Universidade de Aveiro
Departamento de Electrónica, Telecomunicações e Informática,
2019

Bernardo Lopes

Design of Chipless RFID Multi-Resonant Circuits for Barcode Replacement.

Design de Circuitos RFID Multi-Ressonantes sem chip como substitutos dos Códigos de Barras.

Bernardo Lopes

Design of Chipless RFID Multi-Resonant Circuits for Barcode Replacement.

Design de Circuitos RFID Multi-Ressonantes sem chip como substitutos dos Códigos de Barras.

Dissertação apresentada à Universidade de Aveiro para cumprimento dos requisitos necessários à obtenção do grau de Mestre em Engenharia Eletrónica e Telecomunicações, realizada sob a orientação científica do Professor Doutor João Nuno Pimentel da Silva Matos, Professor do Departamento de Eletrónica, Eletrónica Telecomunicações e Informática da Universidade de Aveiro e sob co-orientação científica do Doutor Tiago Miguel Valente Varum, Investigador Doutorado do Instituto de Telecomunicações, poló de Aveiro

o júri / the jury

presidente / president

Professor Doutor Paulo Miguel Nepomuceno Pereira Monteiro
Professor Associado da Universidade de Aveiro (por delegação da Reitora da Universidade de Aveiro)

vogais / examiners committee

Professor Doutor Rafael Ferreira da Silva Caldeirinha
Professor Coordenador do Instituto Politécnico de Leiria (arguente)

Professor Doutor João Nuno Pimentel da Silva Matos
Professor Associado da Universidade de Aveiro (orientador)

agradecimentos / acknowledgements

Obrigado,

Aos meus pais, por me terem apoiado neste caminho.
Á minha irmã, por se esforçar a fingir interessada quando eu começo a falar de coisas técnicas.
Ao meu cão Lobo, por não me ter comido a tese.
À Marlene, por me ter apoiado no meu pior e no meu melhor.
Aos meus amigos de Esgueira, por acreditarem que eu vou ser rico e apadrinhar todos os seus filhos.
Ao Coutinho, Zé e Pedro, por nunca me terem deixado sozinho neste caminho.
Ao corretor gramatical automático, por nunca ter julgado os meus erros.

Um especial obrigado ao meu orientador Professor Matos, por me ter sempre dado um voto de fé, por me ter dado autonomia, por acreditar no meu trabalho e por ter estado sempre disponivel para me ajudar.

Ao Instituto de Telecomunicações por me acolher, guiar e ajudar durante estes dificeis anos.

A todos,
Os meus sinceros agradecimentos!

Palavras chave RFID, RFID sem chip, Tags, FrFT, Circuito Multi-Ressonante, Espiral Ressonante

Resumo

A tecnologia de RFID sem chip, surgiu de um esforço para obter etiquetas RFID de baixo custo sem o uso de circuitos integrados de aplicação especifica (ASICs) que são a restrição à diminuição dos preço dos tipicos sistemas RFID. Desta forma, as tags tornam-se totalmente passivas e sem nenhuma unidade de processamento ativa, passando, os sistemas RFID sem chip a ter mais semelhanças com os sistemas de Radio Detection And Ranging (RADAR) do que com os sistemas RFID comuns.

Esta dissertação esclarece os problemas e desafios que a tecnologia RFID enfrenta enquanto substituta das etiquetas de código de barras apresentando também o estado da arte da tecnologia RFID sem chip. Também apresenta e propõe um modelo para descrever a relação entre a frequência de ressonância do circuito multi-ressonante e o comprimento das espirais ressonantes. Finalmente, um sistema RFID sem chip é simulado usando a transformada fracionária de Fourier como meio de separar sinais modulados linearmente em frequência que colidem simultaneamente no domínio do tempo e da frequência.

Os resultados alcançados com esta dissertação por um lado ajudam os projetistas com a síntese de circuitos multi-ressonantes e por outro provam a confiabilidade do uso da transformada fracionária de Fourier como um meio de manipular o domínio tempo-frequência para recuperar com sucesso informação individual de ID a partir de um sinal que contém mais de um sinal transmistido de uma etiqueta sem chip.

Key words RFID, Chipless RFID, Tags, FrFT, Multi-Resonant Circuit, Spiral Resonator

Abstract

The chipless RFID technology , appears from an effort to design low-cost RFID tags without the use of traditional silicone Application Specific Integrated Circuits (ASICs) that are the price bottleneck of the typicall RFID technology. In this way, tags become fully passive and without any active processing unit, thus the Chipless RFID system have more similarities with the Radio Detection And Ranging (RADAR) systems than with the common RFID systems.

This dissertation sheds light on the problems and challenges that the RFID technology has as replacement of the optical barcode labels, discuss the state of the art of the chipless RFID technology and presents a model to describe the relationship between the multi-resonant circuit resonant frequency and the resonant spirals length. Finally, a chipless RFID system is simulated making use of the fractional Fourier Transform as means to separate linear frequency modulated signals that collide in both time and frequency domain. The results achieved with dissertation not only aid designers with the synthesis of multi-resonant circuits but also prove the reliability of the use of the fractional Fourier Transform as a means of manipulating the time-frequency domain and successfully recovering individual tags' ID from a signal containing more than one collided backscattered signal.

Contents

List of Figures

List of Tables

List of Acronyms

ADC Analog-To-Digital Converter

ADS Advanced Design System

ASIC Application Specific IC

CAD Computer-Aided Design

CAGR Compound Annual Growth Rate

CDMA Code Division Multiple Access

CNL Carbon-Nanotube-Loaded

CST Computer Simulation Technology

DAC Digital-To-Analog Converter

DC Direct Current

EDA Electronic Design Automation

EM Electromagnetic

FMCW Frequency-Modulated Continuous-Wave

FDMA Frequency Domain Multiple Access

FrFT Fractional Fourier Transform

HF High Frequency

IC Integrated Circuit

ID Identification

ISI Inter-Symbol Interference

ISM Industry, Scientific, and Medical

LFM Linear Frequency Modulated

MMIC Monolithic Microwave Integrated Circuit

MoM Method of Moments

MOS Metal Oxide Semiconductor)

QPSK Quadrature Phase Shift Keying

PSK Phase Shift Keying

RF Radio Frequency

RFID Radio Frequency Identification

RO Read Only

R/W Read and Write

SAW Surface Acoustic Wave

SDMA Space Domain Multiple Access

SLMPA Stub Loaded Microstrip Patch Antenna

SMD Surface Mounted Components

SWCNT Single-Walled Carbon Nanotube

TDMA Time Domain Multiple Access

TDOA Time Difference of Arrival

UHF Ultra High Frequency

Chapter 1

Introduction

Automatic identification of products is today one of the major reasons behind the success, expansion and product control of several items from several markets and services. Processes associated with this kind of technology allow the extraction of information through continuous monitoring of items. It's this technology that enables the implementation of a policy of management suitable to keep up with the evolution of the market in a *quasi*-real time fashion [1].

The omnipresent barcode labels that triggered a revolution in identification systems some considerable time ago, are one of the most diffused application of the theory behind automatic identification. Based on the Morse code, the barcode uses the length of interleaved black and white bars to represent data (Figure 1.1). Patented in the United States of America in 1952 this technology began to be explored in the late 1960s and quickly revolutionized the industry's identification systems by allowing to represent digital data in an optical and machine-readable way [2]. According to the website *Stratistics MRC*, the forecasts show that the barcode reader market that was worth 2.12 billion dollars in 2016 will reach the value of 3.18 billion dollars by the end of 2023 with a CAGR (Compound Annual Growth Rate) of 5.9%. Following this growth is the market of the barcode printers: according to the consultant *Global Market Insights, Inc.* it's expected that the value of this market will reach 2.5 billion dollars until 2024, which shows the profound impact that this technology has in our society [3] [4].

Despite being extremely cheap and small, the barcode tags are today an undeniable obstacle to large companies due to its short reading range, clear communication sight and, in most cases, due to the need of human intervention [5].

Figure 1.1: Brief explanation of the numeric values often displayed under a barcode tag. [6]

With all being said, there is a technology capable of surpass the limitation presented by the barcodes: the RFID (*Radio Frequency Identification*) technology.

Radio Frequency Identification is a data capture technique that uses the propagation of electromagnetic waves at RF (Radio Frequency) to automatically identify objects. The success of the use of RFID techniques depends on the propagation of these waves to establish communication between the information carrying device, the RFID tag/transponder, and the interrogator/reader [1], [5].

Figure 1.2 shows the system context diagram of a typical RFID system. Normally, these systems are fundamentally builded with at least two functional blocks:

- **Tag/Transponder** - contains the identification code and it's placed in the item to identify.
- **Interrogator/Read** - sends the interrogation signal to all RFID tags in a nearby area.

The interrogator or reader, can only read tags in its reading range. Typically, it's connected to some sort of device with considerable computing power that is able to process the received information, present it to the user, and save it to a data base to establish worldwide connectivity.

There are a wide range of RFID system that in spite of using the same operating principles, are implemented in different ways. Three criteria are commonly used to distinguish different implementations: frequency of operation, tag power supply, and reading range. Starting with the frequency of operation, depending on the used technology the frequency can go from 125 KHz to 5.8 GHz. The power supply defines if the tag is passive in which case the power is extracted from the interrogation signal or if its active and if so, the tag contains an on board power source. Lastly, the reading range can vary from a few millimeters to a dozen meters [1].

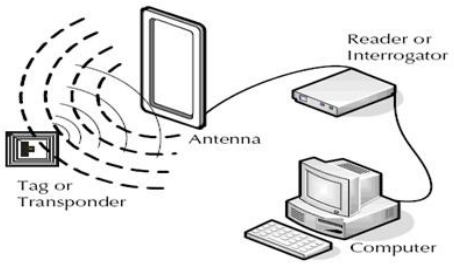

Figure 1.2: System context diagram of a typically RFID system [7].

The general idea is to utilize this technology to build a system in which a costumer with a product using an RFID tag benefits from automatized price recording by simply approaching the balcony without the need to wait for the scanning of every product individually. This saves both the client and the cashier precious time. This is one of many situations that encourage retail and manufacturing companies to adopt RFID technology to tag their products [8].

Considering all the above facts, the researching in the RFID area appears to be a challenging field with plenty of potential. Emerging in an expanding and high valued area, this technology still is in its babyhood but already has the potential to reach the top of the automatic identification market. Through this document it will be presented the motivation to this dissertation, the general planning of the work as well as the goals to achieve, the investigation accomplished, the analysis of the results obtained, and the conclusions drawn.

1.1 Motivation

"*Without hustle, your talent will only get you so far*"
– Gary Vaynerchuk

According to the web-site *Statista*, the RFID market will reach a value of 24.5 billion dollars showing the growing appreciation of this technology in the global economy [9]. The focus on this technology from some companies such as Alien Technology, Motorola, Applied Wireless RFID and Amazon, made the RFID system the major competitor of the until now unswerving market dominated by the barcode (figure 1.3) [10]. The RFID market has the clear advantage of being interdisciplinary, bringing together elements from various fields of knowledge: radio frequency technology, semiconductor technology, data protection and cryptography, telecommunications and many other related areas, which increases its spectrum of applications and stimulates their technological development. However, for RFID technology to be able to replace the use of barcodes, it has to be able to compete with the extremely low price presented by barcodes. This means that the cost of production of RFID tags must be as low as the cost of the barcode labels.

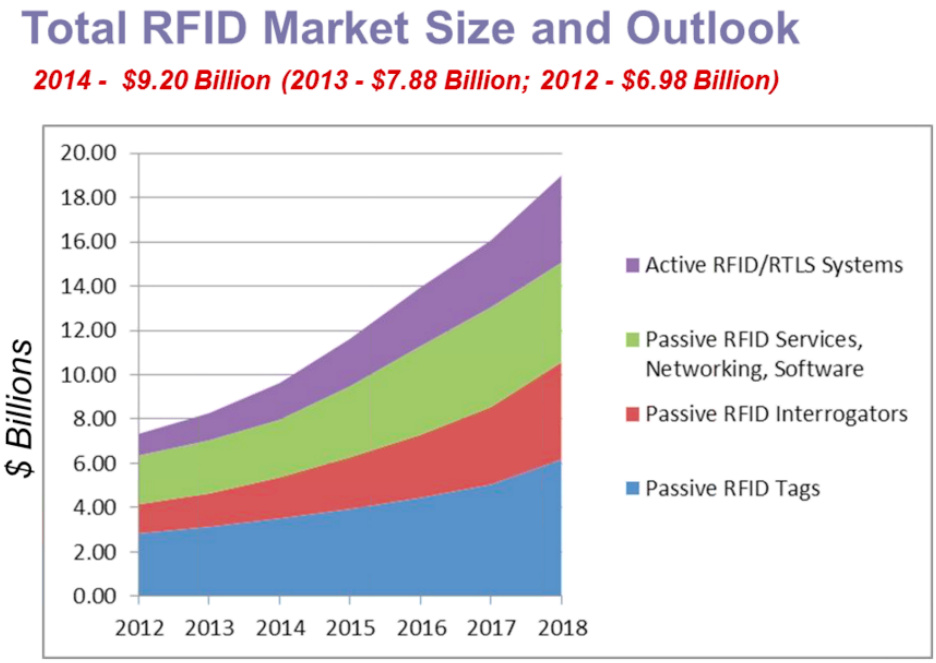

Figure 1.3: Time evolution and projection of the global revenue of the RFID market [10]

Part of the cost of RFID tags is due to their construction: without counting with the power supply in the case of active labels, tags are typically made up of one or more antennas responsible for receiving and / or sending information and an integrated circuit responsible for the signal processing. Depending on the implemented technology, the integrated circuit can store various types of information and / or be reprogrammable.

Typically, made of silicon, the integrated circuit is the main responsible for cost of the tag. The price of this component is at best US$0.05, which means that the cost per label will be

at least close to US$0.1 [5].

Given the higher cost of the silicon circuits implemented in RFID tags (as compared to the cost of printing bar code labels), several efforts are being made to design labels without any integrated circuit. These labels are known as *Chipless RFID tags*, which are devoid of an integrated circuit in their design. The estimated cost for this type of label is less than US$0.01 per label. Most chipless systems use the electromagnetic properties of material and/or the design of various conductive materials to obtain specific electromagnetic behaviour and/or properties that allow each label to have a unique identifiable electromagnetic signature.

The increasing need for efficient product chain management is expected to support the growth of the chipless RFID tag industry. Additionally, these tags can produced by ink-jet printers, which are relatively inexpensive and allow the printing of several labels at the same time, which means that these labels can be easily manufactured. This is another factor responsible for driving the growth of the chipless RFID tag segment [8].

In terms of profit, in North America the chipless RFID tag market is rated as the most attractive of the global chipless RFID, surpassing the value of the chipless RFID Reader and Middleware market (figure 1.4). It is expected that this sector will dominate over the next few years thriving due to the interest of several retail companies such as Walmart who has recently adopted chipless tags in their distributor chains as a way to improve the tracking of their merchandise using an economically viable process. In the European market, manufacturers of textiles, consumer electronics and cultural goods are increasingly adopting chipless RFID technology to improve store inventory management, with this market reaching a respectable value of $50 million in 2016 .

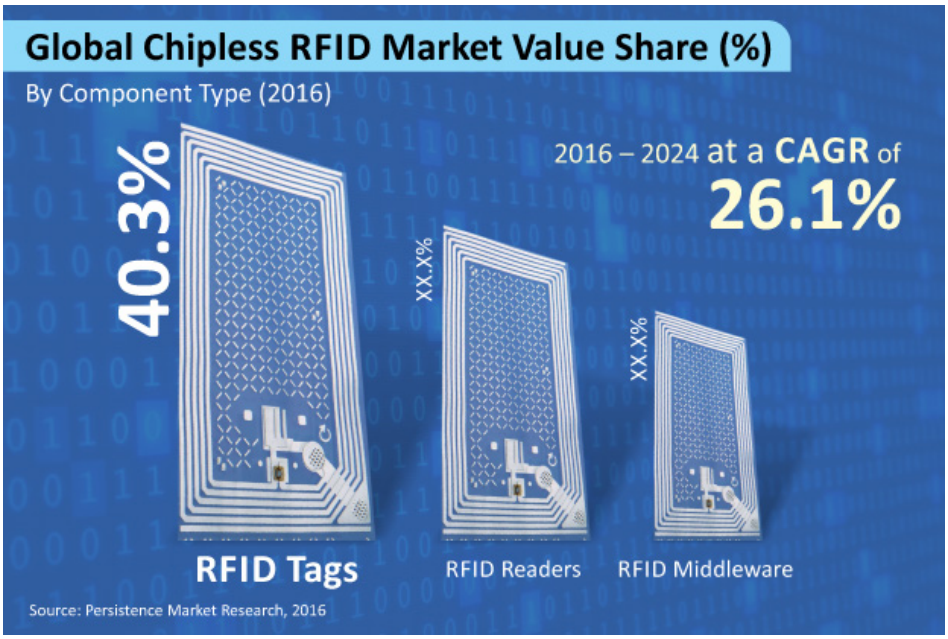

Figure 1.4: Global market share of chipless RFID [8].

Given all the information presented previously, research on chipless RFID tags proves to be quite promising, with room for innovation and improvements. Its positivist projection "promises" positive return of the work done and any implementation with some sort of competitive advantage over other implementations will be quickly recognized and valued. In an

emerging market, the most efficient and economically viable implementation is sought. These points motivated the research presented in this dissertation.

1.2 Main Objectives

This dissertation has the following main objectives:

- Shed light on the problems and challenges that the RFID technology has as a replacement of the optical barcode labels;
- Present the state of the art of the Chipless RFID technology;
- Develop a model capable of describing the multi-resonant circuit frequency behaviour;
- Validate said model by printing and measurement of a multi-resonant circuit designed using the proposed model.
- Implement an algorithm and/or technique capable of separate linear frequency modulated signals that are inseparable both in the time and frequency domain.
- Simulate a Chipless RFID system that successfully achieve all the imposed requirements.

1.3 Document Organization

This document is divided in seven chapters, including the introductory chapter:

- *Chapter 2 - RFID System Overview and Terminology :* this chapter provides the basic knowledge and terminology of the typicall RFID System. By getting better acquainted with these concepts one can better "understand", the limitation, the challenges and the benefits of the use of this technology.
- *Chapter 3 - State Of the Art On Chipless RFID :* chipless RFID is a niche technology within the RFID technology and as such, very specific implementations and technologies have been developed thought the years. This chapter provides an overlook to the state of the art of chipless RFID technology including both tags and advance processing algorithms/techniques used to retrieve the tag's ID.
- *Chapter 4 - Multi-Resonant Circuit Theory :* an introduction to the multi-resonant circuit is done. This chapter covers its operating principle, design implementation and theoretical question. Its main challenges and problems are also addressed. Finally, research on the modelling of the multi-resonant circuit frequency behaviour is presented.
- *Chapter 5 - Multi-Resonant Circuit Characterization :* this chapter presents a characterization of the multi-resonant circuit through simulation of its S-Parameters in *CST Studio Suit 2017* with previous validation of the accuracy of the *CST*. Alternative simulation models are presented, discussed and compared. Finally, a model that relates the resonant frequency of the circuit with the spiral length is proposed and validated thought the printing and measurement of the S-Parameters of a multi-resonant circuit.

- *Chapter 6 - Chipless RFID System Simulation :* a chipless RFID system is simulated in this chapter. The fractional Fourier Transform, a time-frequency analysis technique that allows the recovery of tags ID information from the backscattered signal in a multi-tag environment, is presented, explained and implemented. The system is explained step by step and results are presented for each step.

- *Chapter 7 - Conclusions and Future Work :* lastly, the conclusiond of this dissertation are presented as well some proposals of potential future work that could deepen the understanding of the subjects covered in this work.

1.4 Original Contributions

This dissertation contributed to the scientific community with the publication of a paper *"A Novel Procedure for Chipless RFID Tags Design"* in the proceedings of the conference *YEF-ECE 2019 - 3rd International Young Engineers Forum on Electrical and Computer Engineering*. The paper was written by Bernardo Lopes and João Matos and was orally presented in Lisbon. A copy of this paper is presented in Appendix A.

Furthermore, two other papers written by the same authors are, at the time of write, awaiting approval. Said papers are: *"Modelling of the Multi-Resonant Circuit Frequency Behaviour in Chipless RFID tags"* that is currently submitted to *RFID-TA 2019 - 2019 IEEE International Conference on RFID Technology and Applications* and, *"Simulation of a Chipless RFID System using discreet FrFT to recover individual tags IDs"* that is currently submitted to *IMOC - SBMO/IEEE MTT-S International Microwave and Optoelectronics Conference* .

Chapter 2

RFID System Overview and Terminology

2.1 Introduction

The RFID system has specific architectures and terminologies that one should familiarize with in order to fully understand the work performed in this dissertation. An RFID system is an integrated group of components that implement an RFID solution. These components represent the devices involved in the information exchange and are present in a non-trivial RFID system to some degree.

This chapter will provide the basic knowledge of the most typical RFID system.

2.2 Tag/Transponder

The items that have to be identified are labeled with a tag (also called a transponder). So, the transponder is one of the main components of an RFID system because it contains information about the item which is attached to and has the capability to provide that information upon request, constantly or sporadically.

All the tags offer the same basic functionality: to help identify and track an item. To meet the varied need of different application, transponders come in different forms, shapes, and sizes. The tag must be properly placed on the item so that it could be easily read by the reader. It's, in most cases, the most important part of the RFID system as it defines prices, range and readability.

2.3 Antennas

An antenna can be viewed as a device that converts a guided electromagnetic wave on a transmission line into a plane wave propagating in free space. Thus, one side of an antenna appears as an electrical circuit element, while the other side provides an interface with a propagating plane wave. [11]. The antenna is a component in which the radiation or reception of electromagnetic waves has been optimized for a certain frequency range and its theory has been developed to the point that one can now precisely predict its behaviour and can define it mathematically. The antenna can be viewed as part of the tag in some architectures and as a different device in other cases. This difference, however, has no practical implications.

2.4 Reader

An RFID reader, also called interrogator, is the device responsible to read or read/write data to compatible RFID tags and it behaves both as a slave of the software system and a master of the tags. The software system interacts with the reader through the controller that can either be built into it, or on an external device. Nowadays it's more typical to find the first option and for this reason, we will address the architecture of the reader considering an inbuilt control block.

2.4.1 Reader Architecture

The RFID reader is built off two fundamental function blocks: the control system and the High Frequency (HF) interface as depicted in Figure 2.1.

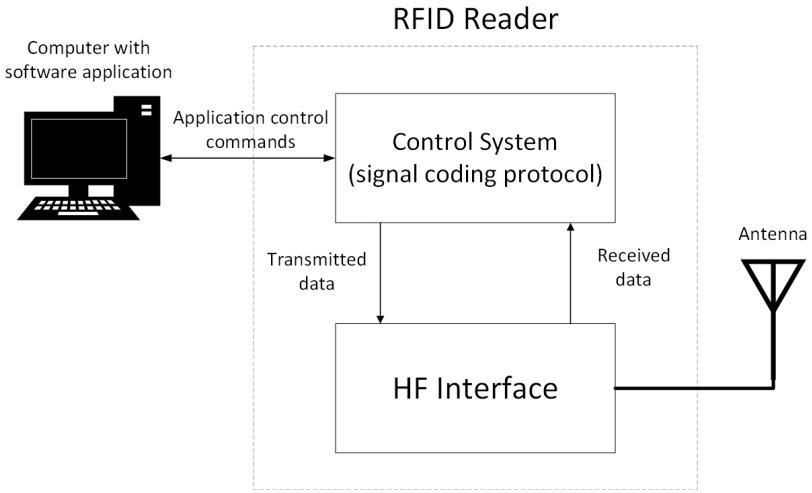

Figure 2.1: Block diagram of a reader consisting of a control system and an HF interface. The entire system is controlled by an external application via control commands.

2.4.1.1 HF Interface

The reader's HF interface is responsible for producing a proper signal to meet the tag's necessities being them in terms of power supply or in terms of communication establishment. This means that the signal generated by this block must be able to establish communication, wake up and/or providing the right amount of power to the tag. It is also responsible for the modulation of the transmission signal, to send data to the transponder, and for the reception and demodulation of HF signal transmitted by the tag.

The HF interface contains two separate channels corresponding to the two directions of data flow: from and to the tag. Data transmitted to the tag travels through the transmitter arm and data received from the transponder is collected by the receiver arm. Figure 2.2 shows a block diagram of the HF interface present in the RFID reader.

In the transmitter arm, a signal at the desired operating frequency is generated by the quartz crystal. To avoid worsening the noise in relation to the extremely weak received signal from the transponder, the oscillator is subject to high demands regarding phase stability and

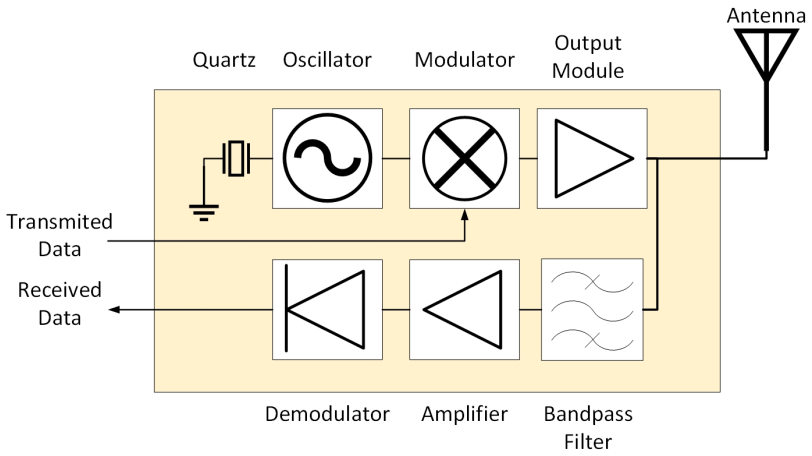

Figure 2.2: Block diagram of an HF interface of an RFID reader.

sideband noise [1]. The generated signal is then feed into in the modulator module which is controlled by the baseband signal of the signal coding system. Finally, the signal is brought to the required level by a power output module. After this stage, some microwave systems employ a directional coupler to separate the system's own transmission signal from the weak backscatter signal of the tag.

In the receiving arm, the incoming signal is filtered by a bandpass filter, amplified and demodulated. Depending on the construction of the reader, this filter can be projected to filter the strong signal from the transmission output module and to filter out justS the response signal from the tag.

2.4.1.2 Control Unit

The control unit of the reader is responsible to establish communication with the application software and to execute the commands received by it. It must also control the communication with the tags in a master-slave principle and perform the necessary coding and decoding of signals. In more complex systems it is expected from this module to execute anti-collision algorithm, encryption and decryption of the data to be transferred between the tag and the reader, and to perform authentication. This model block diagram is depicted in Figure 2.3.

The control unit is typically based upon a microprocessor to support these complex functions. Additionally, there is an additional ASIC module to relieve the processor of some intensive calculation. For performance reasons, the ASIC is accessed via the microprocessor bus (register oriented) [1].

2.4.2 Communication between the Reader and a Tag

The communication between the reader and a tag depends on the type of the tag and can be one of the following:

- **Modulated backscatter**: In this type of communication, the reader sends out a continuous wave RF signal containing AC power and a signal clock to the tag at the working

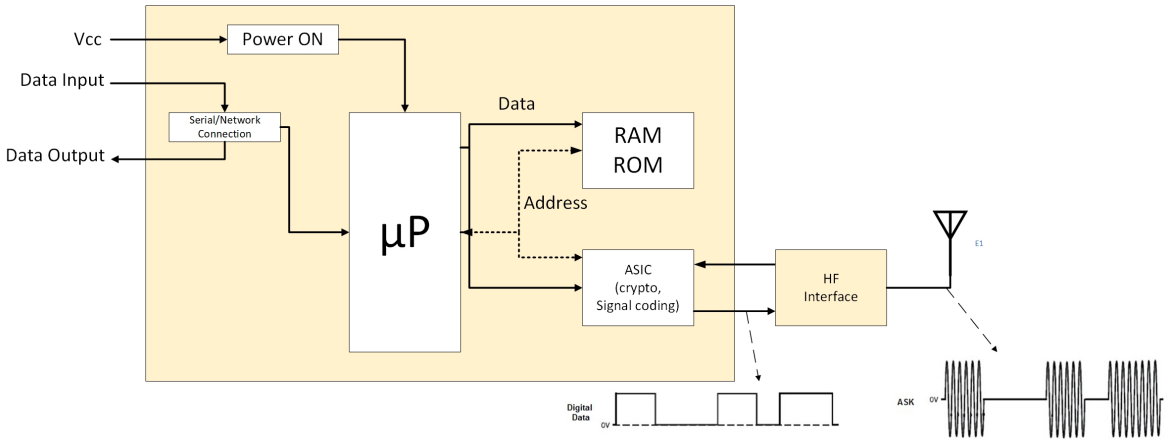

Figure 2.3: Block diagram of a control unit of a reader.

frequency. The tag's antenna absorbs this energy and supplies it to the microchip that modulates or breaks up the input signal into an on/off sequence that represents its data, and transmits it back. Thus, in this type of communication, the reader is the first to make an interaction followed by the tag, so it makes sense to utilize it in passive as well as semi-active tags. The backscatter principle is depicted in Figure 2.4.

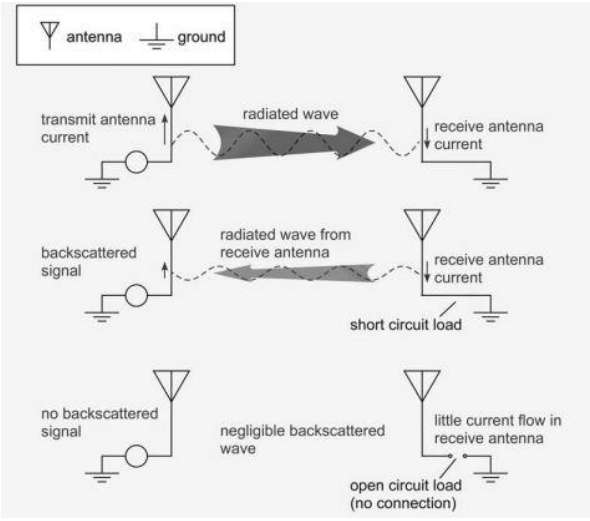

Figure 2.4: Simplified Physics of Backscatter Signaling. Following are the benefits of backscattering Radio waves:- i) Power supply to passive tag. ii) Manage spectral efficiency to manage interference. iii) The need for low complexity RF tags limits modulation and coding options [12].

- **Transmitter type**: In this type of communication the tags broadcast its message to the environment periodically and regardless of the presence or absence of a reader nearby. The communication is initiated always by the tag and thus, only can be implemented in active tags.
- **Transponder type**: In this type of communication, the tag enters a dormant stage

in the absence of interrogation from the reader. When in this stage, it periodically broadcasts a message to check whether any reader is listening to it. When the reader receives this message, it can instruct the tag to end the dormant state and to start to act as a transmitter tag again.

2.5 Interrogation Zones

The area in which the readers and tags establish communication is called the interrogation zone. The configuration of this area has a major impact on the overall performance of the RFID system since multiple readers and tags can create a crowded environment, called a *dense environment*, in which there is loss of efficiency and data.

2.5.1 Dense Environments

There are two major kinds of dense environments (Figure 2.5):

- **Dense interrogator environment** - when multiple interrogators are operating next to each other.
- **Dense tag environment** - when multiple tags are in the reading zone of a certain reader getting all the same interrogation signal.

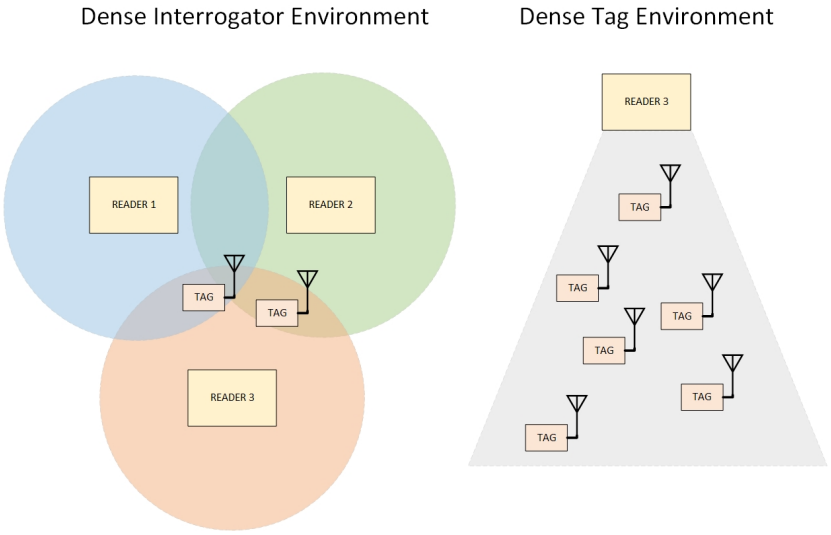

Figure 2.5: Types of dense environments in a typical RFID system.

The main problem with dense environments is the increase in the probability of collisions, since the denser the environment the bigger the probability of collisions. There are basically two types of collision:

2.5.1.1 Reader Collisions

These type of collisions are more likely to happen in the dense interrogator environment for obvious reasons. The main problem is the overlap of the coverage areas of multiple readers. This overlap causes:

- **Multiple Reads** - a tag that is in the overlap area can be read by multiple readers. Depending on the application, these duplicate reads can cause problems.
- **Signal Interference** - when the interrogation zones of multiple readers overlap, the signals from the various interrogators will most likely interact with each other causing constructive or destructive interference. This interference can dramatically change the signal characteristics and information.

2.5.1.2 Tag Collisions

The tags collisions are more prone to happen in dense tag environment and generally occur when multiple tags try to respond to the same interrogation signal at the same time. The multiple responses will confuse the interrogator making it unable to identify correctly the tags. Besides that, in this type of environment, it is not unusual to verify the shadowing effect. This effect happens when tagged item blocks the reader signal from reaching another tagged item hiding behind it. Because of this, the hidden tag can never be read.

2.5.2 Anti-collision Protocols

In order to address the issue of collisions, the developers of RFID systems created several anti-collision protocols.

What one has to understand is that all the tags share the same communication channel every time they try to contact the same reader. Every communication channel has a defined channel capacity which is limited by the highest data rate possible to achieve (which is defined by the readers and transponders antenna) and the time interval in which the channel is available. The channel capacity must be divided between all transponders in such a manner that data can be transferred from several transponders to a single reader. This multi-access problem has been around for quite some time in radio frequency technology (for example, when multiple mobile phones try to access the same base station) and as a consequence of this, multiple workarounds were created in order to solve those problems. The problem with the classical procedures like *frequency domain multiple access (FDMA)*, *space domain multiple access (SDMA)*, *time domain multiple access (TDMA)* and *code division multiple access (CDMA)* is the "*assumption of an uninterrupted data stream from and to the participants (...)* [1]." And as such, designers of RFID systems had to developed/apply specific protocols to adapt to the specific need of the RFID system that they aim to work with. The most common used anti-collision protocols usually fall into one of two categories: Aloha-based protocols and tree-based protocols.

2.6 RFID Transponder Architecture

The main purpose of the transponder is to carry ID (Identification) information regarding the item that it's fixed on. Typically, an RFID transponder is composed by an antenna, an RF section and a digital control section that is either a microprocessor or some other digital system [13]. A basic passive RFID transceiver block architecture is represented in figure 2.6.

Bear in mind that due to the diversity of the now numerous tags typologies, the architecture can dramatically change from one tag to another especially if we are talking about chipless RFID transceivers. Nevertheless, here it will be presented a more high-level architecture that will fit most of the typologies used in the market.

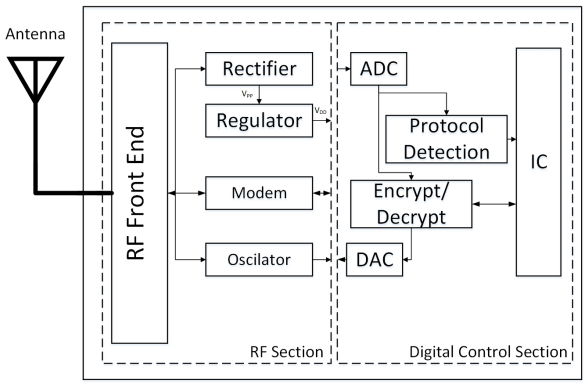

Figure 2.6: Basic passive RFID transceiver block architecture.

2.6.1 Transponder's Antenna

The antenna in the tag acts as a transducer between the electromagnetic wave propagating in free space and the circuitry embedded in the transducer. This operation principle is exemplified in figure 2.7.

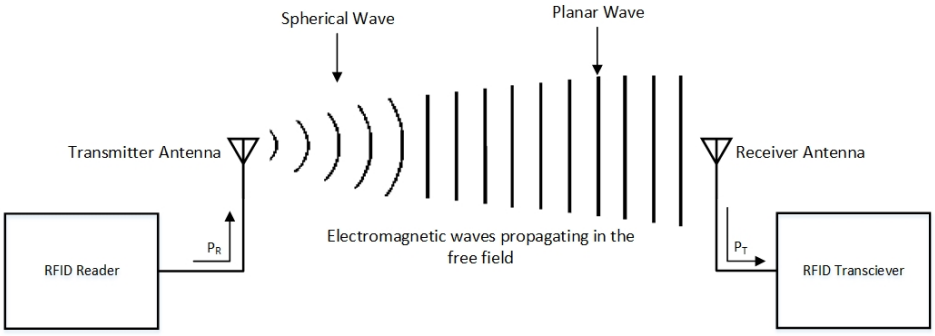

Figure 2.7: Basic operation of transmitting and receiving antennas.

A tag's antenna length is generally much larger than the tag's microchip, and therefore ultimately determines a tag's physical dimensions. An antenna can be designed based on several factors, such as reading distance, known orientation to the tag to the reader and the reader's antenna polarization. The connection point between a tag's microchip and the antenna is the weakest link of the tag. If any of these connection points are damaged, the tag might become non-functional or might have its performance significantly degraded. Changing the antenna geometry can randomly detune the tag, resulting in suboptimal performance.

2.6.2 RF Section

The RF section converts the energy received by the transponder's antenna and converts it to a baseband signal or an equivalent DC voltage. It's also responsible to provide DC power supply for the control section and to modulate and transmit the RF signal so that the ID data can be re-transmitted to the RFID reader.

Depending on the tag's ability to be read-only (RO) or read/write (R/W), the RF section can be modified in such a way that it also extracts the interrogation code from the reader.

The extracted code is transformed from an RF signal to a baseband signal using demodulation circuitry and sent to the control section for further processing [13].

2.6.3 Digital Control Section

The digital section has both analog and digital signal processing subsections. Today's trend is to integrate the digital control section into a single IC so that minimum spacing and package dimensions are achieved.

After the RF signal is received and demodulated in the RF section, the demodulated signal is sent to an analog-to-digital converter (ADC), which converts the RF signal to a low-frequency baseband signal. The baseband signal is then converted to a digital signal and processed further in the protocol detection circuit and decrypted. This signal is then processed by the processing unit, which generates a response signal that is sent to the encryption circuitry and is in turn converted to an analog signal by the digital-to-analog converter (DAC). This signal is then modulated by an RF carrier signal and propagated back to the reader via the tag antenna. This operation is done in the RF section of the tag and the antenna [13].

Chapter 3

State Of The Art On Chipless RFID

3.1 Introduction

Chipless RFID is an ill-defined term: some authors refer to it as tags where all circuits are printed with conductive ink; on the other hand, the majority of the authors and specialists refer to chipless RFID tags as tags that do not have any microchip at all. Through this document the latest definition of chipless RFID is adopted.

The chipless RFID tags and system operate at a completely different principle than that of the conventional RFID and as such, must be addressed in a completely different way. This chapter presents a review of the state of the art of chipless RFID technology. It covers the techniques and technologies used to construct and develop tags as well as some of the most advanced processing algorithms and techniques used to retrieve the tag's IDs.

3.2 SAW Tags

Surface Acoustic Wave (SAW) tags were first proposed in the 1970s but only in recent years technology has reached the maturity required for the mass production of these tags [14]. The operating principle of these tags is based on converting the received interrogation signal from the reader directly into an acoustic wave propagating on the SAW chip surface. This conversion is done by the interdigital transducer (IDT), that is connected to the tag's antenna, and uses the piezoelectric effect of the substrate material. The propagated acoustic wave is then reflected by a number of reflectors, which create a train of pulses with phase shifts. Lastly, the train of pulses returns to the IDT that bears the job of retransmitting the signal back to the reader. This encoding method is based on the time delays of reflected pulses that are controlled by the positioning of the code reflectors[5, 14, 15]. Figure 3.1 shows a typical operation of a SAW tag system.

These types of chipless RFID tags operate in the 2.45-GHz frequency band reserved globally for ISM applications. The literature report reading ranges as large as 10 meters [14] and more than 128 bits of address space [15]. The tag size can be on the order of 1 mm and, reportedly, very robust to high temperatures and is able to achieve greater penetration into pallets containing metal or liquid items [5, 15]. According to the site RFID Journal, "NASA staff will attach RF SAW tags to uniforms and toiletry items placed into each duffel bag assigned to each crew member of a six-month mission" [16] in order to shorten the time taken to audit the possessions of the individual crew members so that NASA's inventory managers

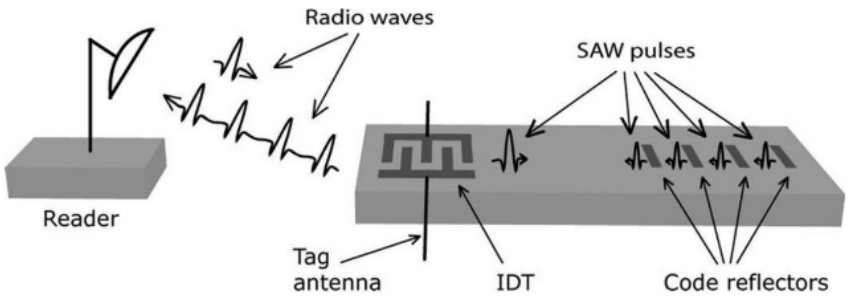

Figure 3.1: Operation of a SAW tag system. [14].

back on Earth can check the supply of these goods and determine which need to be restocked for the next mission.

3.3 Spectral Signature Based Chipless Tags

Spectral Signature Based Chipless Tags use resonant structures to encode data in the form of presence or absence of certain frequencies in the spectrum. The concept of frequency signature is based on encoding an N-bit digital word with N frequencies where each bit is represented by a single frequency and the variation of the amplitude represents the difference between a logic '0' and logic '1' [17]. In [5], the authors point out several types of spectral signature-based tags that had been reported to the time of writing in journals, web articles, white papers and research publication. Thus, in the next subsection, it will be presented a summary of said types based on [5] and complemented with new relevant material.

3.3.1 Chemical Tags

Chemical Tags are designed and implemented making use of target chemical and physical proprieties of certain materials. These, so-called second generation tags, are constructed from resonating deposited fibers or special electronic ink and aim to be cheap, to work on low-grade paper and plastic and to be very tolerant to water and metal as they only work in the KHz range. [17, 18] These tags consist of tiny particles of deposit chemicals, which exhibit varying degrees of magnetism, and, when EM waves are forced on them, they resonate with distinct frequencies, which are picked up by the reader [19]. According to [19], CrossID, an Israeli startup, claims that printing this kind of tags will cost less than 1 cent each and that the company will be able to scan the bar code from 3 meters away, without a line-of-sight requirement. Tapemark, a manufacturer of packaging and packaging materials, claims to be implementing these new tags into packaging, paper and film. The frequencies used by Tapemark range from 24 GHz to over 60 GHz and places the tags priced at five cents each [20].

3.3.2 Ink-Tattoo Chipless Tags

Ink-Tattoo Chipless Tags were developed by SOMARK Innovations, a St. Louis biotech startup, with the goal of innovating cattle identification with a more cheap and reliable solution [21]. These tags use electronic ink patterns embedded into or printed onto the surface of the

objects or live tissue being tagged. SOMARK claims that their tattoos will cost less than the ear tags typically used in livestock and perform well around metal, liquid, and biomass, which is essential for the livestock market. The ink is compatible with multiple frequencies ranging from 100 KHz to the GHz band and is 100% biocompatible and chemically inert [22]. The tattoo's data capacity is related to its size, with a typical cattle tattoo measuring approximately 7.5 by 7.5 centimetres [23]. The reader detection is based on spatial diversity created by the presence or absence of ink particles on the tagged surface [5].

3.3.3 Planar Circuits Chipless Tags

Planar Circuits Chipless Tags are designed using planar microstrip/coplanar waveguide/stripline resonant structures, such as antennas, filters, and fractals [5]. Jalaly and Robertson reported in [24] an RF Barcode prototype using multiple frequency bands consisting of arrays of microstrip dipole-like structures that behave as a resonant bandpass or bandstop filters tuned to predetermined frequencies.

The tags are constructed using frequency selective surfaces designed to perform a (or a combination of) lowpass, bandpass, and bandstop filtering function(s) on the highpass incident plane wave passing through. Detection is based on measuring reflection, where the interrogator emits electromagnetic energy, and the frequency content of the return energy from the RF barcodes in the field is analyzed to determine which barcodes are on the tagged item in the detection zone, hence the item identity [24]. Just like previously mentioned tags, the codification is made by analyzing the presence/absence of certain resonating frequencies.

3.3.4 Space-filing Curves used for Spectral Signature Encoding Chipless Tags

In 2016 a new technique was proposed: the use of Hilbert and Peano space-filling curves in the design of chipless RFID tags [25]. Figures 3.2 and 3.3 show a few iterations of Hilbert and Peano curves respectively.

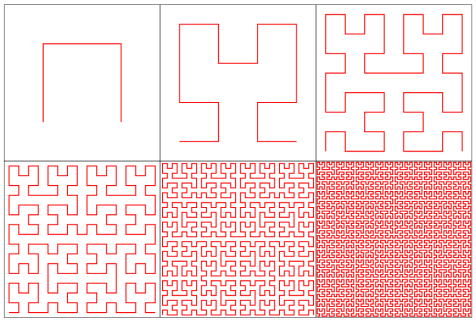

Figure 3.2: Six iterations of the Hilbert curve construction, whose limiting space-filling curve was devised by mathematician David Hilbert. [26].

The most interesting propriety of these curves is the fact that as we move up on the iteration order of these curves, the longer the line is, in the same relatively small surface area. This as some electromagnetic implications: such curves, filling a small footprint can be resonant at a wavelength much longer than its footprint. This is an advantage since it allows the development of small footprint tags at UHF ranges [5]. The major problem of these tags

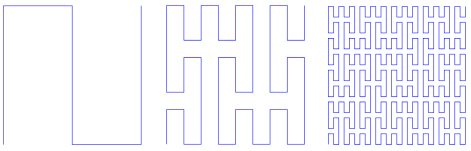

Figure 3.3: Three iterations of the Peano curve construction, whose limit is a space-filling curve. [26].

is in the fact that in order to change a tag's information, several design changes need to be made turning this solution in not so easily scalable technology.

3.3.5 Multi-resonator-based Chipless RFID Tags

The multi-resonator-based chipless RFID tags make use of multi-resonating circuit and a pair of transmitting (Tx) and receiving (Rx) antennas to encode data bits in the form of attenuations and phase jumps at particular frequencies of the spectrum. This technology was patented in 2008 [27] and gives examples of several embodiments of the invention. One of the most well-spread embodiments consists on a resonator/antenna structure comprised by a multi-stop-band filter comprising a plurality of cascaded resonator substructures, each of which corresponding to a stop-band having an associated characteristic frequency, such that information may be encoded in the structure by modifying the resonator substructures. Several adaptations and variations of this embodiment are documented by several researchers - in [28] the authors simulated and implemented a 10-bit chipless RFID tag on Mylar PET substrate using spirals as resonant structures and a pair of UWB short range antennas crossed polarized working in the range of 22-26.5 GHz. The tag consists of two Coplanar Waveguides (CPW) transmission lines each coupled to 5 pairs of resonators which provides 5 distinct frequency signatures. The length of the spirals is the only dimension varied between spirals. The simulated tag presented more than 10 dB depth in the frequency response. The prototype was built on paper subtract and, due to the higher loss factor of the paper, it reduced the lowest tag amplitude depth to 2.5 dB at a reading distance of 10 cm. This prototype provided an experimental validation of an inexpensive and flexible, high information capacity tag; the work presented in [29] is quite similar to the previous one, but the created tag used a bandwidth of 1.76 GHz working on the 1.2-2.96 GHz range and coding 12 bits (1 bit for sensing and 11 for coding) and was bounded into an area of 16.30 cm x 6.63 cm; [30] also presents a prototype of a 6-bit chipless RFID tag operating at 30 GHz using six cascaded and parallel spiral resonators; [31] takes a new approach on the same problem aiming at improving the performance of the tag presented in [32] (a 35-bit chipless tag with a coding density of 0.51 bit/cm^2), miniaturization was design on the transponder to provide a more compact size. This newly introduced tag was based on the same multi-resonating circuit described previously but using four spiral resonators on which were added slots, two U-shaped defected ground structure (DGS) and a 50 Ω microstrip line. By adding slots on the spiral resonator, more bits of information can be stored on the original resonator and the DGS set on the ground plane increase the coding density without adding extra area. Every pair of spirals have the same dimensions in order to accentuate the dip on the spectrum. The spirals are responsible for two dips, the slots are responsible for another two dips and the DGS are responsible for another two. The resonance frequency is shifted by controlling the dimensions of the structure responsible for the dip

and every structure can vary between nine values with a protection bandwidth between 0.1 - 0.2 GHz. Hence, the total combination can theoretically reach the value of $9^6 = 531441$, which is estimated as 19.02 bits in coding capacity within a compact size of 19.89 cm^2 thus achieving a code density of 0.946 bit/cm^2 by applying a frequency shift coding (FSC) coding technique. The results show that the proposed resonators exhibit compact electrical size and small bandwidth.

Typically, the existence of resonant structures is correlated to the existence of '0'. The problem with these structures is that they are not totally reconfigurable, for example, if one desires to code a '1' it can be obtained by four different ways [5]: the first is short-circuiting the resonator; the second is to "open" the resonator leaving the first loop with a discontinuity in the is short-circuiting the resonator; the second is "open" the resonator leaving the first loop with a discontinuity in the conductor; third, reducing the number of turns in order to shift the resonant frequency out of the operation band; and fourth, withdrawing the resonator, although it is an unusual shift the resonant frequency out of the operation band; and fourth, withdrawing the resonator, although it is an unusual option. All are effective, but the first and the second solutions are more advantageous since they preserve the ID of the resonator. In 2015, Alves et al. published a paper [33] on the possibility of implementing silicon optical switch on the spiral resonators in order to create truly reconfigurable RFID chipless tags. The study claimed that each resonator could be at resonance or non-resonance according to the optical switch that was controlled by light. The semiconductor of silicon changes its electromagnetic characteristics when illuminated increasing its conductivity. Thus, integrating a small piece of this material in the construction of the spiral makes this tag a reconfigurable tag having different responses depending on the presence of incident light on the semiconductor strip. The study only reached the simulation phase in 2015, but in 2018 another study was published by Alves et al [34] where it was simulated and implemented a multi-resonator composed of three resonators with only 8.9 mm x 5.4 mm overall size, and its ID states controlled by an optical switch fixed in a 0.3 mm gap. The optical switch was illuminated by a laser source at 980 nm with 17 mW of output power. The final results show that the simulation and measured results showed a remarkable resemblance and that the reconfigurable multi-resonator for chipless tags has a great potential in IoT sensing applications.

3.3.6 Multi-resonator dipole-based Chipless RFID Tags

The multi-resonator dipole-based chipless RFID Tags use the same principle of the tags explained above being the major difference in the choice of the resonant structure. As opposed to the spiral resonators used in the Multi-resonator-based Chipless RFID Tags, these tags use a multi-resonant dipole antenna and only one of the two UWB antennas previously used. At the time of writing, the literature presents some applications of this technology: [35] proposed a chipless RFID sensor tag integrating four tip-loaded dipole resonators as a 4-bit ID encoder and a circular microstrip patch antenna (CMPA) resonator as a crack sensor. The dipole shape was chosen due to the simple geometry and the ability to resonate on a ground plane. This dipole will behave like a half wavelength resonator and will have a resonant frequency depending on its length. In order to reduce the mutual coupling and to shorten the dipole's physical length, the dipole shape was modified with a capacitive tip loading structure, by enlarging both dipole's tips. The overall size of the tag was 35 mm x 15 mm and appears to be legible up to a distance of 120 cm. The results show that the proposed chipless RFID sensor system is only reliable in an anechoic chamber environment. Also, the resonator design

for ID part should be improved to have better resonating/absorption characteristics; [36] took another approach, replacing the spiral resonators by multi-resonant dipole antenna comprised by a set of parallel loop antennas, which resonate at different frequencies. These loop antennas are a series of folded half-wave dipole antennas and by removing any of the half wavelength dipoles, the corresponding resonant peak disappears without influencing the resonances of the other dipoles [5]. The interrogation signal is received by the UWB monopole antenna and is retransmitted only containing certain frequencies, hence encoding a unique spectral signature. The main benefit of using dipole antennas as the resonant structure is the reduction in the size of the tag.

3.4 Amplitude-Phase-Backscatter-Modulation-Based Chipless Tags

These type of tags are the last type covered in this document and are characterised by encoding the information by varying the amplitude or phase of the backscattered signal based on the loading of the chipless tag's antenna. The reactive loading of the tag's antenna is responsible for the variation of the loading thus, influencing the RADAR cross-section of the antenna in amplitude or phase. These variations can be due to the fact that the antenna load is an analog sensor or a left-handed (LH) delay line, or the antenna is terminated by a microstrip-based stub reflector [5]. Karmakar et al. claim, in [5], that based on the data encoding antenna loading element we can distinguish between four types of different backscatter modulation-based chipless RFID tags. The remaining subsection will be dedicated to presenting and analyzing said types.

3.4.1 LH-Delay-Lines-Based Chipless Tags

The motivation for the use of left-handed artificial delay lines and a passive phase shift keying scheme in chipless RFID tags came for the need to replace the mechanical part of the SAW approach by an electromagnetic one. The SAW approach lacked the robustness to high temperatures and had a hard time achieving low construction costs.

Mandel et al described an implementation of this method in [37]. Besides the antenna, the tag is made up of intercalated delay lines and reflectors (or modulators). The interrogation signal is received by the antenna an is delayed by every delay line and reflected by every reflecting element. The superposition of the reflected signals forms the retransmitted signal which codes the information in the phase of the reflected signal with respect to a reference phase.

Using conventional delay lines would imply the fit of extremely large physical lines, which would not be feasible. To surpass this problem, the authors suggested the use of low-wave structures like Left-Handed artificial lines. Since there is no way of building a transmission line with a distributed left-handed lumped element model, the authors had to build an artificial line by cascading unit cells constituted by lumped elements like SMD (Surface-Mounted Device) capacitors and inductors. Yet, there is a drawback of using LH structures: the group velocity of those lines is dispersive. In other words, there is the possibility of inter-symbol interference (ISI) due to pulse broadening. This effect increases with line length, thus, it limits the maximum amount of direct encodable information. The solution is the use of Quaternary Phase Shift Keying (QPSK) to increase the information density along the delay line. The prototype build consists of three delay elements and three passive reflectors/modulators where two of them are built as QPSK modulators while the other one only allows a 2-PSK realized

by an open or short. The prototype is 26 cm long (without the antenna) and is able to code 75 different IDs (≈ 6.2 bit). The simulated and measured results showed good agreement.

3.4.2 Remote-Complex-Impedance-Based Chipless RFID Tags

These kinds of tags encode data by means of loading a scattering antenna with microstrip stubs, which represent different inductances, and therefore manipulating the phase component of the antenna's RADAR cross-section and backscatter signal [5]. The nomenclature "scattering antenna" was proposed in [38] to describe an antenna terminated by a lossless reactance. The scattering antenna should scatter back the same power irrespectively of the type of lossless termination and the backscattered signal should have a constant envelope in absence of frequency selective fading [38]. Such an example of a scattering antenna is the microstrip patch antenna. A novel technique for RFID based on remote measurement of complex impedance at microwave frequencies was presented in [39]: multiple tags are interrogated using a chirp signal with a bandwidth of few hundred MHz to few GHz. The superimposed responses of the individual tags are mixed with the interrogation signal and filtered to generate an intermediate frequency signal. A particular tag is selected by processing this signal even further with a narrow detection bandwidth. The phase-frequency profile (that determines the tag's identity) of the reflection coefficient of the selected tag is recovered with the aid of a reference channel. This technology has some benefits: it uses a large transmission bandwidth allows one to resolve between adjacent tags and provide immunity o multipath; has a better overall Signal to Noise ration when compared to amplitude modulation; it allows operation with low transmitted power and can provide range information.

3.4.3 Stub-Loaded-Patch-Antenna-Based Chipless RFID Tags

The operating principle of the tag is based on the use of vector backscattered signals from multiple planar reflectors to code a bit sequence created using the relative phase difference of the backscatters signals [40]. The main difference between this technology and the above is that the relative phase refers to the difference in phases of the backscattered E-plane and H-plane signals in the reader antenna. The tag's antennas are multiple patch antennas, which are suited due to their scattering antenna properties [5]. The antenna reflector element used in [40] was a square Stub Loaded Microstrip Patch Antenna (SLMPA) consisting of a microstrip patch antenna loaded with an open circuit transmission line. The designed tag contained three antenna elements arranged in a linear array. Each signature frequency contains an absolute phase of between 0-180 degrees. Using a resolution of 5 degrees, each frequency signature can contain 35 bits of data, thus, the three elements tag can then, theoretically, contain 108 bits of data. The prototype showed that a unique code can be extracted with a 30^{o} phase shift and both the simulation and measured results validated the concept.

3.4.4 Carbon-nanotube-loaded (CNL) Chipless tags

In [41], a rather unique chipless RFID tag was proposed. It combines RFID technology and nanotechnology to create an RFID tag that works as ammonia (NH_3) detector sensor. The tag comprises a conformal RFID antenna with a single-walled carbon nanotube (SWCNT) composite in the chipless RFID node for toxic gas detection. The chipless tag antenna is a bowtie meander-line dipole antenna and the SWCNT is placed between at the input port of the antenna in order to enable data encoding [5].

The impedance of the SWCNT is highly sensitive to the concentration of ammonia (NH_3) thus, by varying the concentration of ammonia in the environment one varies the impedance of the SWCNT and consequently the amplitude of the backscattered signal. These variations can be picked up by the reader to infer about the levels of ammonia present in the environment.

3.5 Multi-Tag Identification Algorithm and Techniques

As the reader may have noticed by now, systems using chipless RFID tags differ greatly from the conventional RFID systems in a number of ways. This is due, in great part, to the fact that in typical RFID systems the tag contains onboard active elements (ASIC and/or battery) and hence, the tag is capable of sensing collision in the wireless environment and establishing a two-way communication with the reader by switching between sleep and wake-up state controlled by the reader different query signals. In these type of systems, several common anti-collision protocols that are used in both wireless and network systems (such as Aloha-Based and Tree-Based protocols) have an almost direct adaptation and application. On the other hand, chipless RFID systems are more identical to RADAR systems especially from the tag's perspective as the tags do not possess any intelligence. Just like RADAR systems, the incident signal is backscattered by the different tags in multiple directions. The reader's antenna captures a portion of this signal and analyses its spectrum to find the resonance information that denotes the tag ID. This gives rise to an overlap of the several responses that modulate their ID over the same interrogation signal, which means that they encode the information on the same frequency band. Thus, neither time-domain windowing and frequency-domain filtering are suited to separate the signals. Therefore, the collision tag-detection and collision avoidance issues need to be addressed in the reader using adequate techniques for signal processing. The next points are intended to elucidate the reader about the new techniques introduced to solve this problem.

3.5.1 Block Coding

Overlaps of the backscattered signals is not the only form of interference. The communication channel of most of chipless RFID systems are made of air and the channels are often cluttered with objects, walls and nearby tags thus causing a decrease in the probability of successful identification of a tag's ID due to the inclusion of noise, data collisions, undesired reflection and multipath propagation. Due to this, wrong decoding may occur altering a bit value (or more) of the tag's decoded ID.

Most of the chipless RFID tags presented in the literature focus mainly on incorporating as many data bits as possible within a small footprint. This means that parity and/or error checking bits are not used since the problems of data loss and integrity during transmission are not tackled by the tag's designers. The modification of the encoding method of the tag by using block coding alleviates some of the burden of the reader as the main responsible for the reliability and data integrity by also participating in reliability improvement.

In block coding the original ID binary sequence is segmented into message blocks consisting of m information bits and k parity or error checking bits. A generator matrix is used to generate codewords ID. This matrix defines the range of possibilities of the code words since these words are limited to the set of all linear combinations of the lines of the matrix. The matrix is built up using a certain linear code like, for example, the Hamming code - a linear error-correcting code. The Hamming code is one of the most used codes and it's based on

adding additional check bits to the original code word. These bits are then computed as the XOR operation of certain code bits [42]. Let's take, for example, the Hamming(7,4) code represented in Figure 3.4.

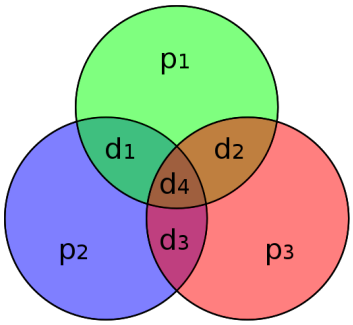

Figure 3.4: Graphic representation of the Hamming(7,4) code with four data bits (d1, d2, d3, d4) and three parity bits (p1, p2, p3). The membership of each data bit shows which parity bits cover said data bit. For example, d3 is covered by p2 and p3, but not p1. [43].

Three parity bits are added to the original four-bit ID word. At the receiving side, the value of the parity bits is checked against the XOR operation of the received corresponding bits. If there is a mismatch between these values, then it's concluded that an error as occurs (the erroneous bit can be the parity bit). This is done by using the parity-check matrix defined by the used code. The result from the multiplication of the seven bit received word with the parity-check matrix is called syndrome (that in this specific case is a three-bit vector) and it gives the position of the bit that occurred the error if the vector is other than a null vector. For example, if the syndrome vector is (1,0,1) then it's assumed that a single bit error has occurred in the fifth position of the received word. On another hand, if the computed syndrome is (0,0,0) then it's assumed that no error has occurred. It's worth noting that the Hamming(7,4) is only able to correct single-bit errors and detect all single-bit and two-bit error [42].

This coding scheme provides a robust decoding method of detecting the presence of bit error in case of singe-tag transmission error and collision in case of multi-tag transmission error. This comes at the cost of adding bits that do not contain identification information in the tag and thus increasing its footprint without increasing the information saved in the tag. Another problem is the lack of distinction between single tag reading error detection and multiple tag detection [44].

3.5.2 Time-Frequency Analysis

The use of narrow-beam antennas with beam steering capability helps to isolate individually the tags in the interrogation zone. However, it's almost impossible to isolate all the tags thus, collisions still happen. Since tags are distributed within the interrogation area and within the narrow-beam of the reading antennas, the geometrical distribution of tags can be exploited as a distinguishing criterion for multiple tags (although this situation is specific only to certain applications). Following this introduction is an overview of a signal separation-based approach through *t-f* analysis.

Due to the spatial positioning of the colliding tags, there may be a time difference of arrival

(TDOA) in the response signals from the multiple tags, which means that resonances may occur at different time instances but at the same frequencies. These different time instances constitute an important parameter that may be used in the separation of the tag's responses. As showed in Figure 3.5, in the *t-f* plane is possible to distinguish multiple tag's responses.

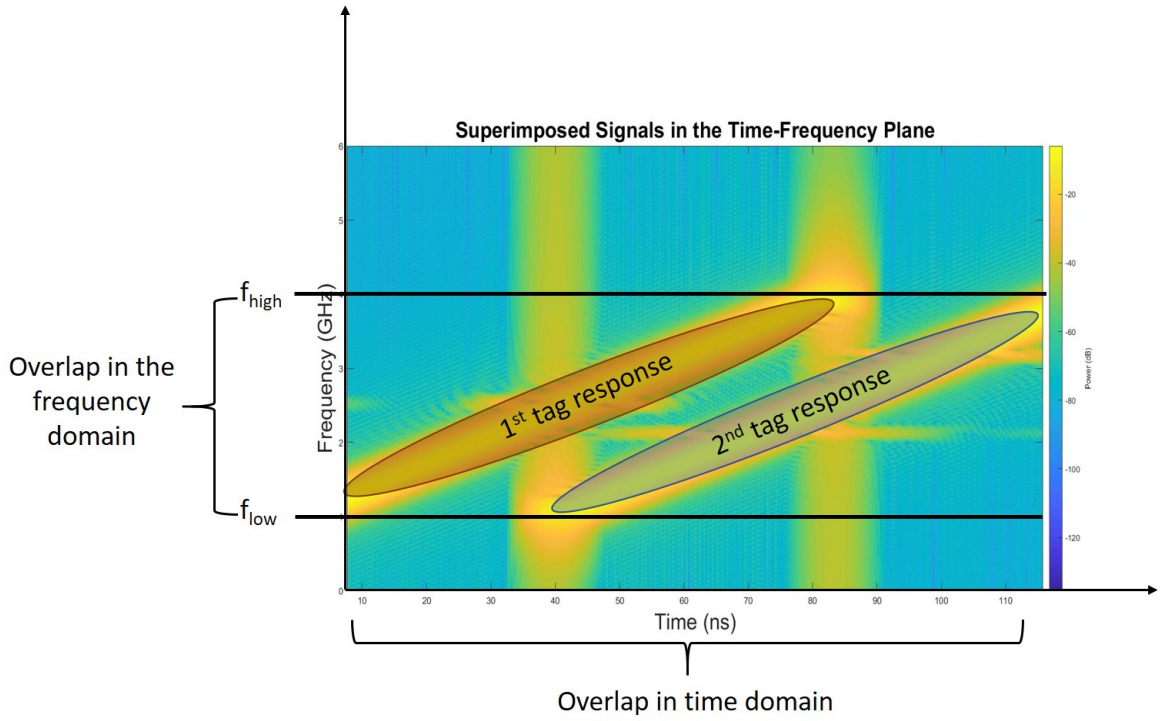

Figure 3.5: Colliding backscatter signals from a multi-tag environment in the time-frequency plane.

The fractional Fourier transform (FrFT) is a group of linear transformations generalizing the Fourier transform. This generalization can be thought as the Fourier transform to the n-th power, where n is an integer - in this way, it can transform a function to any intermediate domain between time and frequency [45]. In this intermediate domain, signals that were once superimposed can now have no to minimum overlap. It can also be viewed as an angle rotation in the *t-f* plane where the signal contains both time and frequency information. Linear Frequency Modulation/ Chirp signals spread over time and frequency, however, in the optimum fractional domain, it can be represented in a compact manner as an impulse/spike [44].

In [44] the authors report that this method successfully extracted individual tag response signals from the collided signal. From the extracted signal, the tag ID was decoded correctly in every case. Despise the great results, this methodology requires a short-duration chirp signal and a high sampling rate.

3.5.3 Frequency-Modulated Continuous-Wave (FMCW) RADAR-Based Techniques

The FMCW RADAR-Based Technique, unlike the previous technique, has the advantage of not only detecting the tag's ID but also its range in the interrogation zone. Besides that, it requires a lower sampling rate and can perform satisfactorily even with longer-duration chirp signals [44].

Chipless RFID systems are a niche within RADAR theory thus, they share a lot of similarities with the typical RADAR system. The commonly used FMCW RADAR technique is used to distinguish between multiple targets in an interrogation zone. In chipless RFID systems, this technique is used to detect and discriminate tags that are near each other.

There are two different antenna configurations used in FMCW RADAR: mono- and bistatic. In a monostatic configuration, the same antenna is used for both transmitting the interrogation signal and receiving the backscattered signal. Differently, the bistatic configuration distributes those tasks by two different antennas. The use of these configurations are very application specific, for example - if the reader is to be hand-held, then a monostatic configuration is more appropriate since the reader must be lightweight, compact and easy to carry. In a monostatic configuration, a circulator is used before the antenna in order to prevent the received signal to come to the transmitter section. In the bistatic RADAR, the received signal is brought to the mixer. In both configurations, a coupler is used to bring a reference of the input signal to the mixer for comparison. The mixer creates a difference frequency signal comparing the reference signal and received signal that is called intermediate frequency (IF) signal. This signal is the target of most of the analysis to extract worthy information about the tags.

There are three main steps for resolving multi-tag collision: 1. Identify that there was a collision; 2. Estimating the probable number of tags involved in the collision; 3. Decoding the individual tag's ID from the collided response.

The process proposed in [44] is showcased in Figure 3.6.

A different set of simulations were carried out for the validation of the methodology proposed. The method was proved to be able to detect the presence of multiple chipless tags within the interrogation zone. Yet, this method fails for monostatic RADAR if the tags reside at a same distance from the receiver.

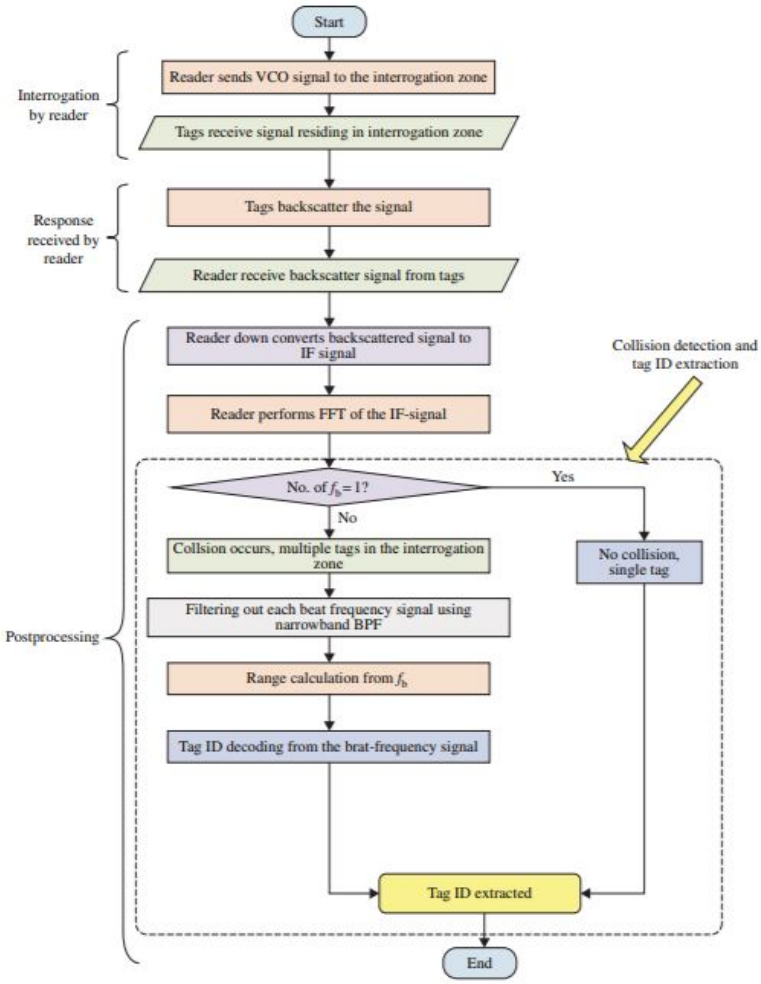

Figure 3.6: Flowchart of the processes for resolving multi-tag collision [44].

Chapter 4

Multi-Resonant Circuit Theory

4.1 Introduction

As stated before, chipless RFID tags can encode data in many different ways. So far, tags that encode their data as a spectral signature are known to be more efficient in terms of coding capacity and, thus, widely research by the scientific community [46]. Within all the different technologies that encode data as a spectral signature, the multi-resonator-based chipless RFID technology presents itself as one of the most suitable solutions to be exploit as a replacement of the common barcode labels: it's designed to operate at a short range (up to 40 cm) and to tag extremely low cost price sensitive items [47]. A multi-resonator-based chipless RFID tag is built from a multi-resonant circuit - responsible for the data encoding, and a pair of antennas - responsible to receive the interrogation signal and to send the modulated version of the same signal back to the reader. The block diagram of said tag is depicted in Figure 4.1.

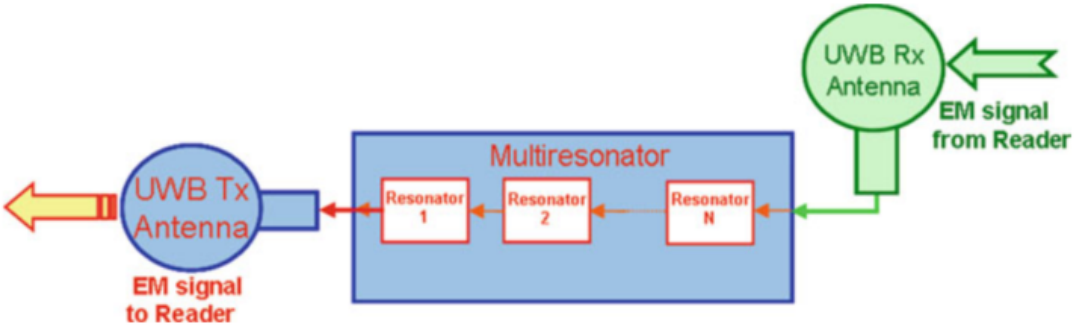

Figure 4.1: Block diagram of a multi-resonator-based chipless RFID tag [47].

It's mainly the multi-resonant circuit that is targeted for research by the scientific community as it defines the codding capabilities of the tag. One of the drawbacks of these type of tags is the complex measurement steps necessary to retrieve information and the effect of the interference suffered when in a real environment. The used detection techniques are mostly based on radar cross-section, and thus, are highly sensitive to noise, reading distance, and other factors [46]. So, improving the codding capabilities of the tag will directly impact the abilities to retrieve a correct identification from the reading process. In this sense, this chapter will study and analyse in detail the multi-resonant circuit.

4.2 Multi-Resonant Circuit

The multi-resonant circuit consist in a series of cascaded resonators coupled to a microstrip line as shown in Figure 4.2 and 4.3.

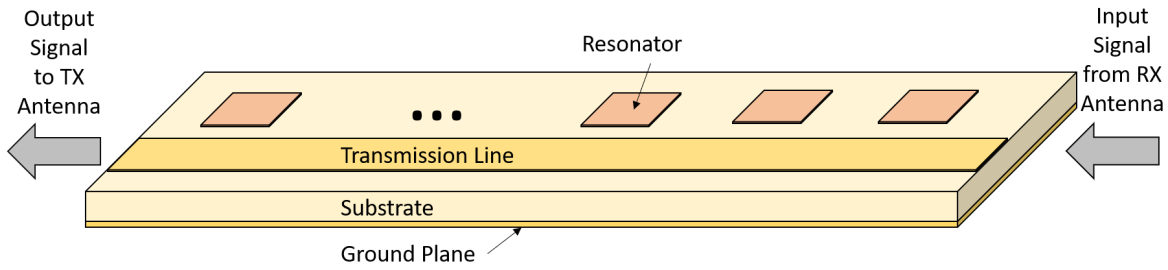

Figure 4.2: Perspective view of the multi-resonator circuit.

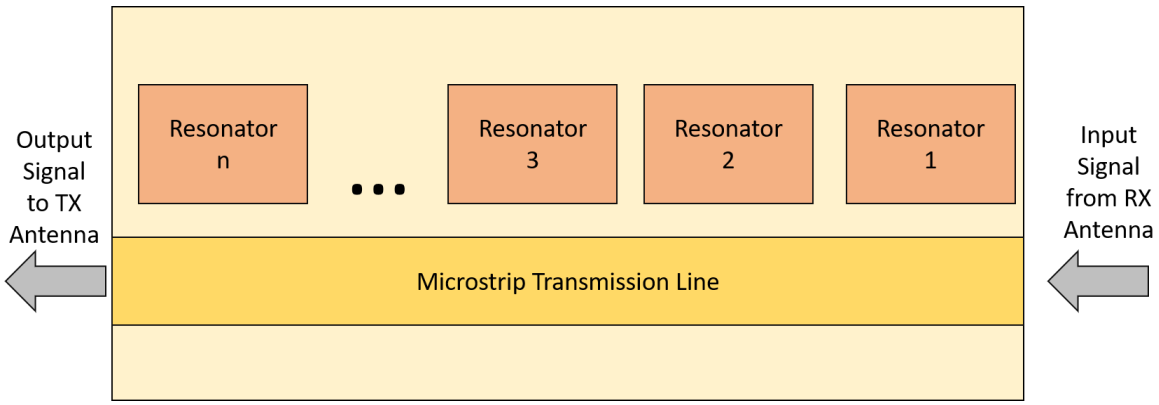

Figure 4.3: Block diagram of the multi-resonator circuit from a top view.

The signal flows from the RX antenna through the transmission line to the TX antenna. All of the n resonators are coupled to the transmission line and, at their specific resonant frequency, create a low impedance path to the ground plane. Because they are coupled to the transmission line, when resonating the signal travelling through the transmission line is deviated to the ground by the resonator, causing a lack of spectral content at that specific frequency. Since information is coded by the presence or absence of spectral content at predetermined frequencies, the resonant structures have a huge impact on the quality of the tag and therefore, the choice of the resonator must be done thoughtfully. Joubert's work [48] sorted out the most important criteria when deciding on which resonator type to use:

- The size of the resonator;
- The spacing/coupling factor relationship between adjacent resonators;
- The position of the first spurious response of the resonator;
- The tunability of the resonator;

Joubert also compared two highly used resonators - the rectangular open-loop resonator and the improved or miniaturised hairpin resonator - with the spiral resonator. All three resonators were built to achieve a fundamental resonance at 1.8 GHz for the specified substrate. The results obtained from that comparison indicate that the surface area of a spiral resonator is smaller by 60% than the square open loop resonator and 17% than the improved or miniaturised hairpin resonator. Therefore spiral resonators can be used to construct very small and compact narrow-stopband filters. An additional advantage is that, by being smaller, the physical spacing between resonators can be increased, resulting in less unwanted coupling between adjacent resonators. The spiral resonator can be easily tuned by varying its physical dimensions and the tag code can be easily modified by shorting specific spirals to the transmission line.

Using spiral resonators, information is encoded in the spectrum of the input signal as attenuations and phase jumps at pre-selected frequencies, as can be seen in Figure 4.4.

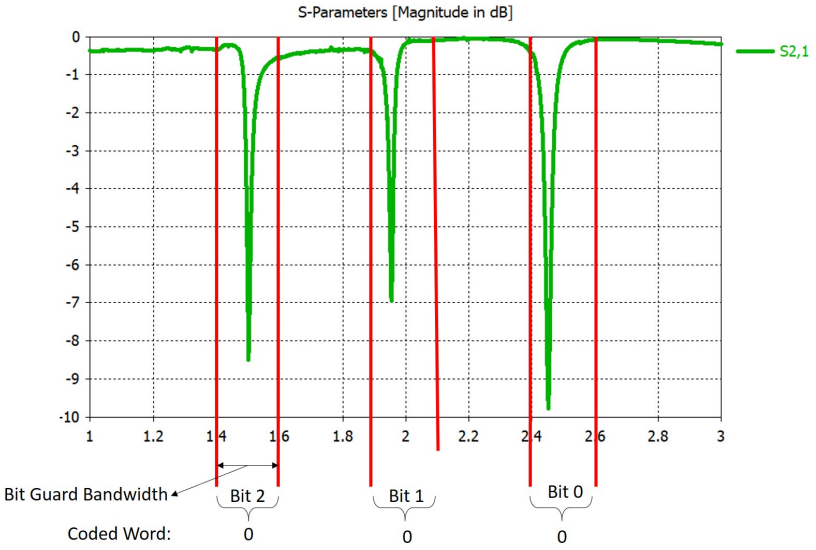

Figure 4.4: Spectrum analysis of the encoded signal. The information is encoded by attenuations in frequency in certain pre-selected frequency. Each pre-selected frequency has an associated bit bandwidth that allows information to be detected correctly even if the resonance deviates slightly from the desired frequency. In this example, the pre-selected resonant frequencies were 1.5, 2 and 2.5 GHz.

For the reasons mentioned above, the spiral resonators were chosen as the resonators to be used in the multi-resonant circuit throughout this work.

4.3 Multi-Resonant Circuit Design

The correct design of the multi-resonant circuit is of utmost importance. Conceptually, the designer has to choose the frequency range of operation, the number of bits to encode within that range, the corresponding frequency were the bits are to be encoded and the guard bandwidth for each bit. The goal is to maximize the number of bits encoded in the spectrum and to minimize the frequency range used, the physical size of the circuit, and the potential

errors caused by unexpected frequency shifts, added noise or other causes. At a physical level, the designer has to compute each dimension of the spiral resonator and the transmission line in order to achieve the desired frequency response. To do that, the relationship between the circuit frequency behaviour and its physical dimensions must be known, which implies the existence of some model capable of describing such behaviour. The multi-resonant circuit has a lot of variables that influence its frequency response. Every spiral resonator has five different physical parameters that directly influence its resonant frequency. Furthermore, the transmission line also has two physical parameters that influence the frequency response of the circuit. Such parameters are depicted in Figure 4.5.

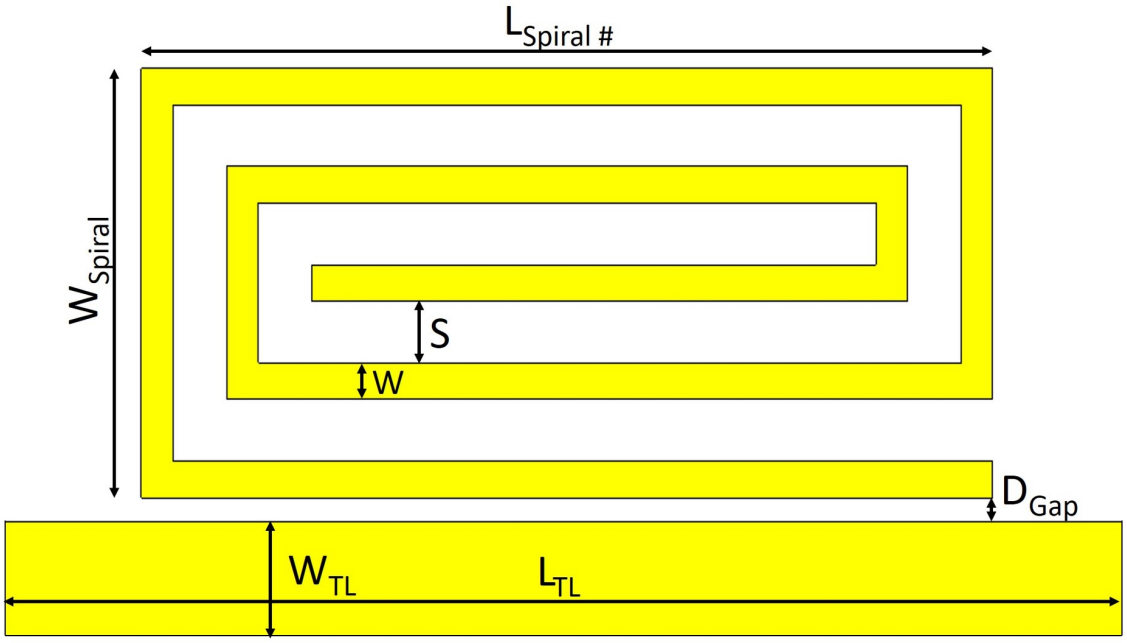

Figure 4.5: Spiral Resonator coupled to a transmission line highlighting the physical parameters of the structure: $L_{spiral\#}$ is the length of the spiral numbered by #; W_{spiral} is the width of the spiral; S is the spacing between turns; W is the width of the spiral arm; D_{Gap} is the distance between the spiral resonator and the transmission line; W_{TL} is the width of the transmission line and the L_{TL} is the length of the transmission line.

Additionally, the number of turns n is also used and it accounts for the number of turns of a spiral resonator.

To the author knowledge, very few information exists on a model capable of accounting for every physical parameter of the circuit. This indicates the lacking of a model capable of aiding designers in the process of projecting multi-resonant circuits. The design process appears to be bounded to the try and error approach using full wave 3D or Method of Moments (MoM) simulators which is a time-consuming process, that is difficult to scale.

Nevertheless, some efforts were made to conceptually better understand the circuit behaviour. Several authors [49, 50, 51] model the circuit as behaving in an equivalent matter to the circuit displayed in Figure 4.6. The overall equivalent circuit behaves as a stop-band filter having one resonant frequency at a predetermined frequency, imitating the behaviour of

a multi-resonant circuit containing only one resonant spiral.

The problem with this model is that, despite providing the designer with a more conceptual visualization of the behaviour of the circuit, it does not relate its lumped element values with the physical units depicted in Figure 4.5.

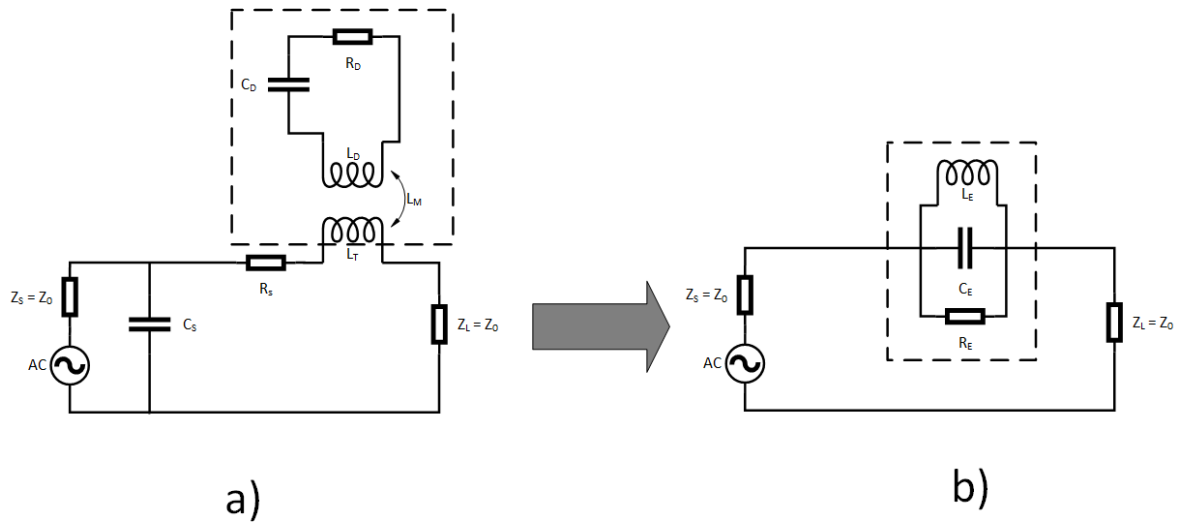

Figure 4.6: Equivalent circuit model of the spiral resonator coupled to a microstrip transmission line. Sub-figure a) is the the equivalent RLC circuit of the spiral resonator that influences the main circuit due to the mutual inductance; Sub-figure b) presents the equivalent simplified circuit.

In this sense, this work sheds some light on the problems with modelling a multi-resonant circuit and tries to provide a solution to this issue. In order to try modelling the multi-resonant circuit, one can first try to fully model the spiral resonator and then define its interaction with the coupled transmission line.

The spiral structures first appear in the literature as an inductor and this constitutes the bulk of the work done on this topic by the scientific community.

4.3.1 Spiral Inductors

The inductor plays a significant role in today's technology. With the tendency to miniaturize every technology, lumped-element design using inductors became a key technique for reducing Monolithic Microwave Integrated Circuits (MMICs) chip area, resulting in more chips per wafer, and thus lowering costs of production. Bellow C-band frequencies, MMICs that use lumped inductors are one order of magnitude smaller that ICs that use distributed matching elements [52]. For these reasons, the study of the inductor as an on-chip passive component was conducted by the scientific community. One of these implementations was the planar spiral/coil version that rises as the most popular one. This type of inductor can take a rectangular or circular shape. The latter one has better performance suffering less resistive and capacitive losses. However, the circular shape is not widely used because only a few commercial layout tools support the manufacturing of it [53] leaving the rectangular spiral as the adopted shape of the planar inductor. Withal, the hexagonal shape, due to its

better similarities to the circular shape, is also used. A scheme of the rectangular inductor is depicted in Figure 4.7.

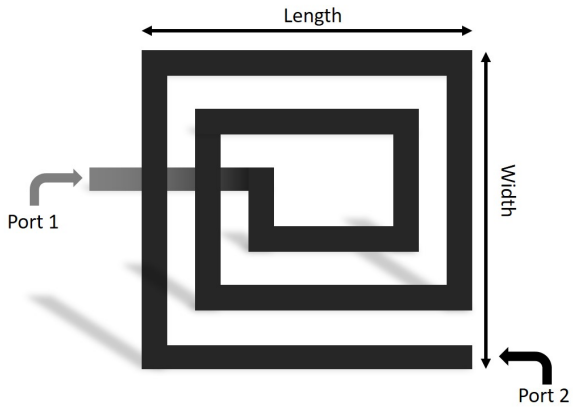

Figure 4.7: Spiral inductor scheme.

Once again, the lack of an accurate model for on-chip inductors is one of the most challenging problems for silicon-based radio-frequency integrated circuits designers [54]. However, this situation is changing as the demand for radio-frequency integrated circuits continues to grow and thus, some models started to appear in the literature. Models can be developed using analytical/semi-empirical, electromagnetic and measurement-based methods as shown in Figure 4.8. Most of the work performed appears to be around the lumped-element method.

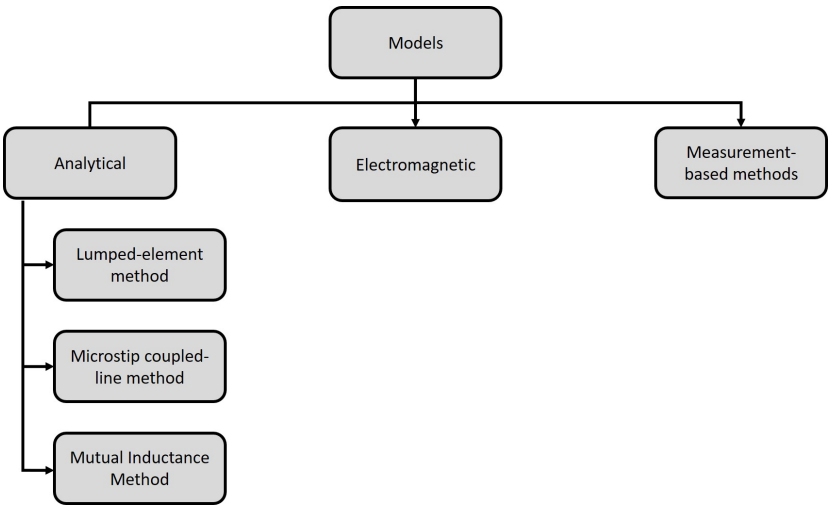

Figure 4.8: Model types that can be developed to describe the spiral inductors behaviour.

4.3.1.1 Lumped-Element method

Within the Analytical/Semi-empirical models, the lumped-element approach uses frequency-independent formulas for free-space inductance with ground plane effects.

The first reported lumped-element model was proposed by Nguyen and Meyer [55] in 1990.

In their work, the authors describe inductors and LC filters fabricated in Si bipolar process with oxide isolation. The lumped-element model presented is the one shown in Figure 4.9.

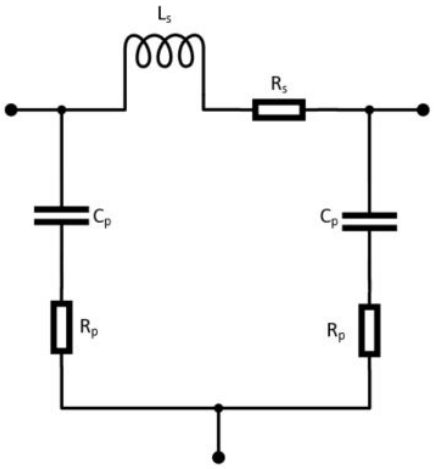

Figure 4.9: Equivalent circuit of the square-spiral inductor proposed by Nguyen and Meyer [55]. In the figure L_s models the self and mutual inductance in the second metal segments, R_s is the accumulated sheet resistance, C_p models the parasitic capacitance from the second metal layer to the substrate, and R_p represents the resistance of the conductive Si substrate.

However, this model does not account with the coupling capacitance between metal segments due to fringing fields in both the dielectric region and the air region. Additionally, the approximations done are only valid because the relative dielectric constant of the oxide is small and the inductor is used at frequencies far below its self-resonant frequency. An improved model was proposed by Ashby et al. [56] by accounting with more physical mechanisms taking place in the inductor. There are two major differences to the previous model: the addition of C_{sub3} and C_{sub4} that allow a good fit with the obtained high frequency measured data, and the use of a frequency dependent resistor to model the series resistance of the inductor. This model is represented in Figure 4.10. However, this model parameters need to be extracted from empirical curve fitting rather than by physical means [53].

Yue and Wong [54] proposed an inductor model similar to the one above but with model parameters more relevant to the inductor geometry. Such model is displayed in Figure 4.11.

All of the values of the circuit elements can be derived using analytical means. Some of the techniques used deduce those values have some limitations such as, for example, being only applicable to square shape spirals.

By this time, the reader must already realize the similarities and differences between the model in Figure 4.11 and Figure 4.6. The first one is built in MOS (Metal Oxide Semiconductor) technology while the latter uses microstrip technology. In the microstrip spiral, power flows through the spiral due to capacitive coupling to a transmission line then to the ground, while that in the MOS spiral, the power is injected through one port of the spiral and it flows to the other port. One other big difference is that the MOS spiral has a feed-through path, meaning that the signal can flow directly from the input to the output port without passing through the spiral, due to the parasitic capacitive coupling between the input and output port model by C_s. This parasitic capacity does not exist in the microstrip spiral model which

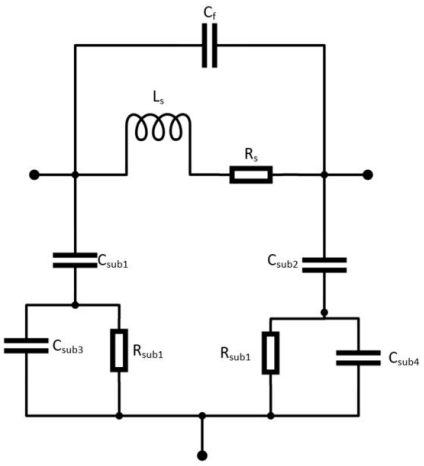

Figure 4.10: Equivalent circuit of the square-spiral inductor proposed by Ashby et al. [56]. In the figure L_s represents the series inductance of the structure, R_s stands for the series resistance of the metallization and includes a frequency dependent term to model skin effect and other high frequency effects, C_f models the fringing capacitance between the metal traces, C_{sub1} and C_{sub2} represent the capacitance from the metal layer to the substrate, R_{sub1} and R_{sub2} model the substrate resistance and, C_{sub3} and C_{sub4} represent the capacitance into the substrate.

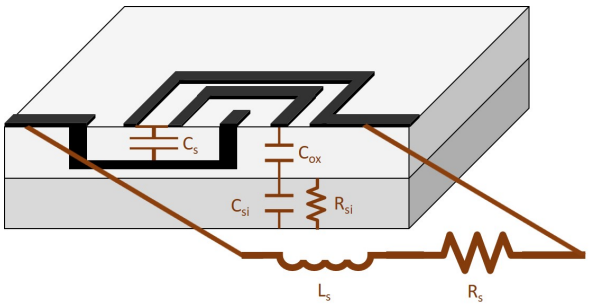

Figure 4.11: Equivalent circuit of the spiral inductor proposed by Yue and Wong et al. [54]. In the figure L_s represents the series inductance of the structure, R_s stands for the series resistance, C_s models the feed-through path, C_{ox} models the oxide capacitance between the spiral and the silicon substrate. The capacitance and resistance of the silicon substrate are modelled by C_{si} and R_{si}.

---

means that the behaviour of these spirals is critically different.

4.3.1.2 Coupled-Line Approach

This technique decomposes the spiral in a set of coupled lines. It's reported to predict the spiral inductor's behaviour reasonably well for spiral up to two turns, with frequencies up to 18 GHz [52] and can only be applied to microstrip spiral inductors. Figure 4.12 shows a modified equivalent circuit of a 1.75-turn rectangular spiral inductor. This model accounts for the crossover capacitance but does not account for the right-angle bend discontinuity effect.

The analysis of these circuits can be done by using either commercial CAD tools or by solving cascaded ABCD or S-parameter matrices for these elements. The solving process is doable for spirals up to two turns, but as more turns are designed the more complex the work becomes and thus, this solution has some drawbacks in terms of complexity.

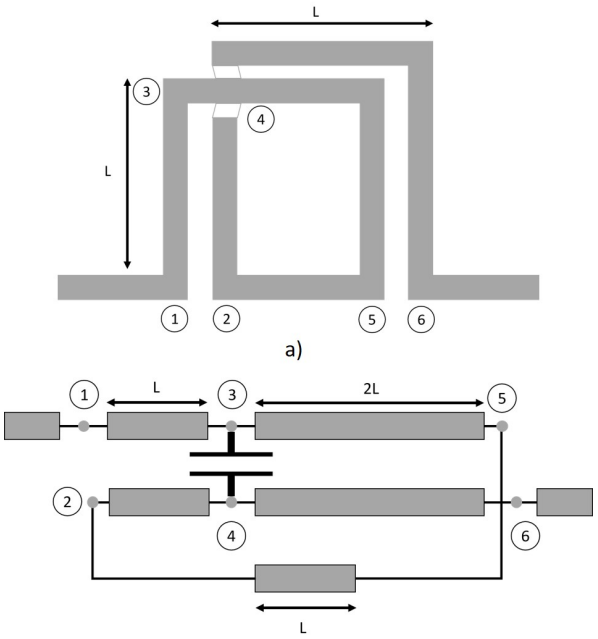

Figure 4.12: a) Spiral Inductor of 1.75 turn; b) Respective Spiral Inductor coupled-line model.

4.3.1.3 Mutual Inductance Approach

The mutual inductance approach aims to derive the inductance value of the spiral. Despite not actually providing a model for the spiral it gives the designers a nominal value for its inductance. The inductance value is derived by subdividing the spiral into rectangular sections and then calculating the self-inductance of all segments and the mutual inductance between all segments just like it's depicted in Figure 4.13. This relationship was first proposed by Greenhouse [57] and then perfected by Krafcsik et al. in his study [58].

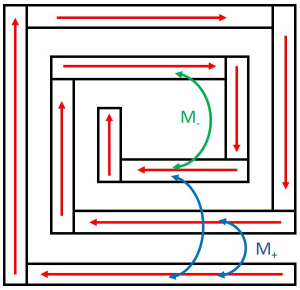

Figure 4.13: Spiral inductor divided in section showing positive and negative mutual inductance path and the current flow direction.

As this model only computes the inductance value of the spiral, no more attention will be given.

4.3.1.4 Electromagnetic Models

The electromagnetic models are generated by simulation that are able to simulate inductors adequately and also provide additional flexibility in terms of layout, complexity and versatility [52]. The most used technique for planar structures is the *method of moments* (MoM) while the *finite element method* (FEM) is used for 3-D structures. Both these techniques perform electromagnetic analysis in the frequency domain. Simulators are becoming designer's most useful designing tool. The behaviour of the spiral inductor can be easily modified by changing the structure of the spiral and rerunning the simulation. The main drawback of this method is that it can be a very time-consuming process based on a *trial and error* approach in order to achieve the desired behaviour of the inductor.

These simulators work by solving Maxwell's equations in terms of electric and magnetic fields or current densities, which are in the form of integro-differential equations, by applying boundary conditions. The structure is fully analysed by exciting the input ports with known sources and then solving numerically the previously mentioned equations in order to determine unknown field or induced current densities. The numerically solving involves discretizing (meshing) the unknown fields or currents. The structure to be simulated is defined in terms of dielectric and metal layers, their thickness and material proprieties. The simulator is designed to be able to solve and simulate the behaviour of arbitrarily shaped strip conductor structures providing data about its frequency and/or time behaviour.

While using EM simulators, one has to compromise among size, speed and accuracy while also having in mind that these simulations are reported to accurately calculate the inductance and resonant frequencies of these inductors but fail to compute their Q-factor [52].

4.3.1.5 Measurement-based methods

The measurement-based methods, as the name implies, are methods that aim to extract a model by performing measurements in specific configurations. This means that the model is extracted after the circuit is constructed, not aiding its design. In this sense, this method will not be explored as it only provides a model for the circuit after it's designed.

4.3.2 Spiral Resonator

As stated before, no accurate model of the frequency behaviour of the spiral resonator is present in the revised literature. As such, characterizing the Multi-resonant Circuit by firstly studying the spiral resonator through an accurate model and then add to that model the coupled line theory becomes impractical and time-consuming. Rather than doing this, the author characterized the multi-resonant circuit as a whole.

Chapter 5

Multi-Resonant Circuit Characterization

5.1 Preliminary Simulation of a Single-Spiral Multi-Resonant Circuit

In order to better understand the behaviour of the multi-resonant circuit, one was designed in *CST STUDIO SUITE 2017*, a simulation software that provides accurate 3D electromagnetic Electronic Design Automation (EDA) solutions for Maxwell's Equations. The circuit was designed using a Rogers RO4725JXR substrate with $height = h = 0.78\ mm$ and $dielectic\ constant = \epsilon_r = 2.55$. The conductor used was copper with $thickness = t = 0.017\ mm$. All other parameters reference Figure 4.5 and are listed in the Table 5.1.

Table 5.1: Design Parameters

Circuit Parameter	**Value [mm]**	**Circuit Parameter**	**Value [mm]**
s	0.5	D_{Gap}	0.2
w	0.3	W_{TL}	1.912
W_{Spiral}	$5 \cdot w + 4 \cdot s$	L_{TL}	$L_{Spiral\#} + 10$

The simulated structure consisted of a multi-resonant circuit with only one resonant spiral of length $L_{Spiral1} = L = 5mm$ with $number\ of\ turns = 2.25$ and occupying a total surface area of 300 mm^2. The value of W_{TL} was computed in order to have a 50 Ω impedance, thus matching the input impedance of the discrete ports used. The circuit was tested in the 1 to 15 GHz frequency band in order to have an accurate understanding of its behaviour within a large range of frequencies. The structure is excited by an auto-generated signal from its ports, which are typically highlighted with a red circle and a corresponding labelling number. The S-Parameters can be analysed in order to perceive the circuit's resonant frequencies. Because the circuit is almost symmetric from the port's point of view, the S_{12} and S_{21} parameter are identical thus, during this dissertation most of the times only one of them will be referred.

Figure 5.1 show the results obtained from the S_{12} parameter simulation in the chosen frequency band. According to the figure, is possible to not that that within that frequency range, the circuit has three clear resonant frequencies and that from approximately 10 to 15 GHz the quality of the circuit is highly deteriorated. From this data is also possible to perceive

that all three resonant peaks have a relatively narrow -3 dB bandwidth that get progressively larger with the rise in frequency.

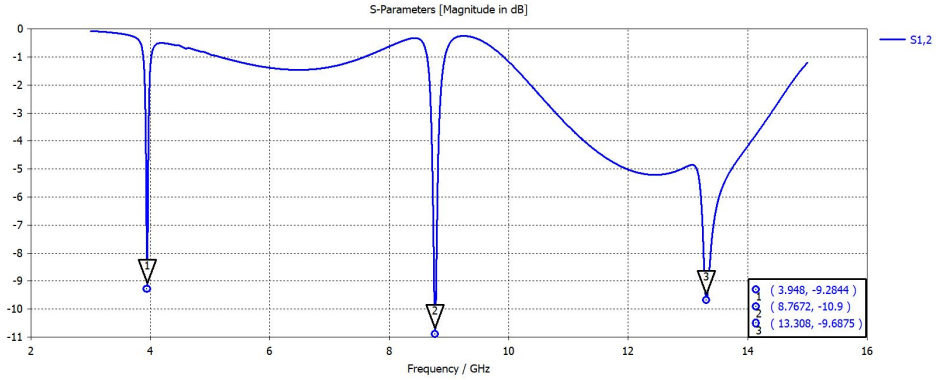

Figure 5.1: CST simulated S_{12} parameter from 1 to 15 GHz of a multi-resonant circuit with a resonant spiral with length of 5 mm.

In order to comprehend the differences in the behaviour of the circuit at both resonant and non-resonant frequencies, two surface current monitors were used in CST simulation software. The resonant monitor was set at 3.948 GHz whereas the non-resonant was set at 3 GHz. Figure 5.2 show the obtained results.

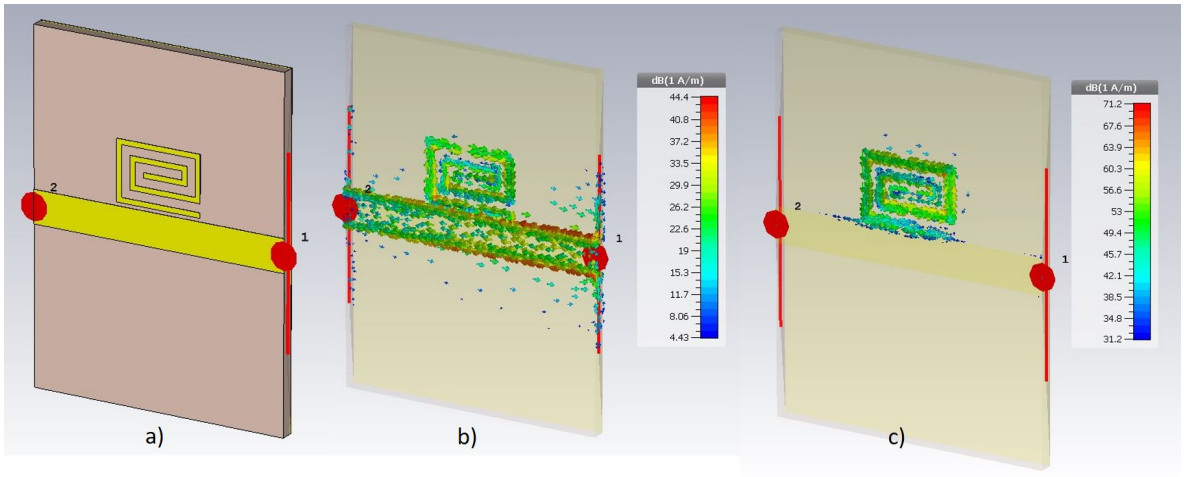

Figure 5.2: a) Simulated Structure; b) Surface current at a non-resonant frequency; c) Surface current at the first resonant frequency.

As expected, it's clear that at a resonant frequency, the flowing current is deviated from the transmission line to the spiral resonator causing a lack of spectral content at that particular frequency in the output port.

5.2 Simulated Models

Throughout the literature, it is possible o find hundreds of cases were the CST is used to simulate multi-resonant circuits. The results obtained in the simulations are in most cases

taken for correct upon comparison with measured data. However, these comparisons are only performed for the first resonant frequency and show a slight deviation both in resonant frequency and in attenuation.

In order to understand the validity of the use of CST as the most reliable simulator, a comparison between three models in two different simulating software was conducted. The three models were: a coupled-line-based model using 20 different components (coupled lines, transmission lines and transmission line square bends and couples square bends) in the *Advance Design System 2017* software; a electromagnetic model in the *Advance Design System 2017* software and the already used 3D model built in CST. All models simulated a spiral resonator coupled to a transmission line with a length of 5 mm, built on Rogers RO4725JXR substrate with $height = 0.78mm$ and $\epsilon_r = 2.55$. The conductor used was copper with $thickness = 0.017mm$. All other parameters reference Figure 4.5 and are listed in the Table 5.1. The results obtained from these models was then compared to the ones obtained by measurements.

5.2.1 Coupled Line Model

The use of coupled-line models was already discussed when reviewing the models for the spiral inductor. In [47] a spiral resonator comprising of 22 section of microstrip components coupled to a transmission line modelled in the ADS Schematic Simulator was proposed. This model was improved by reducing the number of sections to 20 and by adding 90° bends and coupled 90° bends to the schematic. The proposed improved schematic of the circuit is displayed in Figure 5.3.

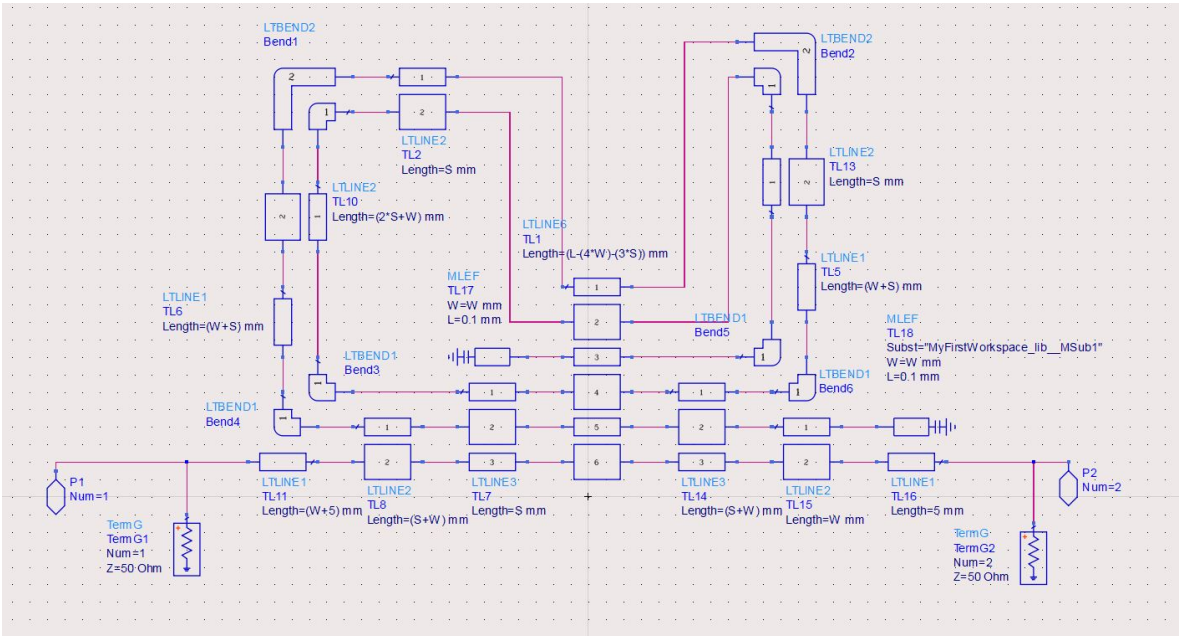

Figure 5.3: ADS Schematic multi-resonant circuit layout.

The main advantage of this model is that it allows a much shorter optimization time due to the fact that the transmission line theory-based simulators take less time to simulate than full wave 3D or Method of Moments solvers. However, this model does not account with coupling between some elements (like the 90° bends and the transmission line) and assumes that some

elements don't have any effect on other elements, due to the distance between them and this may not always be true.

5.2.2 EM ADS Model

The ADS software also has an in-built full wave solver that allows the simulation of the equivalent planar structure of the one used in the coupled line model. The layout of the simulated structure is displayed in Figure 5.4.

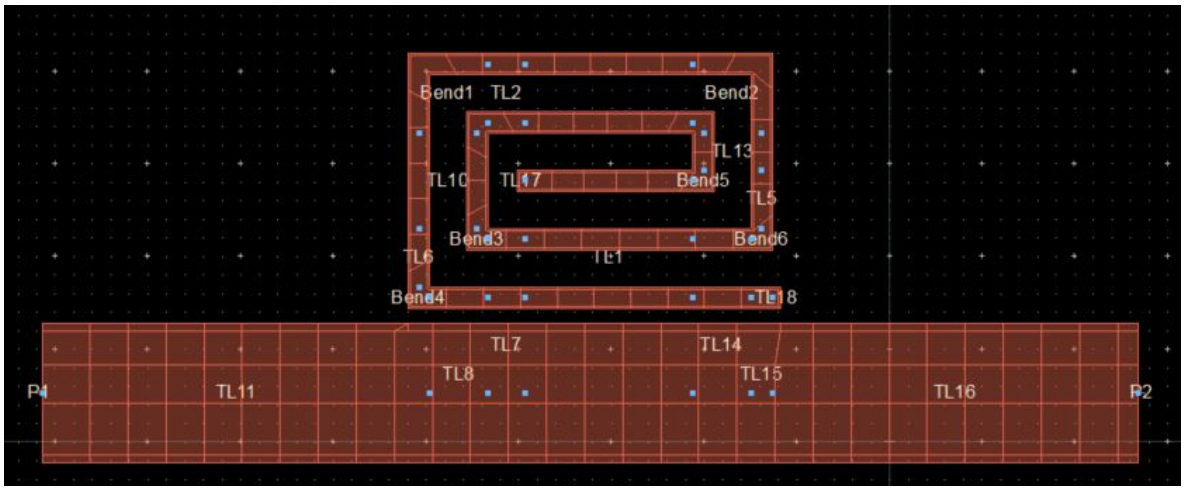

Figure 5.4: ADS Electromagnetic multi-resonant circuit layout.

This method of simulation is also faster then the model in CST, however is much slower that the coupled-line one.

5.2.3 Testing Device

The corresponding multi-resonant circuit was built similarly to the diagram depicted in Figure 4.2 and it's presented in Figure 5.5. The S-Parameters within the 1 to 15 GHz frequency band of the circuit were extracted using an Agilent Technologies's PNA-X Network Analyser.

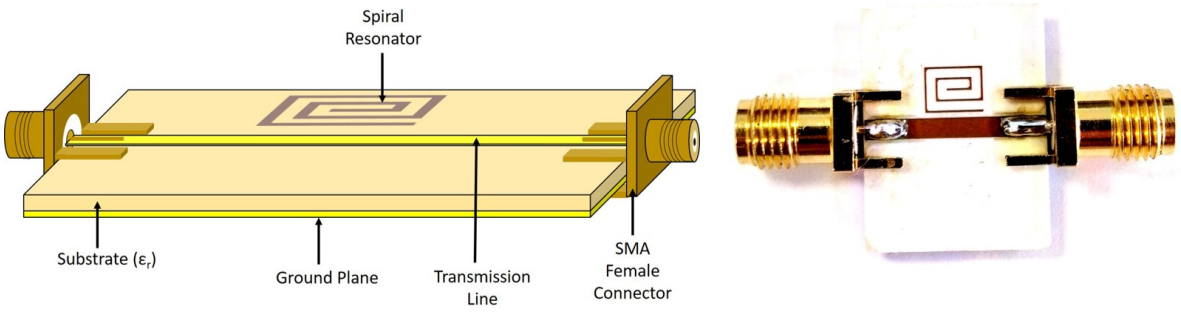

Figure 5.5: In the image, at the right, is the printed Multi-Resonant circuit with one resonant spiral of length 5 mm on a Rogers RO4725JXR substrate, and at the left it is the circuit schematic.

5.2.4 Results

The S_{12} parameter obtained from both the simulated and measured circuits are presented in Figure 5.6.

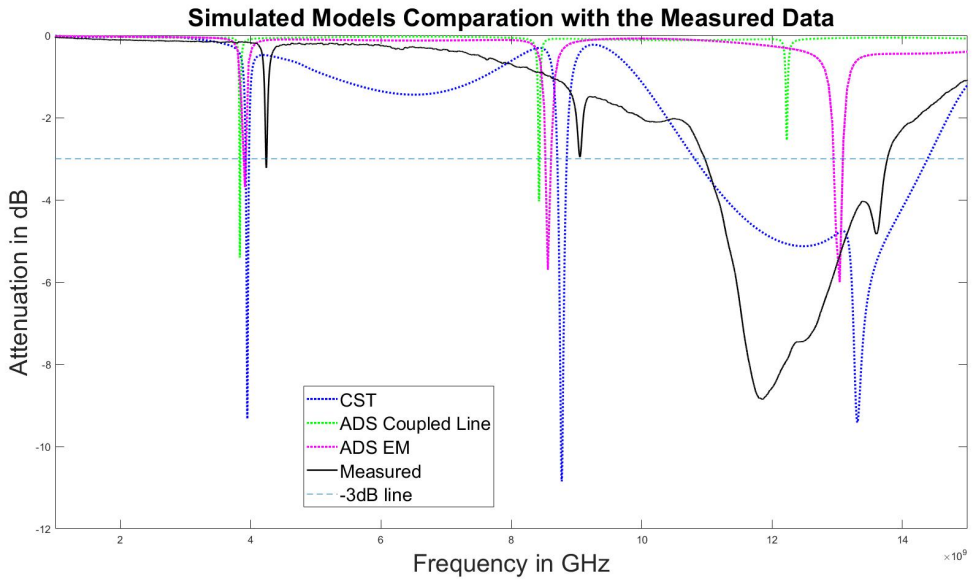

Figure 5.6: S_{12} parameter obtained from both the simulated and measured circuits.

The results show that in terms of the resonant frequencies, the CST is the one that is closer to the measured data, followed by the ADS EM model and lastly the ADS Coupled Line model. In terms of attenuation, the CST is too optimistic while the other two are closer to the measured attenuation, being the ADS EM model the one that better approximates the first resonant frequency whereas the ADS Couples Line has the closest attenuation value to the measured second resonant frequency. The third resonant frequency appears to have an abnormal behaviour: the frequency response deteriorates significantly from 11 GHz and appears to have the predicted third resonant peak as a secondary peak of the resonance peak around 11.8 GHz. In terms of the shape and form of the S_{12} parameter, the CST is arguably the one that better describes the measured data due to its behaviour after the second resonant frequency. For this reason, the CST simulation software will be used as the most reliable software through this study. However, to better study the strange phenomenon happening after the 10 GHz mark the author decided to short the resonant spiral to try to isolate the reason of such behaviour: either it is from the substrate/connectors/welding or from the designed circuit. The S_{12} parameter was measured and it's depicted in Figure 5.7.

The obtained S_{12} parameter shows that this strange behaviour is present in the circuit even when the spiral is shorted to the transmission line. Thus, the expected behaviour of the circuit will be superimposed on this curve resulting in the S_{12} parameter measured in Figure 5.6. This problem, however, does not affect the first resonant mode of the circuit, which is the most used mode for data encoding by the academia.

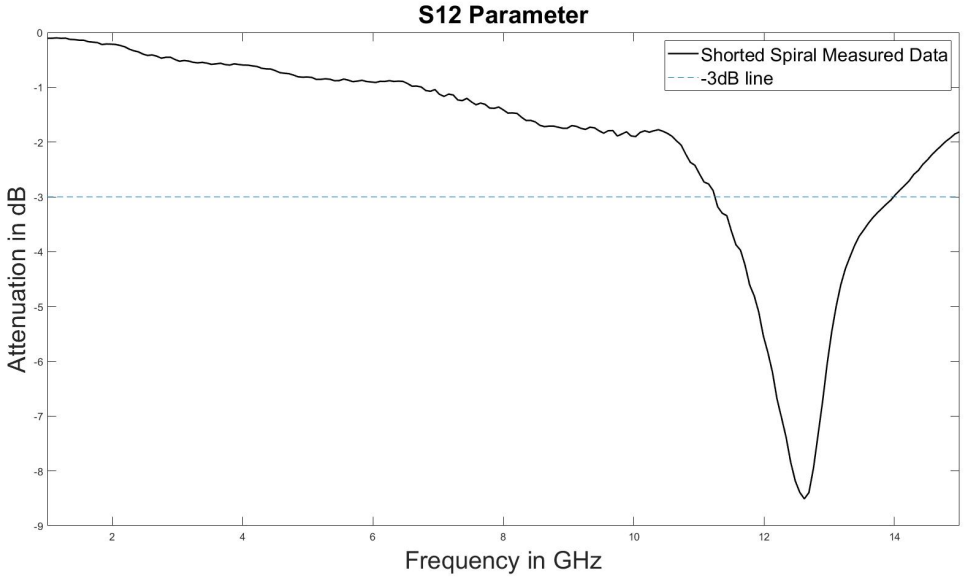

Figure 5.7: S_{12} paramter of the multi-ressonant circuit with the spiral shorted to the transmission line.

5.3 Parametric Analysis

The spiral resonator has four parameters that influence its frequency response: the spacing between arms "s", the width of each arm "w", the length of the spiral "L_{spiral}", and the distance to the transmission line "D_{Gap}". The width of the spiral is a consequence of all other parameters and of the fact that the number of turns of the spiral n is 2.25 ,which will be kept constant throughout this work. In order to observe the impact of the variation of these parameters, a parametric study of the S_{12} parameter was conducted by varying each parameter independently. The reference design is the above depicted and all other parameters without being the one being varied will be kept constant and have the value specified in Table 5.1. Additionally, the default length of the spiral will be 5 mm.

The first parameter studied was the distance between the spiral resonator and the transmission line "D_{Gap}". The value of D_{Gap} was varied between 0.1 mm and 0.8 mm. The first three resonant frequencies within the 1 to 15 GHz spectrum and the value of the attenuation at the resonant frequency were obtained, and are depicted in Figure 5.8. From the results obtained, it's clear that the variation of D_{Gap} doesn't have a significant effect in the first three resonant frequencies of the spiral resonator - it only causes a average deviation approximately of 60 MHz of the resonant peak when compared with the one from Figure 5.1. On the other hand, it has a considerable impact on the attenuation of the referred frequencies. For the first and second resonant frequencies, the attenuations decrease in what appears to be an exponential-like behaviour, the third resonant frequency, however, doesn't appear to have a defined predictable behaviour showing only a slight tendency to decrease.

The second parameter studied was the width of each arm "w" of the spiral resonator. The value of w was varied between 0.1 mm and 0.8 mm. The first three resonant frequencies within the 1 to 15 GHz spectrum and the value of the attenuation at the resonant frequency were obtained and are depicted in Figure 5.9. Once again, like the D_{Gap} parameter, the width of

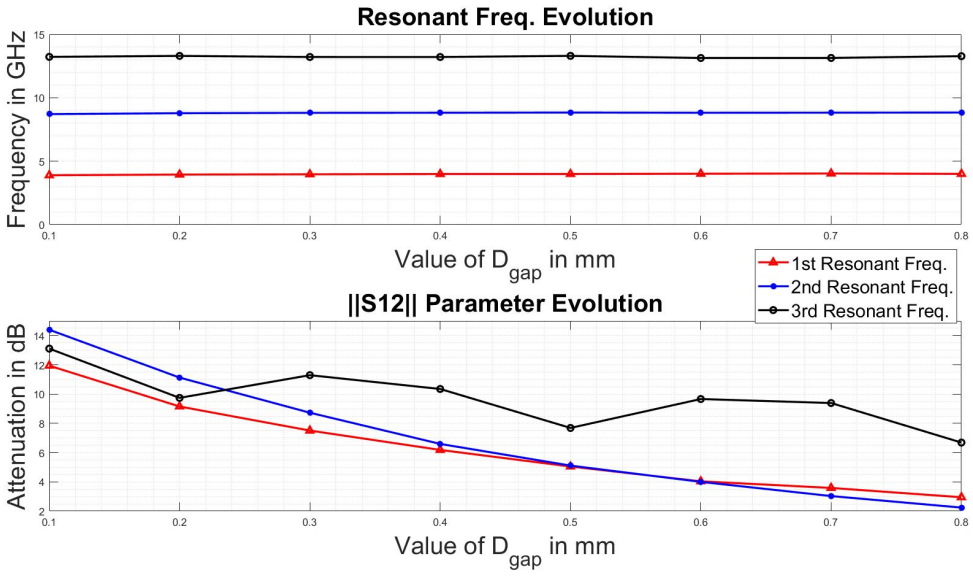

Figure 5.8: Resonant frequency and $||S_{12}||$ parameter evolution with the increase of the distance between a spiral resonator and the transmission line D_{Gap} (all other parameters are presented on Table 5.1).

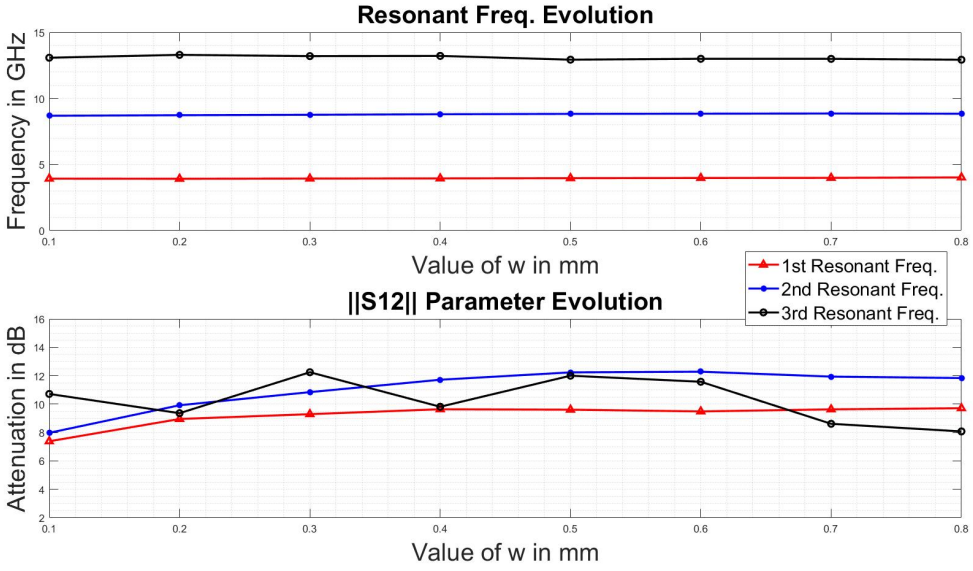

Figure 5.9: Resonant frequency and $||S_{12}||$ parameter evolution with the increase of the width of each arm w of the spiral resonator (all other parameters are presented on Table 5.1).

---

the spirals arms "w" doesn't have a significant influence on the resonant frequencies of the circuit, causing an average deviation of approximately 100 MHz, nevertheless, it has bigger influence than the D_{Gap} parameter had. The attenuation of the first and second resonant frequencies increase with a logarithmic-like behaviour whereas the third resonant frequency

appears to oscillate in attenuation around 10 dB line within a ±2dB amplitude.

While varying the spacing between arms of the spacing between arms of a the spiral resonator "s", from 0.1 mm to 0.8 mm, the first three resonant frequencies within the 1 to 15 GHz spectrum and the value of the attenuation at the resonant frequency were obtained and are depicted in Figure 5.10.

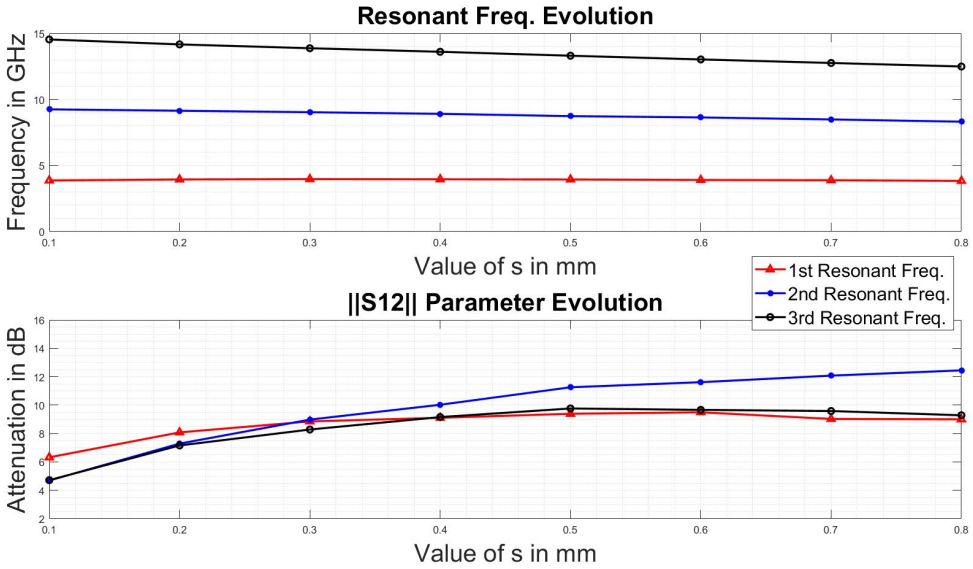

Figure 5.10: Resonant frequency and $||S_{12}||$ parameter evolution with the increase of the spacing between arms of a spiral resonator s (all other parameters are presented on Table 5.1).

Regarding the resonant frequencies, the mean deviation is around 300 MHz is observed. However, the third frequency alone presents a mean deviation of 570 MHz to the values obtained in Figure 5.1. The attenuation at those frequencies increases in what appears to be a logarithmic-like fashion and it's clear that the attenuation value is strongly related with the spacing between arms as the attenuation values have considerable variation with this parameter.

Lastly, the length of the spiral "l" was varied between 1 and 15 mm. Data was collected regarding the first four resonant frequencies, when present, and their respective attenuations. The results obtained are depicted in Figure 5.11.

The results show that the number of resonant frequencies within the analysed spectrum depend on the length of the spiral: larger spirals may have more resonant frequencies. These variations of the resonant frequencies show a great correlation with the variation of the spiral length. For lower values of the spiral length, small variation of the length of the spiral corresponds to considerable variation of the resonant frequencies and higher order resonant frequencies are more sensitive to said variations. The attenuation behaves differently depending on the resonant frequency order: the first resonant frequency has the more stable attenuation value with the increase of the spiral length, the second and third resonant frequency lower their attenuation value with a lower rate when compared to the fourth resonant frequency.

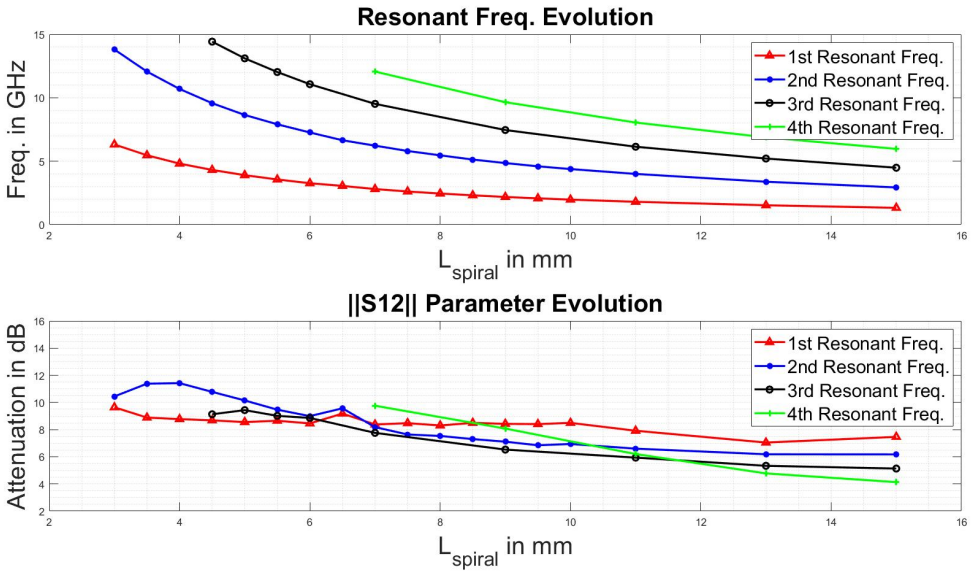

Figure 5.11: Resonant frequency and $||S_{12}||$ parameter evolution with the increase of the spacing between arms of a spiral resonator s (all other parameters are presented on Table 5.1).

5.4 Design Curves Extraction

The performed parametric analysis sheds light on several important points that help to define the multi-resonant circuit behaviour. The first point that is worth noting from the obtained results is that, contrary to what the existing literature indicates, each spiral may cause the appearance of more than one resonant frequency, influencing in this way the frequency response of the circuit. This fact has serious repercussions in the circuit design phase: with the existence of multiple resonant frequencies associated to each spiral, information can be wrongly encoded due to attenuations in the frequency band of interest due to secondary resonances that were not previously accounted for. This new realization is even more important for the fact that is the length of spiral that mainly defines the resonant frequencies of the circuit (all other parameters have an almost negligible contribution to the definition of the resonant frequency) and thus this is the "go-to" parameter when it comes to tuning the circuit.

Because of this, designers must have special care: if they want to work in a continuous frequency range they must select a resonant frequency to work with and a frequency range or a range of lengths of the spiral where no other resonant frequency interferes. This confines the design of spiral resonators to a certain range of length and the usability of the circuit to a certain range of frequencies, which greatly reduces the operating viability of the circuit. Additionally, the designer must account with the 3 dB bandwidth of each resonant peak as it's this bandwidth that ultimately defines the number of bits that one is able to code in a certain frequency range.

The results attained from Figure 5.11 also hint that the evolution of the resonant frequencies, regarding to the length of the spiral, can be accurately described by exponential curves. This means that designers can easily design circuits and spirals to have a specific frequency

response. The author fitted the data point using exponential curves in the form of:

$$f_r = a * exp(b * L_{spiral}) + c * exp(d * L_{spiral}) \tag{5.1}$$

where the constants a, b, c and d are unique for each resonant order and f_r is in GHz, using Matlab. The coefficients obtained for each curve are displayed in Table 5.2.

Table 5.2: Coefficient List

Coefficients	**1st Res. Freq.**	**2nd Res. Freq.**	**3rd Res. Freq.**	**4th Res. Freq.**
a	13.78	28.04	33.47	32.55
b	-0.5032	-0.4657	-0.3878	-0.365
c	4.084	8.496	11.44	14.67
d	-0.07683	-0.07218	-0.06382	-0.06146

The extracted coefficients were used to compute the curves of Figure 5.12. As we can see, these curves fit the data points appropriately which means that one can infer the circuit resonant frequency from the spiral length with a high degree of confidence. Bear in mind that these equations are valid only for the set of design parameters establish in Table 5.1 although the procedure is easily extended to all variations of those parameters.

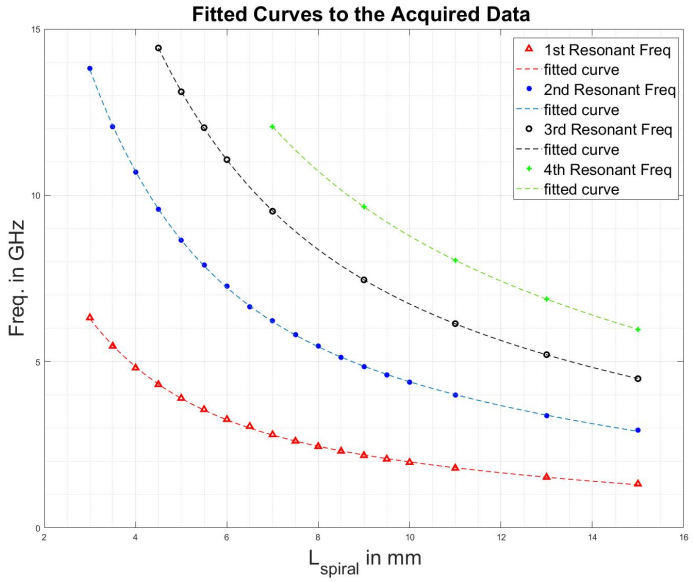

Figure 5.12: Fitted curves in the form of $f_r = a*exp(b*L_{spiral})+c*exp(d*L_{spiral})$, contrasting with the simulated data.

These equations constitute a very simple and intuitive model that relates the circuit's resonant frequency with a physical parameter: the length of the resonant spiral, thus greatly aiding designers in the until now time-consuming and hard task of designing multi-resonant circuits. They can be treated as the first tool used to tuned spiral resonators performing a more careful tuning using a simulator, thus saving precious time to the designer. To the author knowledge, this is the first time that work of this type is done on this topic.

5.5 Multi-Resonant Circuit Synthesis

In order to test the validity of the above equations, a double spiral circuit was projected. The goal was to encode two bits in 1.5 to 3.5 GHz band using 2GHz and 3GHz as the bit frequencies. For that proposed, using the curves from Figure 5.12, only the first resonant mode can be used. Using the equation in the form of $f_r = a * exp(b * L_{spiral}) + c * exp(d * L_{spiral})$ and the parameters extracted for that equation, the length of the spirals was computed. The length of the spiral that resonates at 2 GHz is $L_{spiral\ 1} = 9.92\ mm$ and the one resonating at 3 GHz is $L_{spiral\ 2} = 6.50\ mm$. The spacing between the adjacent spiral is of 4 mm in order to avoid unwanted coupling between the spirals, all other parameters are the ones of Table 5.1. The printed and tested circuit is depicted in Figure 5.13.

Figure 5.13: Image of the printed Multi-Resonant circuit with two resonant spiral projected to resonate at 2 GHz and 3 GHz respectively, on a Rogers RO4725JXR substrate.

The circuit's S-Parameters within the 1 to 15 GHz frequency band were extracted using an Agilent Technologies's PNA-X Network Analyser and then compared to the results from the CST. Such results are shown in Figure 5.14.

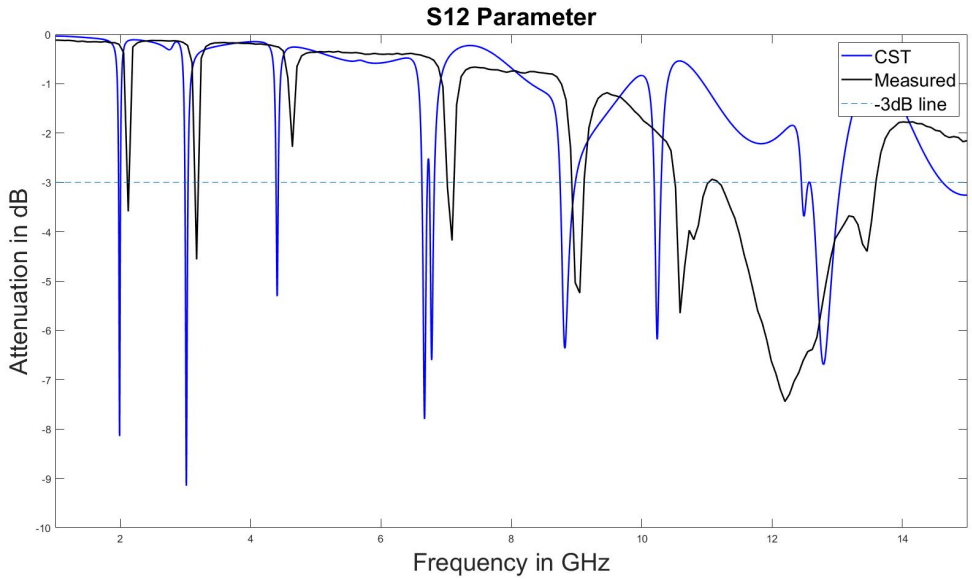

Figure 5.14: S_{12} parameter from the measured multi-resonant circuit with two resonant spirals and the corresponding simulated results from CST.

The curves from Figure 5.14 show a relatively good agreement in terms of frequency between the simulated and measured S_{12} parameter until the 10 GHz mark. As noted above, the CST's attenuation value is not accurate. Data from the first two resonant peaks is summarised in Table 5.3.

Table 5.3: Data from the double resonant spiral multi-resonant circuit frequency response.

	CST	**Measured**	**Difference**
Resonant Peak		**1st**	
Frequency in GHz	1.99	2.12	0.13
Attenuation in dB	8.14	3.58	4.56
Resonant Peak		**2nd**	
Frequency in GHz	3.01	3.17	0.16
Attenuation in dB	9.15	4.56	4.58

The first thing noticed is that the first resonant peak differs in 120 MHz from the desired resonant frequency and the second resonant peak is shifted 170 MHz, values that are easily acceptable. Between the measured and simulated data, the resonant frequency differs in less than 200 MHz - a tolerable value, whereas the attenuation differs in around 4.50 dB proving once again that CST is not suited to provide a good estimative of the attenuation value.

This validates the utility of the proposed design equations as a mean to provide a first value of the spiral length to resonate at a predetermined frequency. Bear in mind that these equations do not account with undesired coupling between adjacent spirals and do not provide any information about the attenuation value at each resonant peak.

Chapter 6

Chipless RFID System Simulation

6.1 Introduction

In the preceding chapter, the multi-resonant circuit was studied. A simple model capable of describing the behaviour of the multiple resonant-modes of the multi-resonant circuit as function of the length of the spiral was proposed and validated through comparison with measured data. This model allows an easy and fast primary design of the circuit. With this model proposed and validated, it is possible to project a way to correctly recover the ID information from the tags. The collision of tag's responses is the main cause of problems in RFID systems as they make challenging the information recovery process. This fact is even more exacerbated in the chipless RFID systems.

As previously mentioned, the chipless RFID systems are more similar to RADAR systems than to the typical RFID systems. Similarly to RADAR targets, the chipless RFID tags backscatter the interrogation signal to the surrounding space. The reader's antenna captures a portion of that backscatter signal and analyses its spectrum to find the resonance information that encodes the tag's ID. Because several tags share the same interrogation zone, collisions among backscatter signals occurs. An example of a chipless RFID system is depicted in Figure 6.1.

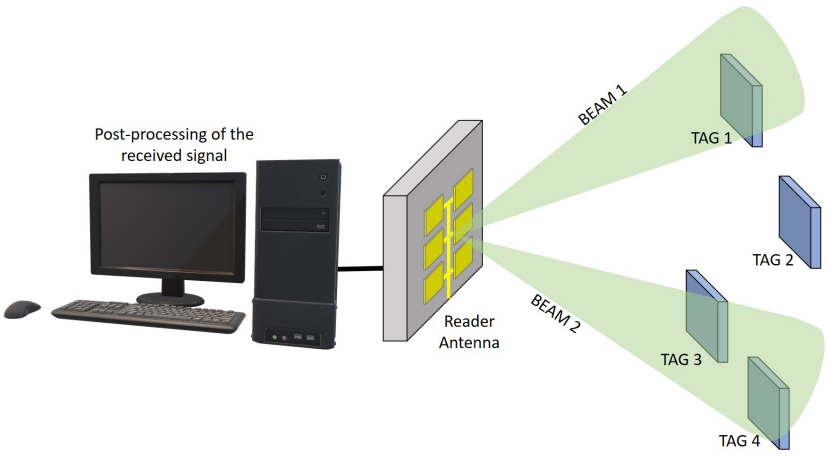

Figure 6.1: Chipless RFID system scheme.

In this example, four tags share the same interrogation zone. The reader uses a narrow-beam antenna with beam steering capabilities to try to isolate tags in its reading range. This works for the case of TAG 1, however, TAG 3 and 4 fall in the same beam which will cause a collision between both backscattered signals. The spatial filtering implemented by having narrow-beam antennas minimizes collision but isn't fully capable of avoiding it. Thus spacial-filtering alone is not enough to guarantee the correct decoding of each tag ID, this problem must be addressed from the signal processing point of view.

All tags in the same interrogation zone backscatter the same interrogation signal, encoding each different information in the same frequency band. Hence, the collision occurs both in the time and frequency domain which in turn means that neither time-domain windowing nor frequency-domain filtering will be capable of separating the colliding signals. However, because the tags may be at different distances from the reader, there may be a time difference of arrival (TDOA) among the response signals from multiple tags. This means that resonances may occur at different time instances but at the same frequency and if so, it's possible to distinguish between responses from several different tags in the *t-f* plane.

The signals used to interrogate the tags are Linear Frequency Modulated (LFM) signals. These signals increase in frequency linearly with time, which means that their frequency spectrum will be constant within the starting and stopping frequency, as can be seen in Figure 6.2.

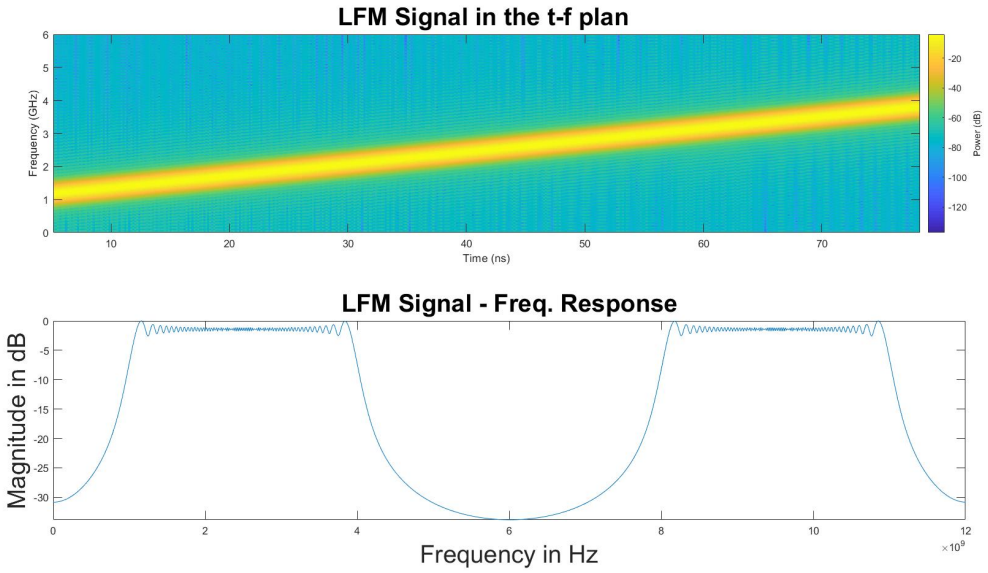

Figure 6.2: Above: Spectrogram of a linear chirp. The spectrogram plot demonstrates the linear rate of change in frequency as a function of time. The intensity of the plot is proportional to the energy content in the signal at the indicated frequency and time. Bellow: frequency response of the signal.

Different types of *t-f* analysis method such as the Fourier Transform, Wigned Distribution, the Ambiguity Function, the Short-Time Fourier Transform (STFT), the Spectrogram and the fractional Fourier Transform are often used in speech processing, radar or quantum physics for time-varying signals [59]. It has been found that FrFT suffers less from cross terms than

STFT and also provides compact support for LFM signals [60] so, the FrFT was used in this work with the goal to retrieve individual tags ID from colliding signals.

In this section, a chipless RFID system is simulated using *Matlab*. The tags frequency response is emulated by FIR filters based on practical measurements obtained. An FrFT algorithm is implemented in order to extract individual IDs from colliding signals. The implementation, results and considerations of this system are presented and discussed.

6.2 Background Theory

Before explaining in detail the system, the mathematical representation of the LFM signal and the FrFT theoretical basis are required.

6.2.1 Linear Frequency Modulated Signal

LFM signals are usually designated by chirps and so, both designations will be used through this chapter. The LFM signal is mathematically defined by Equation 6.1:

$$x(t) = \begin{cases} e^{(j2\pi)\left[\frac{B}{2T}t^2 + \left(f_c - \frac{B}{2}\right)t\right]} \text{ , } 0 \leq t \leq T \\ 0 \text{ , otherwise} \end{cases} \tag{6.1}$$

where B is the total bandwidth of the signal, T is the duration of the signal and f_c is the center frequency of sweep. The rate of which the frequency changes is called the chirp rate and is defined by Equation 6.2:

$$\alpha = \frac{B}{T} \tag{6.2}$$

The LFM signal is not narrowband, but because its instantaneous phase is differentiable, its instantaneous frequency can be interpret as the dominant frequency at each instant in time, thus allowing the use of the formula for the instantaneous frequency of a narrow-band signal [61] represented in Equation 6.3.

$$f_i(t) = \frac{1}{2\pi}\phi'(t) \tag{6.3}$$

where $\phi(t)$ is the instantaneous phase of the signal. Combining Equations 6.1 and 6.3 one can confirm the linear relationship between frequency and time of the chirp signal - Equation 6.4.

$$f_i(t) = \frac{d}{dt}\left(\frac{B}{2T}t^2 + \left(f_c - \frac{B}{2}\right)t\right) = \frac{B}{T}t + f_c - \frac{B}{2} \tag{6.4}$$

6.2.2 Fractional Fourier Transform

Whereas the traditional Fourier Transform allows signals in the time domain to be transformed to the frequency domain and vice-versa, the Fractional Fourier Transform transforms signals to a fractional domain. This fractional domain has no physical meaning, as it is neither time nor frequency but an intermediate domain between them. The Fractional Fourier

Transform can be considered as a generalization of the Fourier Transform [59]. The definition of $f(t)$ in FrFT domain is given by Equation 6.5:

$$f_p(t) = \int_{-\infty}^{\infty} f(t)K(\alpha; u; t)dt \tag{6.5}$$

where p is the order of the FrFT and α is the rotational angle between the time axis and the FrFT axis. The FrFT can be interpreted as a rotation of the *t-f* plane of a signal by α creating a *t-f* mapping of the signal whose frequency varies with time - Figure 6.3.

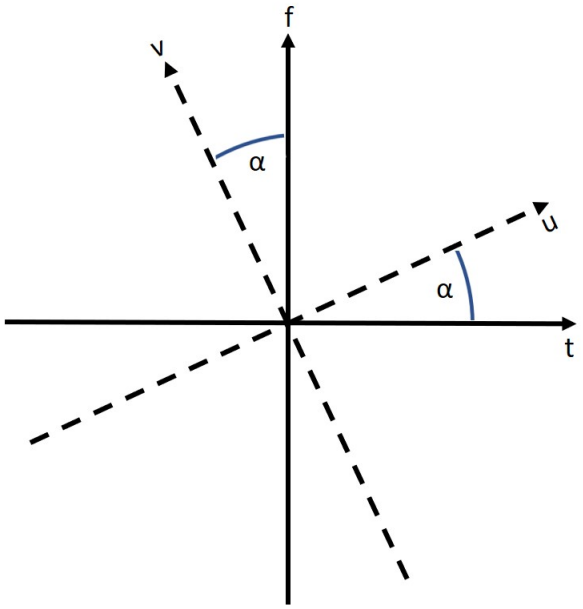

Figure 6.3: Rotation of the t-f plane through FrFT.

The rotational angle α can be related to the order of the transform through Equation 6.6:

$$p = \frac{2}{\pi}\alpha \tag{6.6}$$

α is valid in the interval from $[-\pi, \pi]$ an p is valid in the interval from $[-2, 2]$. Some transform orders are interesting as the result of the FrFT is identical to certain mathematical transforms commonly used: when p is equal to 0 ($\alpha = 0$) the result is identical to the time domain signal; when p is equal to 1 ($\alpha = \frac{\pi}{2}$) the result is equal to the Fourier Transform; when p is equal to -1 ($\alpha = -\frac{\pi}{2}$) the result is equal to the inverse Fourier Transform.

The kernel $K(\alpha; u; t)$ is defined as in Equation 6.7:

$$K(\alpha; u; t) = \sqrt{\frac{1 - i\cot(\alpha)}{2\pi}} e^{\left[i\left(\frac{u^2+t^2}{2}\cot(\alpha) - ut\operatorname{cse}(\alpha)\right)\right]} \tag{6.7}$$

The FrFT is a very complex and hard to understand technique, that in itself, is a topic more than sufficient to write a dissertation. So in order to better comprehend it and to keep it simple this work will rely more on visual guidance in order to both understand and achieve the goals proposed.

6.3 FrFT for Multiple Overlapping Signal Separation

The rotation of the *t-f* plane means that there is an order of transformation where the chirp signal is compacted even if the chirp is neither compact in the time nor in the frequency domain. It's this fact that allows the recovery of multiple overlapping signals as their compact form do not overlap in the fractional domain thus, by windowing each signal in this domain and perform the inverse process it is possible to recover each individual signal without changing its characteristics.

The FrFT Matlab algorithm used in this work is described in [62]. The algorithm receives samples of the signal and the order of transformation to be performed "p" and outputs the fast Fractional Fourier transform of the input signal. The transformation is done in four steps:

1. Chirp Pre-Multiplication;
2. Chirp Convolution;
3. Chirp Post-Multiplication
4. Normalizing Constant;

The optimum order of transformation "p_{opt}" is the one required to maximally separate the individual LFM signals, or in other words, the transformation order that achieves higher rates of compactness of the individual signals in the fractional domain. As the rate of change of frequency df/dt of each signal defines the rotation of the individual LFM signals within the *t-f* plane, p_{opt} is defined as [63]:

$$p_{opt} = \frac{2}{\pi}\alpha = -\frac{2}{\pi}\tan^{-1}\left(\frac{1}{2\mathrm{a}}\right) \tag{6.8}$$

where $a = B/T$ is the chirp rate, B is the bandwidth in hertz, and T is the total signal duration is seconds. However, as the input signal is time-sampled calculation of p_{opt} requires knowledge of time and frequency resolution of the system:

$$p_{opt\ (discrete)} = -\frac{2}{\pi}\tan^{-1}\left(\frac{df/dt}{2\mathrm{a}}\right) \tag{6.9}$$

where $df = f_s/N$ and $dt = 1/f_s$, thus,

$$p_{opt\ (discrete)} = -\frac{2}{\pi}\tan^{-1}\left(\frac{f_s^2/N}{2\mathrm{a}}\right) \tag{6.10}$$

6.4 System Description and Implementation

In order to test the viability of using a FrFT algorithm to recover the ID information of tags sharing the same interrogation zone, a Chipless RFID System was simulated in *Matlab*. The system simulates the transmission of a LFM signal from the reader to two tags with different distances from the reader, the encoding of their ID in the signal, the corresponding backscattered signal of each tag, the received signal composed of the overlap of the two backscatter signals and the extraction of the both tags' ID from that signal. The equivalent implemented system is displayed in Figure 6.4. It does not account for any loss of power in the propagation of the signals, the existence of noise and assumes that the receiving and

transmitting antenna are orthogonal thus not existing collision between the transmitted and received signal in the tag and reader.

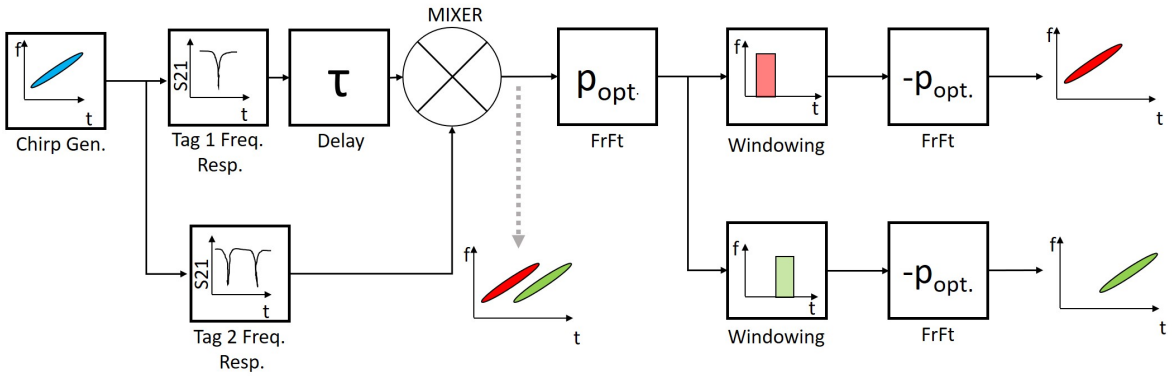

Figure 6.4: Block diagram of the simulated Chipless RFID System.

First, a chirp signal is generated, emulating an interrogation signal created from a reader. This signal is then captured by both tags that encode their unique ID by removing certain frequencies of the signal. The signal from one of the tags is then delayed simulating a scenario where tags are not at the same distance from the reader, and thus, one of the backscatters signals will arrive later. The signals are then mixed together simulating the interference that may occur when the tags share the same interrogation zone. The ouput signal from the mixer is the one received by the reader that will start an algorithm to extract both tags' unique ID. This is achieved by performing the FrFT algorithm with an order of transformation p_{opt} and then isolating each signal with rectangular windows. The opposite process is then made in order to fully recover the original signals. The system was fully simulated in *MATLAB*. To fully understand this process the implementations and results will be given step by step in the following subsections.

6.4.1 Chirp Generator

The band of interest was defined from 1 to 4 GHz and the coding frequencies as 2, 2.5 and 3 GHz. As such, an LFM signal was generated occupying the 1 to 4 GHz band and with a duration of 83.25 ns. This signal is called interrogation signal and is depicted in Figure 6.5. It's over this signal that the tags' ID information will be encoded.

6.4.2 Digital Filter Synthesis

Most of the work performed uses simulated multi-resonant circuits responses in order to approximate their real behaviour. However, since two multi-resonant circuits were already designed we will make use of those results. Real measured data was used, however, in order to facilitate the integration of the data with *MATLAB* two FIR digital filters were implemented approximating the measured data from the tags. The comparations between the measured data and the synthesised equivalent filters are depicted in Figure 6.6.

As we can see, there is a good agreement between the measured data from the multi-resonant circuits and the simulated one from the FIR filters.

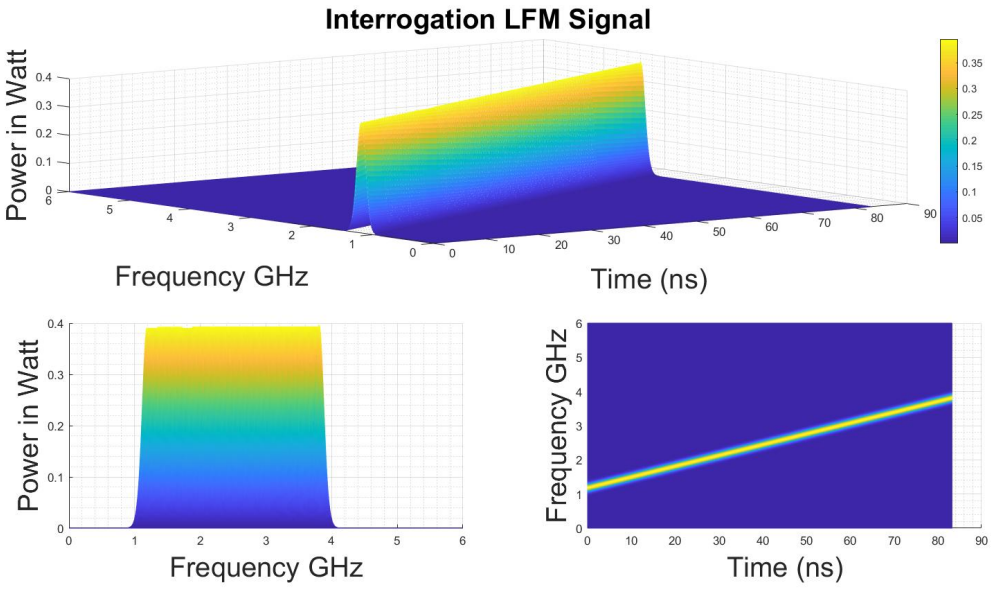

Figure 6.5: Interrogation Signal Spectrogram.

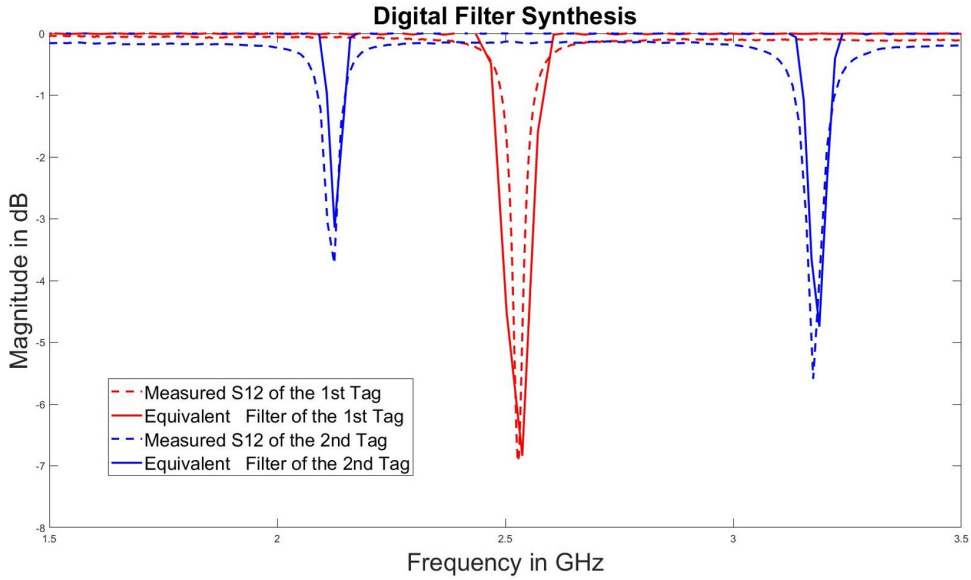

Figure 6.6: Multi-resonant circuit S12 parameter versus the synthesised FIR filters frequency response.

6.4.3 Data Encoding

The data is encoded by convulsing the LFM interrogation signal with the filters responses. This procedure is done individually for each tag and the results are depicted in Figure 6.7 and 6.8.

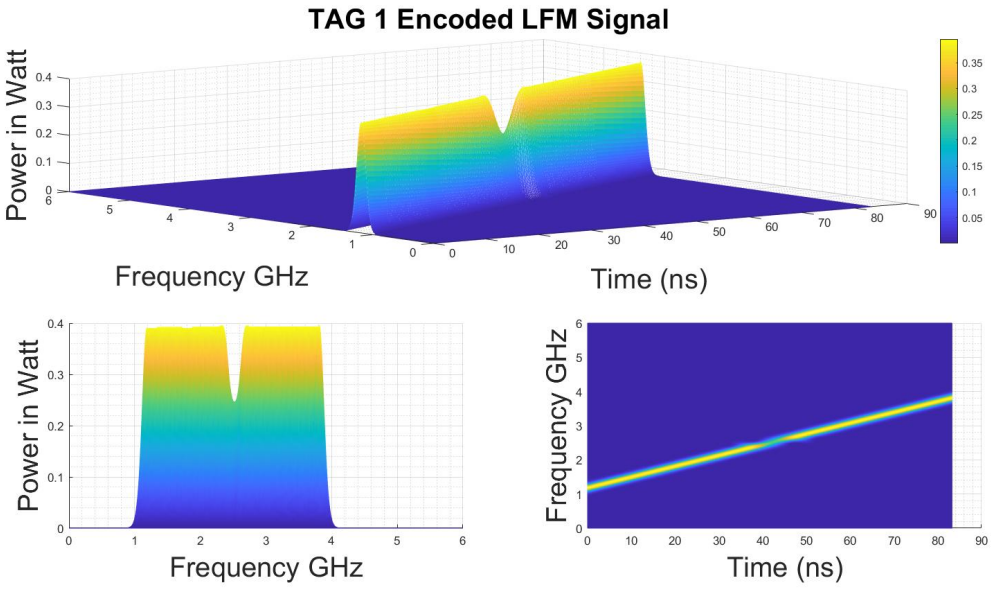

Figure 6.7: Tag 1 encoded LFM Signal Spectrogram.

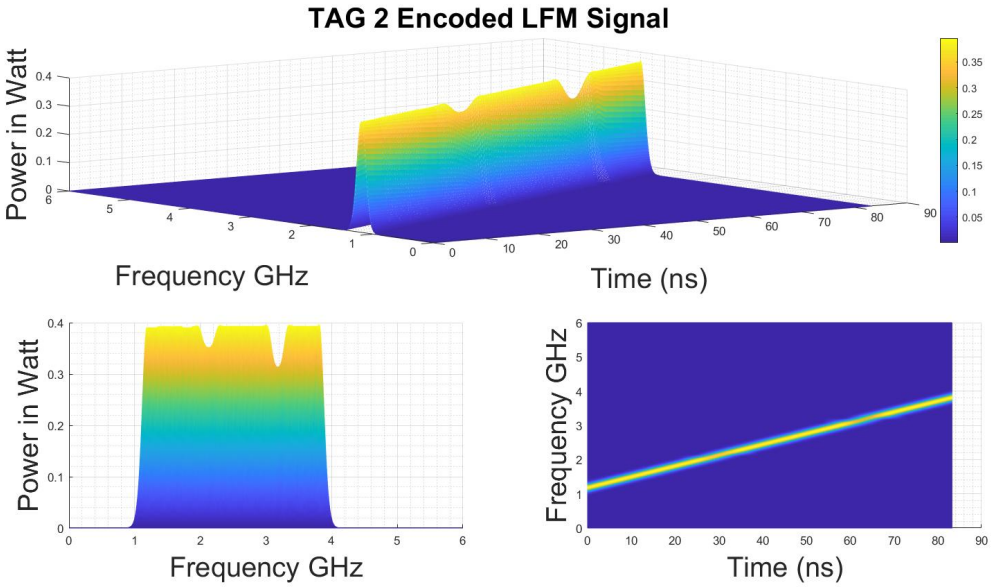

Figure 6.8: Tag 2 encoded LFM Signal Spectrogram.

6.4.4 Mixing

The encoded LFM signal from tag 2 is delayed 40 ns and mixed together with the encoded LFM signal from tag 1. The resulting signal is the one depicted in Figure 6.9.

From its spectrogram it's evident that the signals are not distinguishable neither in the time domain nor in the frequency domain.

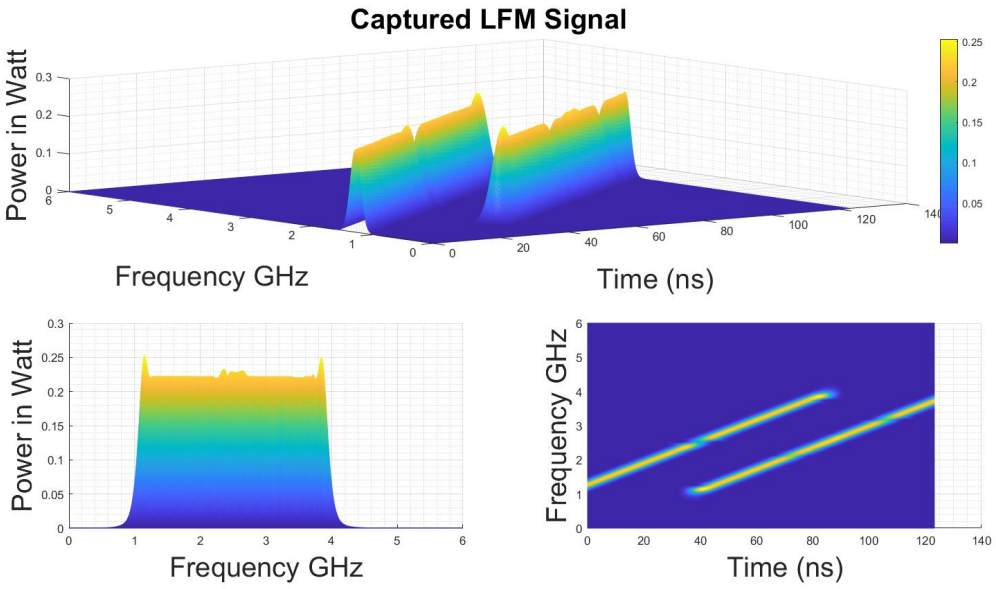

Figure 6.9: Mixed Signal Spectrogram.

6.4.5 FrFT and Windowing

The mixed signal is then fed through the FrFT algorithm. However, neither equations 6.10 and 6.8 computed the value of p_{opt} that most compacted the LFM signals. Perceiving this, and in order to keep the implemented solution simple, a quick iterative program was written allowing us to view the mixed signal in the fractional domain while varying the value of p_{opt}. The value that maximized the compaction of the encoded LFM signals within the mixed signal is $p_{opt} = -0.223$. Figure 6.10 shows clearly the compaction of the LFM signals in the fractional domain.

The windowing of each signal was done using rectangular windows and conserving 50 samples to each side of the two points of maximum power along the u axis. All other samples outside the rectangular window were considered 0.

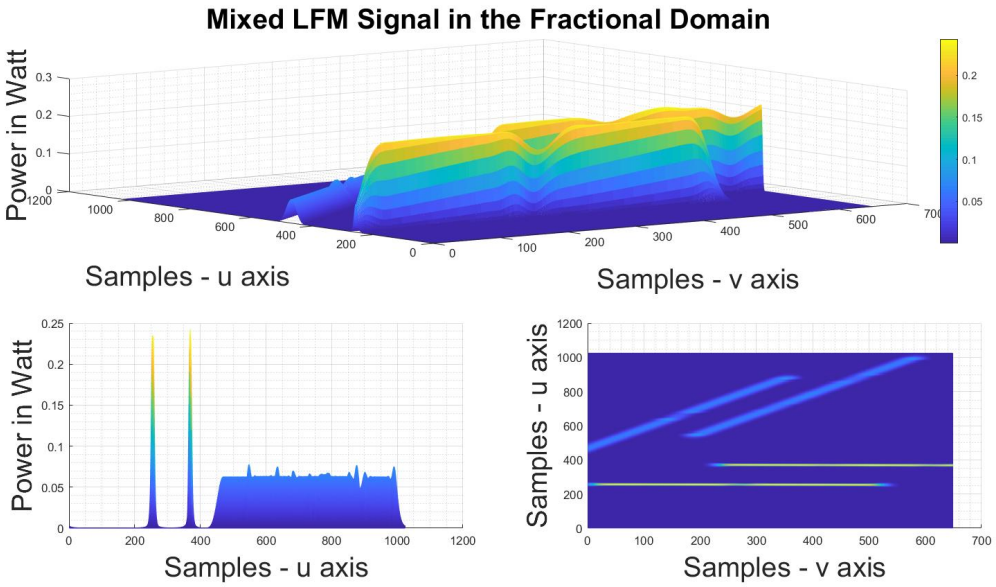

Figure 6.10: Mixed LFM Signal in the fractional domain Spectrogram.

6.4.6 Signal Recovery

In order to retrieve the windowed signals to the t-f plan, each signal goes through an FrFT with $p = -p_{opt} = 0.223$ reversing the signals to their original domain. The recovered signal spectrogram for both tag 1 and 2 are depicted in Figure 6.11 and 6.12 respectively.

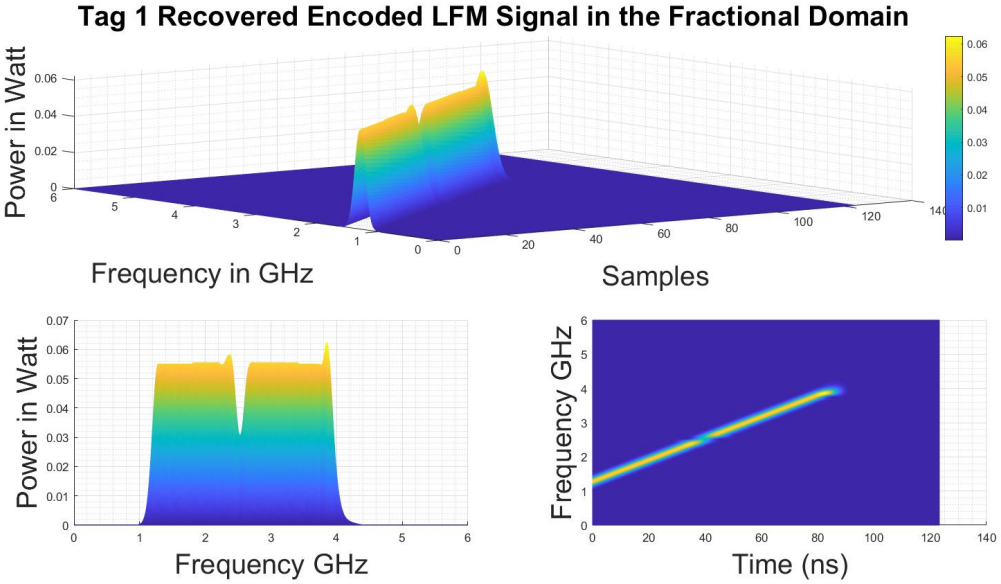

Figure 6.11: Tag 1 Recovered encoded LFM Signal Spectrogram

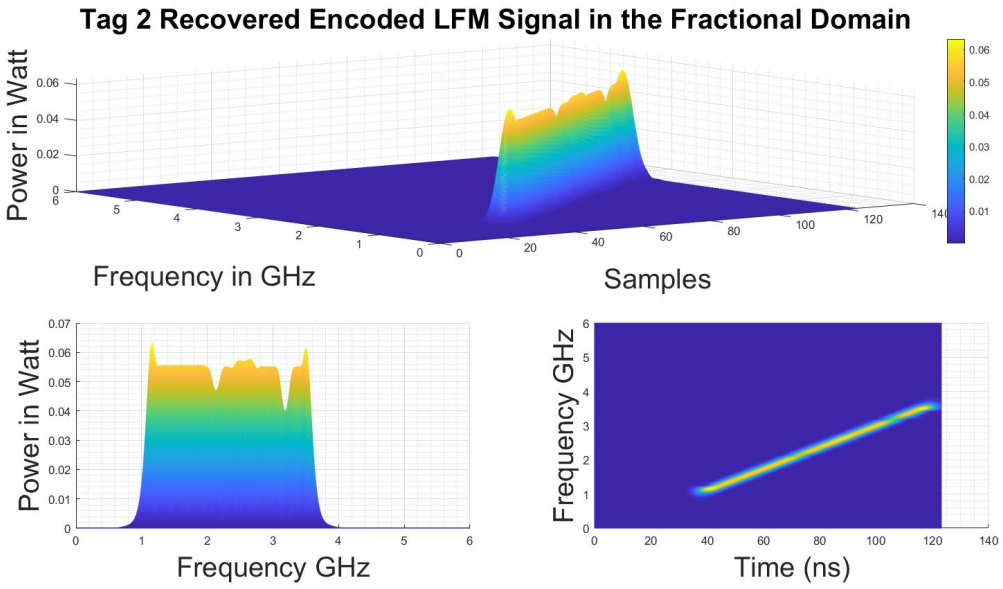

Figure 6.12: Tag 2 Recovered encoded LFM Signal Spectrogram.

6.5 Result Analysis

The recovered signals conserved relatively well both the time and frequency original information. Table 6.1 summarises the results obtained with the simulation of the implemented chipless RFID system using FrFT. From these results, we can see that the maximum deviation between the original resonant frequencies and the decoded one is 24 MHz which is an acceptable value. However, the original signals had around 0.4 Watt within the 1 to 4 GHz band, that is a value considerably greater than the 0.055 watt within the 1 to 4 GHz band of the recovered signal - about 13.75% of the original power value. This is in part due to the power lost by performing the windowing of each peak represented in Figure 6.10 thus losing the power contained between sample 400 and 1000.

The automation of this method is yet a challenge as several critical points in this process become hard to fully predict. The number of backscattered signal within the received signal is evaluated by the number of peaks that the compact version of the signal has in the fractional domain. This peaks become clear and easy to identify if the signals are distanced enough in time, however, if the delay between signals is very small the rotation of the *t-f* plane is not always fully capable of removing the interference from other tags' response signal, which means that secondary peaks may form. These peaks may wrongly be interpreted as additional backscattered signals contained in the received signal. Additionally, the computation of the optimum order of transformation p_{opt} is yet done by visual interaction although some authors use the aforementioned equations.

This method has successfully extracted individual tag response signals from the collided signal. Furthermore, the ID of each tag was successfully retrieved, proving that the *t-f* analysis method can be successfully used for multiple tag identification for chipless RFID tags. In a environment with more than two tags, the same method can be applied by isolating one signal from all the others and then repeating this process until every signal is isolated.

Table 6.1: Results from implemented the simulated chipless RFID system.

	Original Tag 1 Signal	**Recovered Tag 1 Signal**	**Original Tag 2 Signal**		**Recovered Tag 2 Signal**	
Ressonant Frequency (GHz)	2.552	2.528	2.129	3.173	2.129	3.185
Power (Watt)	0.25	0.03	0.35	0.31	0.05	0.04
Time (ns)	42.58	39.18	28.84	62.91	72.47	105.9
	||Difference||		**||Difference||**			
Ressonant Frequency (GHz)	0.024		0		0.012	
Power (Watt)	0.22		0.30		0.27	
Time (ns)	3.4		26.37		42.99	

Chapter 7

Conclusions and Future Work

7.1 Conclusions

The main objectives proposed for this dissertation were achieved. This work not only used state of the art techniques but also provided new knowledge promoting the advance of this technology in the scientific community.

The problems with the RFID technology in penetrating the labelling market were highlighted as well as the motivation and motives behind the uprising of the chipless RFID technology. The state of the art was presented, providing an overlook of the advances made in the last era within this topic.

The main problem behind the Multi-resonator-based Chipless RFID Tags was presented focusing on the lack of models capable of accurately describing the multi-resonant circuit. This issue was addressed in depth by presenting its working principle, the advances made in the modelling of this circuit and by providing an answer to this problem. In order to reach the proposed answer, three models were developed using two different simulating software and then compared with the S-Parameters measured from a printed multi-resonant circuit. From these models, the one that better simulated the measured data was selected in order to simulate the circuit's frequency behaviour by varying several physical lengths of the spiral resonator that constitute it. The results clearly show that the resonant frequencies of the circuit are mainly defined by the length of the spirals, and as such, an equation that relates the length of the spirals with the multi-resonant circuit resonant frequencies was proposed, based on the interpolation of the data simulated. The proposed equation is only usable if all other variables are the ones fixed in this dissertation, however, the methodology used to derive the proposed equation is transversal to all other sets of variables and thus, not only the presented equation has value but the procedure as well. The proposed equation was then validated by designing a multi-resonant circuit using said equation and then comparing the simulated frequency response with the measured one. The results from the simulation show a tolerable deviation from the measured ones. As this equation serves mainly as a first approach to the tag design, the deviation obtained is tolerable as it can be easily tuned by slightly modifying the spiral length. Although data is presented between 1 to 15 GHz, from 9 to 15 GHz the measured data is not reliable due to a non-expected behaviour of the multi-resonant circuit was observed. The tests performed indicate that this problem is not due to the design of the circuit but to an external parameter related to the construction of the circuit - like the connectors or the substrate. However, this doesn't affect the work performed. Part

of this work was presented in the *YEF-ECE 2019 - 3rd International Young Engineers Forum on Electrical and Computer Engineering conference* as an accepted paper. A more complete paper on the subject was also submitted to the *RFID-TA 2019 - 2019 IEEE International Conference on RFID Technology and Applications*, and is, at the time of write, waiting for approval.

Lastly, a chipless RFID system was simulated. One of the main struggles with chipless RFID systems is implementing an algorithm/technique capable of retrieving the ID information from individual tags from a signal containing multiple tags' backscattered signals. These signals collide both in the time and frequency domains thus making most signal processing techniques useless. In order to overcome this problem, the fractional Fourier Transform is presented as a form of analysing and manipulating the time-frequency plane where multiple signals are distinguishable. The FrFT is analysed and then implemented as part of the chipless RFID system. This system uses FIR filters to accurately emulate the responses of two multi-resonant circuits printed and measured. It does not account with noise, loss in power due to the propagation of the waves and any problem related to antennas. The results are very positive and promising as the ID from both tags was retrieved successfully. Part of this work was submitted to the *SBMO/IEEE MTT-S International Microwave and Optoelectronics Conference (IMOC)*, and is, at the time of write, waiting for approval.

This dissertation tackles a very important and current topic both from the scientific and industry point of view. It gives a clear contribution to the advance of this subject as well as performing important groundwork that can serve as a basis for further improvements.

7.2 Future Work

For future work, it would be interesting to further test the behaviour of the multi-resonant circuit. The printing of the circuit on a non-conventional substrate like plastic should be investigated as the final goal is to apply it to cheap market products. The study of the impact of the antennas should be looked into as it's an important part of the chipless RFID tag.

Regarding the simulated system, it would be interesting to account with antennas and losses of power on a very dense interrogation zone where tags are randomly scatted. A solution to the shadowing effect that can occur is also of great research importance. Lastly, the implementation of the system should be done, thus providing important data to the further improvement of each part of the system, contributing in this way to the upcoming of the chipless RFID technology as a reliable barcode replacement.

Bibliography

[1] K. Finkenzeller, *RFID Handbook: Fundamentals and Applications in Contactless Smart Cards and Identification*. Wiley, 2003.

[2] Wikipedia contributors, "Barcode — Wikipedia, the free encyclopedia." `https://en.wikipedia.org/w/index.php?title=Barcode&oldid=846826829`, 2018. [Online; accessed 21-June-2018].

[3] Stratistics, "Barcode scanner - global market outlook (2017-2023)." `http://www.strategymrc.com/report/barcode-scanner-market`, 2017. [Online; accessed 26-June-2018].

[4] Global Market Insights, Inc., "Barcode printers market worth $3.5bn by 2024." `https://www.gminsights.com/pressrelease/barcode-printers-market`, 2018. [Online; accessed 26-June-2018].

[5] S. Preradovic and N. C. Karmakar, "Chipless rfid: Bar code of the future," *IEEE Microwave Magazine*, vol. 11, pp. 87–97, Dec 2010.

[6] Computalable, "Upc." `https://www.computalabel.com/aboutupc.htm`. [Online; accessed 12-July-2018].

[7] Elprocus, "Rfid – a basic introduction & simple application." `https://www.elprocus.com/rfid-basic-introduction-simple-application/#comments`, 2015. [Online; accessed 03-July-2018].

[8] Persistence Market Research (PMR), "Global market study on chipless rfid: Rfid tags segment projected to record double digit cagr over the forecast period." `https://www.persistencemarketresearch.com/market-research/chipless-rfid-market.asp`, 2017. [Online; accessed 26-June-2018].

[9] Statista, "Projected size of the global market for rfid tags from 2016 to 2020 (in billion u.s. dollars." `https://www.statista.com/statistics/299966/size-of-the-global-rfid-market/`, 2018. [Online; accessed 26-June-2018].

[10] RFID 24-7 , "Rfid market exceeds $9b in 2014; retail drives strong growth." `http://rfid24-7.com/2014/03/13/rfid-market-exceeds-9b-in-2014-retail-drives-strong-growth/`, 2014. [Online; accessed 26-June-2018].

[11] D. Pozar, *Microwave Engineering*. Wiley, 2004.

[12] Tanim, M M Zaman, "How does passive rfid works, briefly explained. - scientific figure on researchgate." `https://www.researchgate.net/Simplified-Physics-of-Backscatter-Signaling-Following-are-the-benefits-of_fig6_310465148`, 2014. [Online; accessed 10 Sep, 2018].

[13] S. Preradovic, N. C. Karmakar, and I. Balbin, "Rfid transponders," *IEEE Microwave Magazine*, vol. 9, pp. 90–103, Oct 2008.

[14] V. P. Plessky, S. Member, and L. M. Reindl, "Review on SAW RFID Tags," vol. 57, no. 3, pp. 654–668, 2010.

[15] I. RFSAW, "The Global SAW Tag - a New Technical Approach to RFID," *Reading*, 2004.

[16] Mary Catherine O'Connor, "NASA to Launch RFID Test to Track Crewmember Supplies - 2007-06-04 - Page 2 - RFID Journal," 2017.

[17] S. Preradovic, I. Balbin, N. C. Karmakar, and G. Swiegers, "Chipless frequency signature based RFID transponders," *Proceedings of the 38th European Microwave Conference, EuMC 2008*, no. October, pp. 1723–1726, 2008.

[18] Das Raghu, "Chipless RFID - The End Game," 2006.

[19] B. Violino, "Firewall Protection for Paper Documents," pp. 1–2, 2004.

[20] J. Collins, "RFID fibers for secure applications," *http://www.rfidjournal.com/article/articleprint/845/-1/1/, RFID Journal*, pp. 1–2, 2004.

[21] Bacheldor Beth, "RFID Tattoos for Livestock," p. 1, 2017.

[22] K. C. Jones, "Invisible RFID Ink Safe For Cattle And People, Company Says - InformationWeek."

[23] "RFID Tattoos to Make a Mark on Cattle Tagging," p. 1, 2008.

[24] I. Jalaly and I. D. Robertson, "RF barcodes using multiple frequency bands," *IEEE MTT-S International Microwave Symposium Digest*, vol. 2005, no. C, pp. 139–142, 2005.

[25] J. McVay, A. Hoorfar, and N. Engheta, "Space-filling curve rfid tags," 07 2006.

[26] Wikipedia the free encyclopedia, "Space-filling curve,"

[27] S. Preradovic, N. C. Karmakar, I. Balbin, S. M. Roy, and G. F. Swiegers, "Radio frequency transponder," 2008.

[28] S. Dey and N. C. Karmakar, "An iot empowered flexible chipless rfid tag for low cost item identification," in *2017 IEEE Region 10 Humanitarian Technology Conference (R10-HTC)*, pp. 179–182, Dec 2017.

[29] A. Habib, M. A. Afzal, H. Sadia, Y. Amin, and H. Tenhunen, "Chipless rfid tag for iot applications," in *2016 IEEE 59th International Midwest Symposium on Circuits and Systems (MWSCAS)*, pp. 1–4, Oct 2016.

[30] O. Necibi, S. Beldi, and A. Gharsallah, "Design of a Chipless RFID TAG Using Cascaded and Parallel Spiral Resonators at 30 GHz," *2015 2nd World Symposium on Web Applications and Networking (WSWAN)*, pp. 1–5, 2015.

[31] Y. Ni, X.-d. Huang, and C. Cheng, "Improved chipless tag based on multifilters," *Microwave and Optical Technology Letters*, vol. 59, pp. 1890–1896, 08 2017.

[32] S. Preradovic, I. Balbin, N. C. Karmakar, and G. F. Swiegers, "Multiresonator-based chipless rfid system for low-cost item tracking," *IEEE Transactions on Microwave Theory and Techniques*, vol. 57, pp. 1411–1419, May 2009.

[33] A. A. de Castro Alves, L. L. B. Roger, and F. J. Arnold, "Prediction of the performance of a reconfigurable resonator for rfid chipeless tags," *IEEE Latin America Transactions*, vol. 13, pp. 623–627, March 2015.

[34] A. A. C. Alves, D. H. Spadoti, and L. L. Bravo-Roger, "Optically controlled multiresonator for passive chipless tag," *IEEE Microwave and Wireless Components Letters*, vol. 28, pp. 467–469, June 2018.

[35] A. M. J. Marindra and G. Y. Tian, "Chipless rfid sensor tag for metal crack detection and characterization," *IEEE Transactions on Microwave Theory and Techniques*, vol. 66, pp. 2452–2462, May 2018.

[36] I. Balbin and N. Karmakar, "Novel chipless rfid tag for conveyor belt tracking using multi-resonant dipole antenna," pp. 1109 – 1112, 11 2009.

[37] C. Mandel, M. Schussler, M. Maasch, and R. Jakoby, "A novel passive phase modulator based on lh delay lines for chipless microwave rfid applications," in *2009 IEEE MTT-S International Microwave Workshop on Wireless Sensing, Local Positioning, and RFID*, pp. 1–4, Sep. 2009.

[38] S. Mukherjee, "Antennas for chipless tags based on remote measurement of complex impedance," in *2008 38th European Microwave Conference*, pp. 71–74, Oct 2008.

[39] S. Mukherjee, "Chipless radio frequency identification by remote measurement of complex impedance," in *2007 European Conference on Wireless Technologies*, pp. 249–252, Oct 2007.

[40] I. Balbin and N. C. Karmakar, "Phase-encoded chipless rfid transponder for large-scale low-cost applications," *IEEE Microwave and Wireless Components Letters*, vol. 19, pp. 509–511, Aug 2009.

[41] L. Yang, R. Zhang, D. Staiculescu, C. P. Wong, and M. M. Tentzeris, "A novel conformal rfid-enabled module utilizing inkjet-printed antennas and carbon nanotubes for gas-detection applications," *IEEE Antennas and Wireless Propagation Letters*, vol. 8, pp. 653–656, 2009.

[42] Wikipedia contributors, "Hamming code — Wikipedia, the free encyclopedia." `https://en.wikipedia.org/w/index.php?title=Hamming_code&oldid=883005043`, 2019. [Online; accessed 27-February-2019].

[43] Wikipedia contributors, "Hamming(7,4) — Wikipedia, the free encyclopedia." https://en.wikipedia.org/w/index.php?title=Hamming(7,4)&oldid=883398123, 2019. [Online; accessed 27-February-2019].

[44] N. Karmakar, P. Kalansuriya, R. Azim, and R. Koswatta, *Chipless radio frequency identification reader signal processing.* Wiley Series in Microwave and Optical Engineering, United States: John Wiley & Sons, 1 ed., 4 2016.

[45] Wikipedia contributors, "Fractional fourier transform — Wikipedia, the free encyclopedia." https://en.wikipedia.org/w/index.php?title=Fractional_Fourier_transform&oldid=884297015, 2019. [Online; accessed 27-February-2019].

[46] Y. Ni, X.-d. Huang, and C. Cheng, "Improved chipless tag based on multifilters," *Microwave and Optical Technology Letters*, vol. 59, pp. 1890–1896, 08 2017.

[47] S. Preradovic and N. Karmakar, *Multiresonator-Based Chipless RFID - Barcode of the Future.* 03 2014.

[48] J. Joubert, "Spiral microstrip resonators for narrow-stopband filters," *IEE Proceedings - Microwaves, Antennas and Propagation*, vol. 150, pp. 493–496, Dec 2003.

[49] Young-Taek Lee, Jong-Sik Lim, Chul-Soo Kim, Dal Ahn, and Sangwook Nam, "A compact-size microstrip spiral resonator and its application to microwave oscillator," *IEEE Microwave and Wireless Components Letters*, vol. 12, pp. 375–377, Oct 2002.

[50] Young-Taek Lee, Jong-Sik Lim, Chul-Soo Kim, Dal Ahn, and Sangwook Nam, "A compact-size microstrip spiral resonator and its application to microwave oscillator," *IEEE Microwave and Wireless Components Letters*, vol. 12, pp. 375–377, Oct 2002.

[51] A. Khanna and Y. Garault, "Determination of loaded, unloaded, and external quality factors of a dielectric resonator coupled to a microstrip line," *IEEE Transactions on Microwave Theory and Techniques*, vol. 31, pp. 261–264, Mar 1983.

[52] I. J. Bahl, *Lumped elements for RF and microwave circuits.* Artech house, 2003.

[53] J. Chen and J. Liou, "On-chip spiral inductors for rf applications: An overview," *JOURNAL OF SEMICONDUCTOR TECHNOLOGY AND SCIENCE*, vol. 4, 09 2004.

[54] C. P. Yue and S. S. Wong, "Physical modeling of spiral inductors on silicon," *IEEE Transactions on Electron Devices*, vol. 47, pp. 560–568, March 2000.

[55] N. M. Nguyen and R. G. Meyer, "Si ic-compatible inductors and lc passive filters," *IEEE Journal of Solid-State Circuits*, vol. 25, pp. 1028–1031, Aug 1990.

[56] K. B. Ashby, I. A. Koullias, W. C. Finley, J. J. Bastek, and S. Moinian, "High q inductors for wireless applications in a complementary silicon bipolar process," *IEEE Journal of Solid-State Circuits*, vol. 31, pp. 4–9, Jan 1996.

[57] H. Greenhouse, "Design of planar rectangular microelectronic inductors," *IEEE Transactions on Parts, Hybrids, and Packaging*, vol. 10, pp. 101–109, June 1974.

[58] D. M. Krafcsik and D. E. Dawson, "A closed-form expression for representing the distributed nature of the spiral inductor," in *Microwave and Millimeter-Wave Monolithic Circuits*, vol. 86, pp. 87–92, May 1986.

[59] L. B. Almeida, "The fractional fourier transform and time-frequency representations," *IEEE Transactions on Signal Processing*, vol. 42, pp. 3084–3091, Nov 1994.

[60] N. Karmakar, P. Kalansuriya, R. Azim, and R. Koswatta, *Chipless Radio Frequency Identification Reader Signal Processing*. 03 2016.

[61] D. M. J. Cowell and S. Freear, "Separation of overlapping linear frequency modulated (lfm) signals using the fractional fourier transform," *IEEE Transactions on Ultrasonics, Ferroelectrics, and Frequency Control*, vol. 57, pp. 2324–2333, October 2010.

[62] H. M. Ozaktas, O. Arikan, M. A. Kutay, and G. Bozdagt, "Digital computation of the fractional fourier transform," *IEEE Transactions on Signal Processing*, vol. 44, pp. 2141–2150, Sep. 1996.

[63] C. Capus and K. Brown, "Short-time fractional fourier methods for the time-frequency representation of chirp signals," *The Journal of the Acoustical Society of America*, vol. 113, pp. 3253–63, 07 2003.

Appendices

A Appendix A

YEF-ECE 2019 - 3rd International Young Engineers Forum on Electrical and Computer Engineering conference

A Novel Procedure for Chipless RFID Tags Design

Bernardo Lopes
Universidade de Aveiro
Instituto de Telecomunicações
Aveiro, Portugal
bernardobentolopes@ua.pt

João N. Matos
Universidade de Aveiro
Instituto de Telecomunicações
Aveiro, Portugal
matos@ua.pt

***Abstract*—This paper presents a novel procedure to obtain behaviour defining equations able to aid designers in the design architecture of spiral resonators coupled to a transmission line. Besides demonstrating this procedure, a 3-bit chipless RFID multi-resonator circuit was designed and simulated in the 1 - 7 GHz frequency band using the extracted equations. The results show a maximum error of 1.936 % relative to the frequency of resonance, showcasing the good agreement between the extracted equations and the simulated results.**

***Index Terms*—Chipless RFID, tags, spiral resonators**

I. Introduction

Radio-Frequency Identification (RFID) is an emerging technology that allows data capturing based on the propagation of radio frequency (RF) electromagnetic waves through open space. The advent of the development of this technology within the labelling and smart-identification industry, brought hope on making the now almost seventy year old barcode technology obsolete. The goal is to use RFID to give an answer to the bottleneck that the use of optical reading printed barcode labels created: the need of a clear line-of-sight between the reader and the label, the short-range readability and the non-automated tracking [1].

The typical RFID system is made up of two major components: the transponder/tag, which is located on the object to be identified and the interrogator/reader, which, depending on the technology used, my be a read or write/read device [2]. However, the penetration of the RFID technology in this market is hindered due to the high price of transponder when compared to the simple printed barcode [3]. Within the tree of RFID tags technologies, the chipless RFID is the *go-to* technology when it comes to keep it cheap [4]. The chipless RFID tags, appears from an effort to design low-cost RFID tags without the use of traditional silicone Application Specific Integrated Circuits (ASICs) that were the price bottleneck of the tags. Within all of the reported chipless RFID tags developments the Multi-Resonator-based chipless RFID tags are considered one of the more feasible, commercially viable, efficient in terms of coding capacity and thus, more researched [4]–[6]. The multi-resonator-based chipless RFID tags make use of a multi-resonating circuit and a pair of transmitting (Tx) and receiving (Rx) antennas to encode data bits in the form of attenuations and phase jumps at particular frequencies of the spectrum.

This paper presents an analysis of the multi-resonating circuit as well as the study of its behaviour in the 1-7 GHz frequency band. It also provides empirical equations describing its behaviour in the simulated environment and conditions. Additionally, a 3-bit multi-resonating circuit was designed using the referred equations. This work provides a new set of guide-lines to the synthesis of multi-resonating circuits.

II. Working Principle

As stated above, multi-resonator-based chipless RFID tags make use of a multi-resonating circuit and a pair of Tx and Rx antennas to encode data bits in the form of attenuations and phase jumps at particular frequencies of the spectrum. One of the most well spread embodiments of this principle consists on a multi-stop-band filter comprising a plurality of cascaded resonating substructures, each corresponding to a stop-band having an associated resonating frequency, such that information may be encoded in this scheme by modifying the resonator substructures. Several adaptations and variations of this embodiment are documented by several researchers [7]–[9]. The presence/absence of frequency content in a predetermined frequency is encoded as '1' or '0' and is controlled by the existence/absence of the resonating substructure associated to said frequency.

The resonating structure creates a low impedance path to the ground plane at its resonant frequency. This structure is coupled to the the transmission line thus having an direct influence on the structure frequency behaviour.

III. Layout of the multi-resonating circuit

In order to make the system scalable, adequate and feasible There are several RFID system design requirements that need to be accounted for. Although some of this requirements are highly application specific, there are a few critical ones:

1) **Cost** - The bottleneck of the new chipless RFID systems are the cost of the transponder. Ideally, the goal is to keep the tags bellow 1 cent to make it suitable for labelling low cost items.
2) **Size** - The tag's size is to be kept as small as possible while retaining all critical characteristics such as readability and reading distance. Logically, smaller tags are cheaper. Nevertheless, the size of the tag is intrinsically

978-1-5386-9281-3/19/$31.00 ©2019 IEEE

bounded to the frequency of operation and the size of the item to be tagged.

3) **Scalability** - Transponders that can have their ID easily changed are preferred. This will result in a cheap and quick building process that overall facilitate the successful design of the system.

Taking this into account, several efforts were made in order to determine the choice of the resonator type. Joubert in his work [10], conducted a comparative study between two widely used resonator types (a rectangular open-loop resonator and the miniaturised hairpin resonator) and a proposed compact rectangular spiral resonator. Results show that the spiral resonator due to its much smaller size, and hence the larger gap between spirals, has less unwanted coupling between adjacent resonators. Furthermore, spiral resonators are easily modifiable for data encoding, have narrow bandwidth (20 MHz), considerably high attenuation at its resonant frequency ($>$ 7 dB) and have a single-sided layout [4] when comparing to the other resonator types. Due to these reasons, several authors use spiral resonators as the resonator type.

The typical layout of a conventional spiral resonating structure is depicted in Figure 1. This layout consists on a microstrip line and a spiral resonator, both on the top layer, and separated from the continuous ground plane in the bottom layer by a dialectic layer. The spiral resonator is gap coupled to the 50 Ω microstrip line.

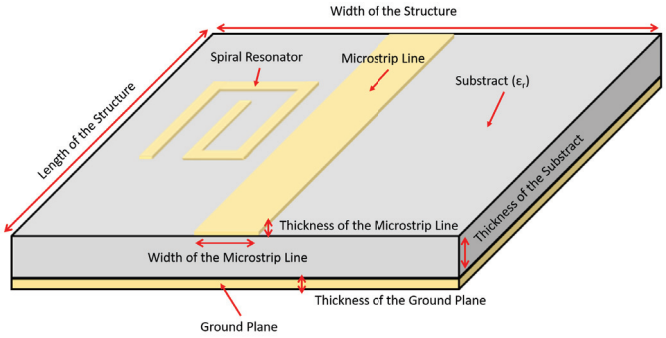

Fig. 1. Layout of the resonating circuit.

IV. Theoretical Modelling of a Spiral Resonator

The creation of models that can accurately describe the behaviour of resonators are of great importance since they are the go-to models for any designer that needs to project any type of resonator and intents to predict the behaviour of the resonator in function of certain variable parameters. To the authors knowledge, few efforts were made to fully model the spiral as a resonating structure coupled to a transmission line. Withal, there are some work on the characterization of this structure as a planar inductor. Most of these characterizations and models lack practicality and intuitiveness to be of help to designers.

Several authors [11]–[15] agreed on a analytical lumped-element circuit capable of describing the behaviour of the resonant spiral and its influence on the microstrip line. Said circuit is represented in Figure 2. In the image, in a), Z_0 is the characteristic impedance, Z_S is the source's impedance, C_S is the source capacitance, R_S is the source restive loss, R_D is the distributed resistive loss of the spiral, C_D is the distributed capacitance of the spiral, L_D is the distributed inductance of the spiral, L_T is the distributed inductance of the transition line, Z_L is the load impedance. In b), the subscript $_E$ stands for "equivalent" and it represents the behaviour and influence of the resonator in the transmission line.

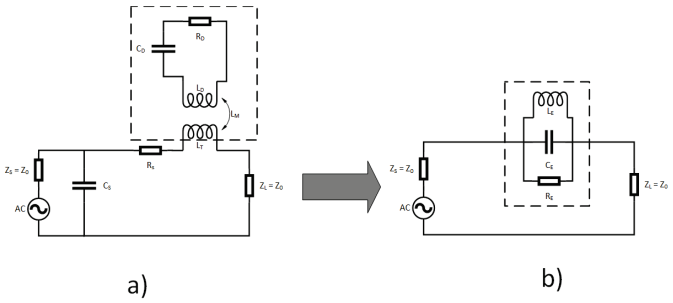

Fig. 2. Equivalent circuit model of the spiral resonator coupled to a microstrip line. In a) is the the equivalent RLC circuit of the spiral resonator that influences the main circuit due to the mutual inductance; In b) is the equivalent circuit of the spiral resonator imitating the behaviour of it when coupled to the transition line having a stop-band characteristic.

From the equivalent circuit is easy to extrapolate that the resonant frequency f_r of the spiral resonator coupled to a microstrip line is :

$$f_r = \frac{1}{2\pi\sqrt{L_E C_E}} \tag{1}$$

The problem arises when trying to find the circuit resonant frequency. From the designer point of view, it would be adequate to write f_r as a function of the resonant spiral building parameters, represented in Figure 3 and, finding out the dependencies between such parameters and L_E and C_E.

Based in [16], Bahl et al. presents in [11] a general expression for inductance of an arbitrary shape. Yet, the list of shapes from which the coefficients were determined does not contain the rectangular shape (only square, hexagonal, octagonal and circle shapes). Several authors also cite [12] as providing a method for calculating the distributed capacitance C_D and the resonant frequency f_r of the spiral resonator. However, this work was perform only taking into account the circular shape, thus not being accurate for describing the behaviour of a rectangular shaped spiral. On a better note, Hejazi et al. [13] developed a procedure for calculating the distributed inductance of a rectangular spiral by calculating the inductance of individual turn and the mutual inductance between turns of the spiral resonator. Despite the resulting equation coming in function of the defined design parameters, its very unfriendly to deal with and does not provide an intuitive notion.

Another way of modelling the spiral resonator is to model the frequency characteristics of the resonator based on the layout of the resonator using coupled line theory. Preradovic

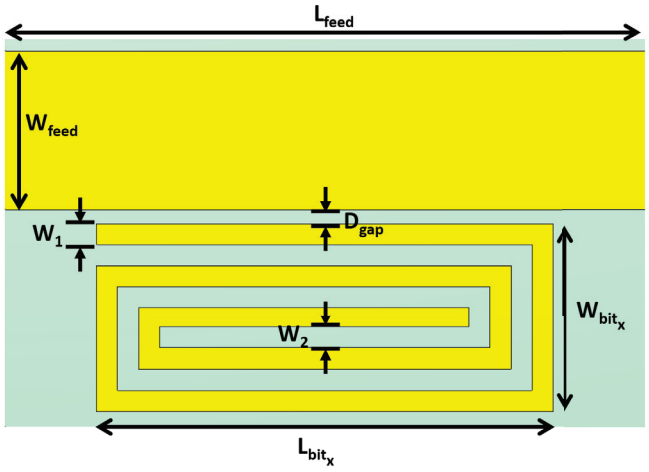

Fig. 3. Spiral resonator design parameters: L_{feed} is the length of the microstrip line, W_{feed} is the width of the microstrip line, D_{gap} is the distance between the micrsotrip line and the spiral resonator, W_1 is the width of the spiral arms, W_2 is the width of the spacing between spiral arms, L_{bit_x} is the length of the spiral were x identifies the spiral (ex: x = 1) and W_{bit_x} is the width of the spiral.

et al. proposed, in [17], a transition line model of a two turn resonator spiral coupled to a microstrip line. The spiral was model in ADS Schematic Simulator and it has a total of 22 section represented by schematic microstrip components. This model enables faster and easier design of the resonator by achieving a shorter simulation time when compared with the typical full wave 3D or Method of Moments (MoM) solvers. However, once again, this model works on the basis of simulating the structure and then interacting and tweaking it's parameters until the desired behaviour is achieved.

The most used model is the one created from electromagnetic (EM) simulators. These simulators simulate the structure adequately and also provide flexibility in terms of layout, complexity and versatility. The most commonly used technique for planar structure is the MoM, and for 3-D structures, the finite element method (FEM) [11]. Both of these techniques perform EM analysis in the frequency domain. Once again, like the above, this model is based on the try-error approach to built the resonating structure.

V. Parametric Analysis

In order to understand the behaviour of the rectangular spiral resonator, one was designed by fixing several parameters and by varying the length of the spiral L_{bit_x}. The simulation was done with *CST STUDIO SUIT 2017* software with the following parameters fixed: $L_{feed} = 5mm$, $W_{feed} = 2.26mm$, $D_{gap} = 0.2mm$, $W_1 = 0.3mm$, $W_2 = 0.3mm$ and $W_{bit_x} = 2.7mm$. The layout is that of Figure 1, using a loss free substrate (with $\epsilon_r = 3.4$ and height of $h = 0.787mm$) and Copper (pure) (with thickness of $t = 0.017mm$) as the conductive material. The spiral has two turns and is made of nine arms just like the one in Figure 3.

The variation of the spiral length is the most common way of tuning the frequency of resonance of the spiral. For this reason, the impact of the variation of the length on the f_r in the 1 - 7 GHz frequency band was studied. This band was chosen to provide quicker simulation results and as a prove of concept. The value of L_{bit_1} was varied between $3mm$ and $9.5mm$. The simulation results are presented in both Table I and in Figure 4.

TABLE I
1st Resonance frequency variation as a function of L_{bit_1}

L_{bit_1} [mm]	1st Frequency of resonance [GHz]	S21 [dB]
3	5,3983	-7,7704
3,5	4,5656	-9,7094
4	3,9738	-10,613
4,5	3,5932	-10,718
5	3,2687	-10,836
5,5	2,9717	-10,675
6	2,7506	-10,315
6,5	2,5193	-10,154
7	2,326	-9,8598
7,5	2,1808	-9,4637
8	2,0367	-9,2119
8,5	1,9344	-8,836
9	1,8266	-8,7046
9,5	1,7254	-8,5752

The points in the above table with the pair of coordinates (L_{bit_1},$f_r^{1^{st}}$) were graphically represented in the graph depicted in Figure 4. The points were fitted with a exponential curve.

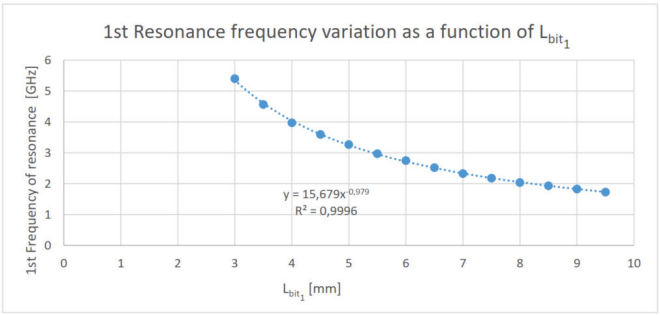

Fig. 4. 1st Resonance frequency variation as a function of L_{bit_1}

The results show that, the behaviour of the f_r in function of L_{bit_1} is highly predictable and can described by the following equation:

$$f_r^{1^{st}} = 15.679 {L_{bit_1}}^{-0.979} \quad (2)$$

Bear in mind that this equation only describes the behaviour of the f_r in the simulated conditions.

It was observed that by continually increasing L_{bit_1} the spiral resonator developed a second f_r for $L_{bit_1} > 6mm$. This phenomenon is represented in table II by the points that depicted this behaviour in the simulation.

Similarly to that previously done, the points in the above table with the pair of coordinates (L_{bit_1},$f_r^{2^{nd}}$) were graphically represented in the graph depicted in Figure 5. The points were fitted with a exponential curve.

TABLE II
2ND RESONANCE FREQUENCY VARIATION AS A FUNCTION OF L_{bit_1}

L_{bit_1} [mm]	2nd Frequency of resonance [GHz]	S21 [dB]
6,5	5,5974	-6,78118
7	5,1728	-6,7371
7,5	4,8615	-6,633
8	4,5425	-6,9511
8,5	4,3005	-7,0045
9	4,0563	-7,2041
9,5	3,833	-7,391

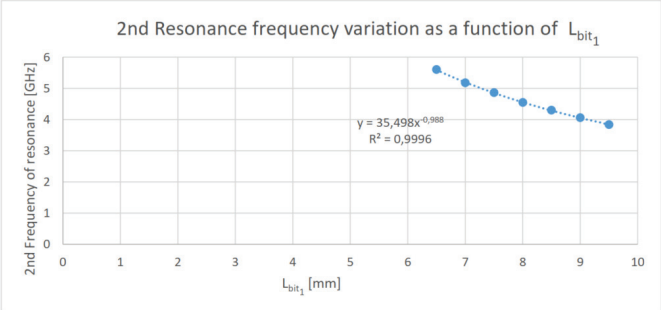

Fig. 5. 2nd Resonance frequency variation as a function of L_{bit_1}

This resonance frequency also has a predictable behaviour when variations of L_{bit_1} are made. It can be described by the following equation:

$$f_r^{2^{nd}} = 35.498 {L_{bit_1}}^{-0.988} \quad (3)$$

In order to test the validity of these equations, a 3 bit multi-resonating circuit was simulated. The tag is to operate from 1 to 3 GHZ with three frequency of resonance at 1.5 GHz, 2 GHz and 2.5 GHz. Using equation 2 and 3 the length of each of the three spirals L_{bit_x} was computed and shown in Table III.

TABLE III
COMPUTATION OF THE VALUES OF L_{bit_x}

Desired Resonance Frequency [GHz]	Value of L_{bit_x} [mm]	2nd Resonance Frequency [GHz]	bit_x
1.5	10.99	3.32	1
2	8.19	4.44	2
2.5	6.52	5.56	3

As the second resonance frequency is out of the interest frequency band, no further adjustments were needed. In order to reduce the inter-spiral coupling, the two smaller spirals were built in one side of the transition line and the bigger spiral was built in the other (Figure 6).

The 3 bit multi-resonant circuit was built with the same material and the same fixed parameters as the ones stated before. Besides that, the length of the spirals are $L_{bit_1} = 10.99mm$, $L_{bit_2} = 8.19mm$, $L_{bit_3} = 5.23mm$ and the width is $W_{bit_1} = W_{bit_2} = W_{bit_3} = 2.7mm$. The layout is showed in Figure 6 and the distance between the bit_2 and bit_3 tags is of $7.142mm$.

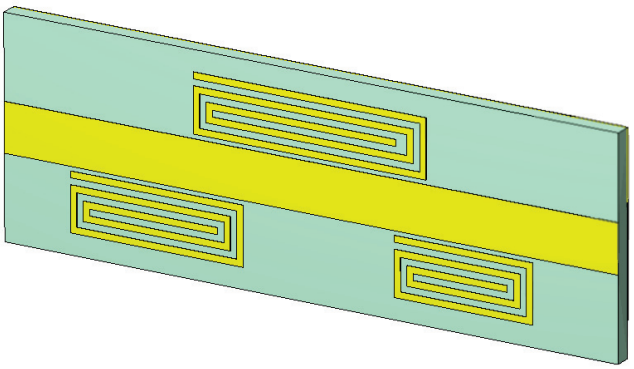

Fig. 6. Design layout of the 3 bit multi-resonant circuit using spiral resonators.

The S21 parameter behaviour in frequency is depicted in Figure 7. The important points were extracted from the frequency response of the tag and are displayed in Table IV. It's clear that the 3 bit multi-resonant circuit behaves as expected in term of its frequency response which validates the used equations as predictors on the frequency response of the tag.

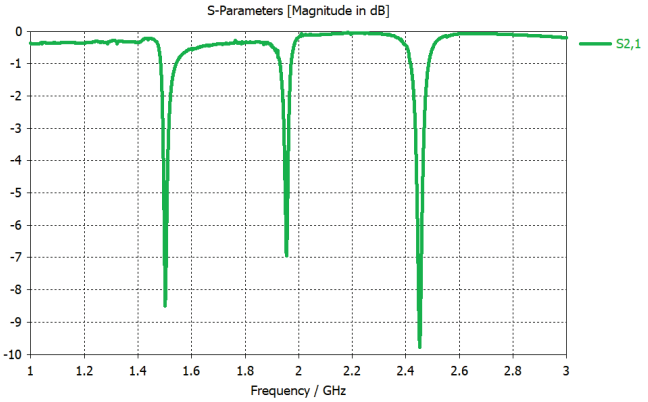

Fig. 7. 3 bit multi-resonant circuit's S21 parameter behaviour.

TABLE IV
RESULTS EXTRACTED FROM THE 3 BIT MULTI-RESONANT CIRCUIT'S FREQUENCY RESPONSE.

1st Resonance Frequency [GHz]	S21 [dB]	3dB bandwidth [MHz]	Error [%]
1.502	-8.4909	218.69	0.13
1.954	-6.9406	177.57	2.3
2.4516	-9.7863	326.42	1.936

VI. CONCLUSIONS

This paper presents a method for developing intuitive and accurate design equations that can greatly aid the design of multi-resonant structures for chipless RFID tags. This process is rather effortless and time saving as it can be easily made using any full wave or MoM solver. Also, this paper showcases the possibility of a single resonant spiral having multiple

resonant frequencies, thus, the modelling as a single RLC circuit is inaccurate to fully describe the behaviour of the referred structure.

ACKNOWLEDGEMENT

This work is funded by FCT/MEC through national funds and when applicable co-funded by FEDER – PT2020 partnership agreement under the project UID/EEA/50008/2019

REFERENCES

[1] S. Preradovic and N. C. Karmakar, "Chipless RFID: Bar Code of the Future," in IEEE Microwave Magazine, vol. 11, no. 7, pp. 87-97, Dec. 2010. doi: 10.1109/MMM.2010.938571,URL:http://ieeexplore.ieee.org/stamp/stamp.jsp?tp=&arnumber=5590347&isnumber=5590337

[2] Finkenzeller, Klaus. (2005). RFID Handbook: Fundamentals and Applications In Contactless Smart Cards and Identification. 10.1002/0470868023.ch1.

[3] Karmakar, N. C., Kalansuriya, P., Azim, R. E., & Koswatta, R. (2016). Chipless radio frequency identification reader signal processing. (1 ed.) (Wiley Series in Microwave and Optical Engineering). Hoboken NJ USA: John Wiley & Sons.https://doi.org/10.1002/9781119215783

[4] Preradovic, S., Karmakar, N.C., & Balbin, I. (2008). RFID Transponders. IEEE Microwave Magazine, 9.

[5] Ni, Yi-Zhan & Huang, Xiao-dong & Cheng, Chong-Hu. (2017). Improved chipless tag based on multifilters. Microwave and Optical Technology Letters. 59. 1890-1896. 10.1002/mop.30647.

[6] C. Herrojo, J. Mata-Contreras, F. Paredes, A. Núñez, E. Ramon and F. Martín, "Near-Field Chipless-RFID System With Erasable/Programmable 40-bit Tags Inkjet Printed on Paper Substrates," in IEEE Microwave and Wireless Components Letters, vol. 28, no. 3, pp. 272-274, March 2018. doi: 10.1109/LMWC.2018.2802718, URL: http://ieeexplore.ieee.org/stamp/stamp.jsp?tp=&arnumber=8299452&isnumber=8310744

[7] Casula, G & Montisci, Giorgio & Maxia, Paolo & Mazzarella, Giuseppe. (2014). A narrowband chipless multiresonator tag for UHF RFID. Journal of Electromagnetic Waves and Applications. 28. 214-227. 10.1080/09205071.2013.862187.

[8] Ni, Yi-Zhan & Huang, Xiao-dong & Cheng, Chong-Hu. (2017). Improved chipless tag based on multifilters. Microwave and Optical Technology Letters. 59. 1890-1896. 10.1002/mop.30647.

[9] S. Preradovic, I. Balbin, N. C. Karmakar and G. F. Swiegers, "Multiresonator-Based Chipless RFID System for Low-Cost Item Tracking," in IEEE Transactions on Microwave Theory and Techniques, vol. 57, no. 5, pp. 1411-1419, May 2009. doi: 10.1109/TMTT.2009.2017323 URL: http://ieeexplore.ieee.org/stamp/stamp.jsp?tp=&arnumber=4814553&isnumber=4909499

[10] J. Joubert, "Spiral microstrip resonators for narrow-stopband filters," in IEE Proceedings - Microwaves, Antennas and Propagation, vol. 150, no. 6, pp. 493-496, 8 Dec. 2003.

[11] Bahl, I. J. (2003). Lumped elements for RF and microwave circuits. Boston: Artech House.

[12] Zunfu Jiang, P. S. Excell and Z. M. Hejazi, "Calculation of distributed capacitances of spiral resonators," in IEEE Transactions on Microwave Theory and Techniques, vol. 45, no. 1, pp. 139-142, Jan. 1997. doi: 10.1109/22.552045, URL:http://ieeexplore.ieee.org/stamp/stamp.jsp?tp=&arnumber=552045&isnumber=11976

[13] Z. M. Hejazi, P. S. Excell and Z. Jiang, "Accurate distributed inductance of spiral resonators," in IEEE Microwave and Guided Wave Letters, vol. 8, no. 4, pp. 164-166, April 1998. doi: 10.1109/75.663521, URL: http://ieeexplore.ieee.org/stamp/stamp.jsp?tp=&arnumber=663521&isnumber=14529

[14] Young-Taek Lee, Jong-Sik Lim, Chul-Soo Kim, Dal Ahn, & Sangwook Nam. (2002). A compact-size microstrip spiral resonator and its application to microwave oscillator. IEEE Microwave and Wireless Components Letters, 12(10), 375–377. doi:10.1109/lmwc.2002.804556

[15] Elelimy, A. M., Ahmed, H. N., & El-Tager, A. M. (2010). A low phase noise microwave oscillator based on a planar microstrip spiral resonator. IEEE Middle East Conference on Antennas and Propagation (MECAP 2010). doi:10.1109/mecap.2010.5724202

[16] S. S. Mohan, M. del Mar Hershenson, S. P. Boyd and T. H. Lee, "Simple accurate expressions for planar spiral inductances," in IEEE Journal of Solid-State Circuits, vol. 34, no. 10, pp. 1419-1424, Oct. 1999. doi: 10.1109/4.792620, URL: http://ieeexplore.ieee.org/stamp/stamp.jsp?tp=&arnumber=792620&isnumber=17209

[17] Preradovic, Stevan & Karmakar, Nemai. (2014). Multiresonator-Based Chipless RFID - Barcode of the Future. 10.1007/978-1-4614-2095-8.

B Appendix B

RFID-TA 2019 - 2019 IEEE International Conference on RFID Technology and Applications

Modelling of the Multi-Resonant Circuit Frequency Behaviour in Chipless RFID tags

Bernardo Lopes
Universidade de Aveiro
Instituto de Telecomunicações
Aveiro, Portugal
bernardobentolopes@ua.pt

João N. Matos
Universidade de Aveiro
Instituto de Telecomunicações
Aveiro, Portugal
matos@ua.pt

***Abstract*—This paper presents a model able to relate the resonant frequency of the multi-resonant of Chipless RFID tags with the spiral resonator structure length. This model is computed from simulated data that was previously validated by comparison with practical data. In this work, the existence of multiple resonant frequencies per resonant spiral is highlighted as well as its implication to the tag design. Lastly, the behaviour of the circuit is studied providing important knowledge to the circuit's designer.**

***Index Terms*—Chipless RFID, Tags, Spiral Resonators, Multi-Resonant Circuit**

I. Introduction

Radio-Frequency Identification (RFID) is an emerging technology that allows data capturing based on the propagation of radio frequency (RF) electromagnetic waves through open space. The advent of the development of this technology within the labelling and smart-identification industry, brought hope on making the now almost seventy year old barcode technology obsolete. The goal is to use RFID to give an answer to the bottleneck that the use of optical reading printed barcode labels created: the need of a clear line-of-sight between the reader and the label, the short-range readability and the non-automated tracking [1].

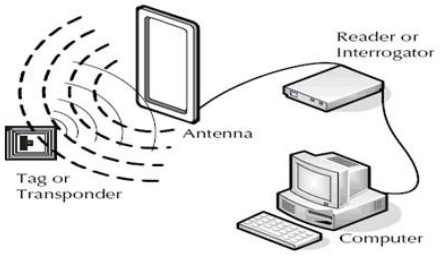

Fig. 1. Typical RFID system [2].

The typical RFID system is made up of two major components: the transponder/tag, which is located on the object to be identified and the interrogator/reader, which, depending on the technology used, may be a read or write/read device [3]. However, the penetration of the RFID technology in this market is hindered due to the high price of transponder when compared to the simple printed barcode [4]. Within the tree of RFID tags technologies, the chipless RFID is the *go-to* technology when it comes to keep it cheap [5]. The chipless RFID tags, appears from an effort to design low-cost RFID tags without the use of traditional silicone Application Specific Integrated Circuits (ASICs) that are the price bottleneck of the tags.

This paper presents a comprehensive understanding of the problems that arise when trying to model a multi-resonant circuit based of spiral resonators structures coupled to a transmission line. It also provides a simple comparative study between three different models created using simulators and a set of equations capable of describing the behaviour of the circuit's resonance frequency in function of the spiral resonator's lengtho. These equation constitute a great aid to the designers as they define the ability to encode data on the spectrum by varying the length of the spiral. To further aid this task, the relationship between the $\|S12\|$ parameter of the circuit and its resonant frequency as the spiral length increases is studied while considering the multiple resonant frequencies of the structure.

II. Working Principle

Data can be encoded in many ways in chipless RFID tags. So far, tags that encode their data as a spectral signature are known to be more efficient in terms of coding capacity and, thus, are more studied by the scientific community [6]. Within all the different technologies that are able to encode data as a spectral signature, the multi-resonantor-based chipless RFID technology presents itself as one of the most suitable solutions to be exploit as a replacement of the common barcode labels: it's designed to operate at a short range (up to 40 cm) and to tag extremely low cost price and sensitive items [7]. A multi-resonantor-based chipless RFID tag is built from a multi-resonant circuit - responsible for the data encoding - and a pair of antennas responsible to receive the interrogation signal and send the modulated version of the same signal back to the reader. The block diagram of said tag is depicted in Figure 2.

The multi-resonant circuit is the main target of the scientific community when it come to defining the codding capabilities of the tag. One of the drawbacks of this type of tags is the complex measurement steps and the interference suffer when the tag is subjected to real environment conditions. The used detection techniques are mainly based on radar cross-section

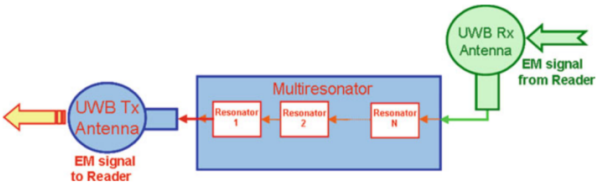

Fig. 2. Block diagram of a multi-resonantor-based chipless RFID tag [7].

information capture techniques and thus are highly sensitive to noise, reading distance and other factors [6]. Improving the codding capabilities of the tag will directly impact the abilities to retrieve a correct identification from the reading process. The information is encoded in the spectrum of the input signal as attenuations and phase jumps at pre-selected frequencies as explained in Figure 3. In this way, the information is coded in bits as '1' if there is spectral information at a specific frequency, and as '0' if there is not.

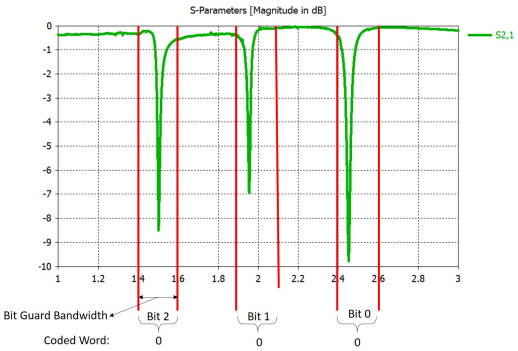

Fig. 3. Frequency response for a tag with pre-selected resonant frequencies at 1.5, 2 and 2.5 GHz.

III. Layout of the Multi-Resonant Circuit

The multi-resonant circuit consist in multiple cascaded resonators coupled to a microstrip line as showed in by Figure 4 and 5.

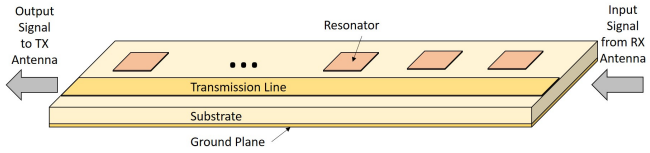

Fig. 4. Block diagram of the multi-resonantor circuit from a perspective view.

The signal flows from the RX antenna through the transmission line to the TX antenna. All of the n resonators are coupled to the transmission line and, at their specific resonant frequency, create a low impedance path to the ground plane. Because they are coupled to the transmission line the signal travelling through the transmission line is deviated to the ground, at the resonate frequency of the resonator, causing a lack of spectral content at that specific frequency in the

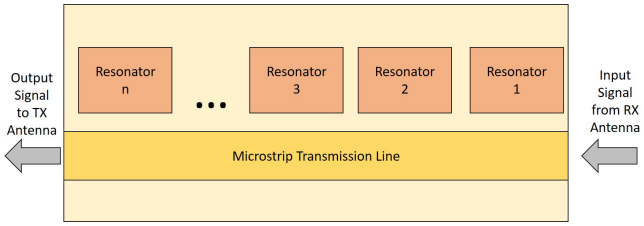

Fig. 5. Block diagram of the multi-resonantor circuit from a top view.

output signal. Since information is coded by the presence or absence of spectral content at predetermined frequencies, the resonant structures have a huge impact on the quality of the tag and therefore, the choice of the resonator must be done thoughtfully. In his work [8], Joubert sorted out the most important criteria when deciding on which resonator type to use:

- The size of the resonator;
- The spacing/coupling factor relationship between adjacent resonators;
- The position of the first spurious response of the resonator;
- The tunability of the resonator;

With the previous in mind, Joubert compared two highly used resonators - the rectangular open-loop resonator and the improved or miniaturised hairpin resonator - with the spiral resonator. All three resonators were built to achieve a fundamental resonance at 1.8 GHz for the specified substrate. The results obtained from that comparison indicate that spiral resonator is about 60% smaller in surface area that the square open loop resonator, and 17% smaller that the improved or miniaturised hairpin resonator. This indicates that spiral resonators can be used to construct very small and compact narrow-stop-band filters. A secondary advantage is that, being smaller, the physical spacing between resonators can be increased, result in in less unwanted coupling between adjacent resonators. This study was one of several that led the designers to opt for spiral resonators as the resonanting structure. For the above mentioned reasons, the authors also used spiral resonators in the design of the multi-resonant circuit.

The structure is built by etching two conductive layers at the top and bottom layer of a dielectric material as the one represented in Figure 6. The dielectric material has hight h and a relative permittivity and permeability ϵ_r , μ_r respectively. The conductive layer as a thickness of t and a width of w.

IV. Theoretical Modelling of the Multi-Resonant Circuit

The correct design of the multi-resonant circuit is of utmost importance. Conceptually, the designer must choose a frequency range of operation, the number of bits to encode within that range, the corresponding frequency were the bits are to be encoded and a guard bandwidth for each bit. The goal is to maximize the number of bits encoded in the spectrum and

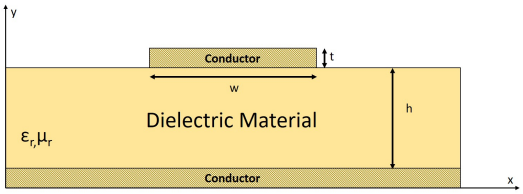

Fig. 6. Cross sectional view of a basic structure of a microstip line.

to minimize the frequency band used and the potential errors caused by unexpected frequency shifts, added noise or other causes. At a physical level, the designer has to compute each dimension of the spiral resonator and the transmission line in order to achieve the desired frequency response. In order to do that, the relationship between the circuit frequency behaviour and its physical dimension must be known, which implies the existence of some model capable of describing such relationship. The multi-resonant circuit has a lot of variable that influence its frequency response. Every spiral resonator has five different physical parameters that directly influence its resonant frequency. Additionally, the transmission line also has two physical parameters that influence the frequency response of the circuit. Such parameters are depicted in Figure 7. Additionally, the number of turns n is also used and it accounts for the number of turns of a spiral resonator.

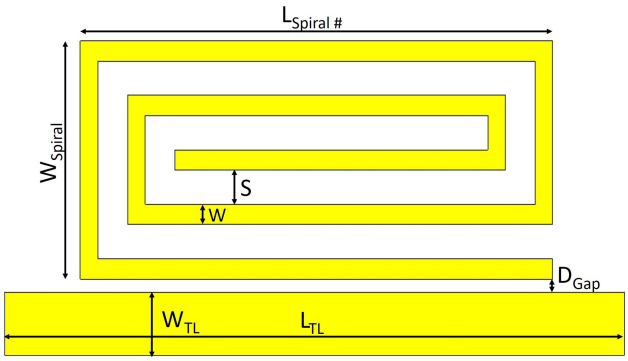

Fig. 7. Spiral Resonator coupled to a transmission line highlighting the physical parameters of the structure: $L_{spiral\#}$ is the length of the spiral numbered by #; W_{spiral} is the width of the spiral; S is the spacing between turns; W is the width of the spiral arm; D_{Gap} is the distance between the spiral resonator and the transmission line; W_{TL} is the width of the transmission line and the L_{TL} is the length of the transmission line.

The creation of models that can accurately describe the behaviour of the multi-resonant circuit is of great importance since the models provide the first interaction for any designer that needs to project a circuit and intents to predict its behaviour in function of certain variable parameters. To the authors knowledge, few efforts were made to fully model the spiral as a resonant structure coupled to a transmission line. Withal, there are some work on the characterization of this structure as a planar inductor. Most of these characterizations and models lack practicality and intuitiveness to be of help to designers.

Several authors [9]–[13] agreed on a analytical lumped-element circuit, presented in Figure 8, capable of describing the behaviour of the resonant spiral and its influence on the microstrip line. In the image, in a), Z_0 is the characteristic impedance, Z_S is the source's impedance, C_S is the source capacitance, R_S is the source restive loss, R_D is the distributed resistive loss of the spiral, C_D is the distributed capacitance of the spiral, L_D is the distributed inductance of the spiral, L_T is the distributed inductance of the transition line, Z_L is the load impedance. In b), the subscript $_E$ stands for "equivalent" and it represents the behaviour and influence of the resonator in the transmission line.

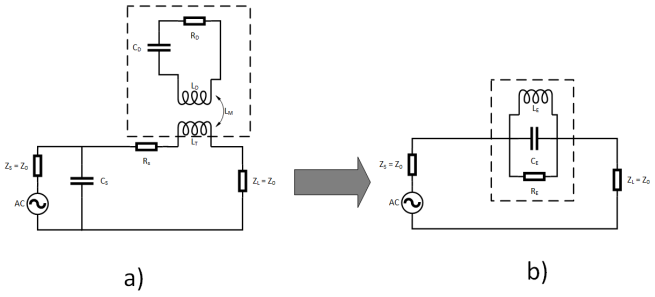

Fig. 8. Equivalent circuit model of the spiral resonator coupled to a microstrip line. In a) is the the equivalent RLC circuit of the spiral resonator that influences the main circuit due to the mutual inductance; In b) is the equivalent circuit of the spiral resonator imitating the behaviour of it when coupled to the transition line having a stop-band characteristic.

From the equivalent circuit is easy to extrapolate that the resonant frequency f_r of the spiral resonator coupled to a microstrip line is :

$$f_r = \frac{1}{2\pi\sqrt{L_E C_E}} \tag{1}$$

The problem arises when trying to find the circuit resonant frequency. From the designer point of view, it would be adequate to write f_r as a function of the resonant spiral building parameters, represented in Figure 7 and, finding out the dependencies between such parameters and L_E and C_E.

Based in [14], Bahl et al. presents in [9] a general expression for inductance of an arbitrary shape. Yet, the list of shapes from which the coefficients were determined does not contain the rectangular shape (only square, hexagonal, octagonal and circle shapes). Several authors also cite [10] as providing a method for calculating the distributed capacitance C_D and the resonant frequency f_r of the spiral resonator. However, this work was perform only taking into account the circular shape, thus not being accurate for describing the behaviour of a rectangular shaped spiral. On a better note, Hejazi et al. [11] developed a procedure for calculating the distributed inductance of a rectangular spiral by calculating the inductance of individual turn and the mutual inductance between turns of the spiral resonator. Despite the resulting equation coming in function of the defined design parameters, its very unfriendly to deal with and does not provide an intuitive notion.

Another way of modelling the spiral resonator is to model the frequency characteristics of the resonator based on the layout of the resonator using coupled line theory. Preradovic et al. proposed, in [15], a transition line model of a two turn resonator spiral coupled to a microstrip line. The spiral was model in ADS Schematic Simulator and it has a total of 22 section represented by schematic microstrip components. This model enables faster and easier design of the resonator by achieving a shorter simulation time when compared with the typical full wave 3D or Method of Moments (MoM) solvers. However, once again, this model works on the basis of simulating the structure and then interacting and tweaking its parameters until the desired behaviour is achieved.

The most used model is the one created from electromagnetic (EM) simulators. These simulators simulate the structure adequately and also provide flexibility in terms of layout, complexity and versatility. The most commonly used technique for planar structure is the MoM, and for 3-D structures, the finite element method (FEM) [9]. Both of these techniques perform EM analysis in the frequency domain. Once again, like the above, this model is based on the try-error approach to build the resonant structure.

V. Multi-Resonant Circuit Analysis

In order to compute a model capable of describing the multi-resonant circuit frequency behaviour, the authors tested the approach of two different simulators: the *CST STUDIO SUIT 2017* and the *Advance System Design 2017* (ADS) . While using the last, the authors simulated the structures using an electromagnetic simulator and using a 20 section model based on coupled and microstrip lines. All three structures were built with the exact same dimensions on a Rogers RO4725JXR substrate with $h = 0.78mm$ and $\epsilon_r = 2.55$. The conductor used was copper with $t = 0.017mm$. All other parameters were kept constant throughout this work and are listed in the Table I. The simulated structure was a multi-resonant circuit with only one resonant spiral of length $L_{Spiral1} = L = 8mm$.

TABLE I
Design Parameters

Circuit Parameter	Value [mm]	Circuit Parameter	Value [mm]
S	0.5	D_{Gap}	0.2
W	0.3	W_{TL}	1.912
W_{Spiral}	3.5	L_{TL}	$L_{Spiral\#} + 10$

The simulated circuit was printed and it's showcased in Figure 9. The S-Parameters of the circuit were extracted using a Agilent Technologies's PNA-X Network Analyser.

The results obtained from the simulations were compared with the one obtained from the physical device testing and are depicted in Figure 10. The circuit is symmetric and thus the following relationships are valid and were confirmed by measured results: $S12 = S21$ and $S11 = S22$. For this reason, throughout this paper only the S12 and S11 will be showcased. Results show that is the ADS coupled-line model that better mirrors the correct resonant frequency while the

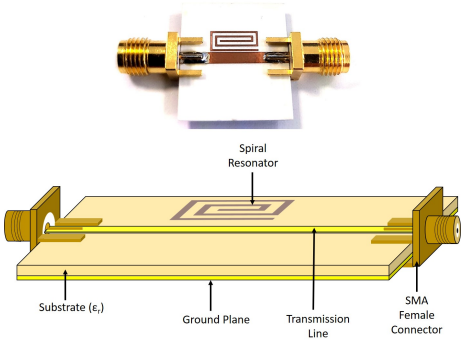

Fig. 9. Above is the device that was tested and under that is a schematic of a typical multi-resonant circuit test device (that can have more than one resonant spiral).

ADS electromagnetic model better agrees with the correct attenuation. The *CST STUDIO SUIT 2017*'s electromagnetic model is a good compromise between correct resonant frequency and attenuation being chosen as the simulator to be used throughout this work.

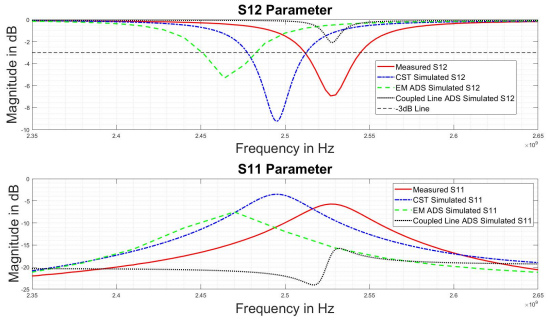

Fig. 10. Compilation of the S12 and S11 parameters from the simulated and physical multi-resonant circuit.

In order to better understand the behaviour of the multi-resonant circuit, using *CST STUDIO SUIT 2017*, a parametric simulation was performed varying the spiral resonator's length $L_{spiral1}$. The multi-resonant circuit as the same structure as the one depicted in Figure 9 and the same parameter values as the ones in Table I. The simulation was performed in the 1 to 15 GHz band by varying the $L_{spiral1} = L$ from 3 to 15 mm.

The first thing that is worth noting from the obtained results is that, contrary to what the existing literature indicates, each spiral may have more than one resonant frequency influencing in this way the frequency response of the circuit. For example, when the length of the spiral is 7 mm, the circuit has four resonant frequencies in the 1 to 15 GHz band, as could be seen in Figure 11.

This fact as serious repercussions in the circuit design phase. By existing multiple resonant frequencies for each spiral, information can be wrongly encoded due to attenuations in

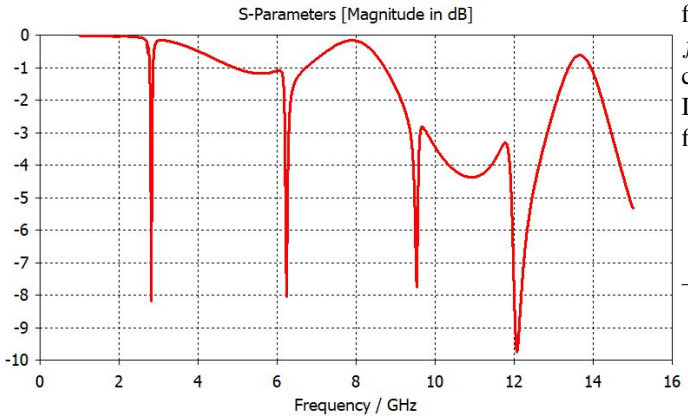

Fig. 11. S12-Parameter obtained in the parametric simulation using CST and by establishing the length of the spiral as 7 mm

the frequency band of interest due to secondary resonances that were not accounted for.

To further understand the frequency behaviour of the multi-resonator circuit, the authors related the first four resonant frequencies with the length of the spiral by analysing both S12 and S11 parameters. The results obtained are presented in Figure 12.

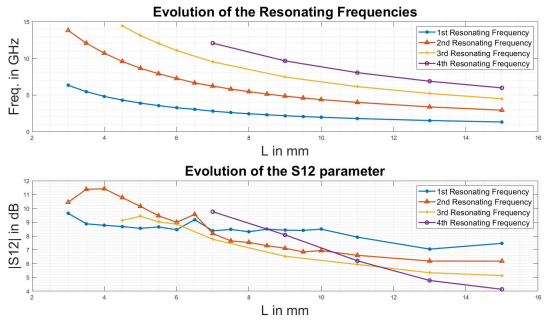

Fig. 12. Results obtained from the parametric simulation of the single spiral resonator multi-resonant circuit.

The results indicate that designers must have special care: if they want to work in a continuous frequency range they must select a resonant frequency to work with and a frequency range or a range of length's of the spiral where no other resonant frequency interferes. This confines the design of spiral resonators to a certain range of length and the usability of the circuit to a certain range of frequencies, which greatly reduces the operating viability of the circuit. Additionally, the designer must account with the 3dB bandwidth of each resonant peak as it's this bandwidth that ultimately defines de number of bits that one is able to code in a certain frequency range. The results attain also hint that the the evolution of the resonant frequencies with regards to the length of the spiral can be accurately described by exponential curves. This means that designers can easily design circuits and spirals to have a specific frequency response. The authors fitted the data point using exponential curves in the form of $f_r = a * exp(b * L) + c * exp(d * L)$ using Matlab. The coefficients obtained for each curve are displayed in Table II. These coefficients are used to generate design curves that fit the data points and are displayed in Figure 13.

TABLE II
COEFFICIENT LIST

Coefficients	1st Resonant Freq.	2nd Resonant Freq.
a	13.78	28.04
b	-0.5032	-0.4657
c	4.084	8.496
d	-0.07683	-0.07218
Coefficients	**3rd Resonant Freq.**	**4th Resonant Freq.**
a	33.47	32.55
b	-0.3878	-0.365
c	11.44	14.67
d	-0.06382	-0.06146

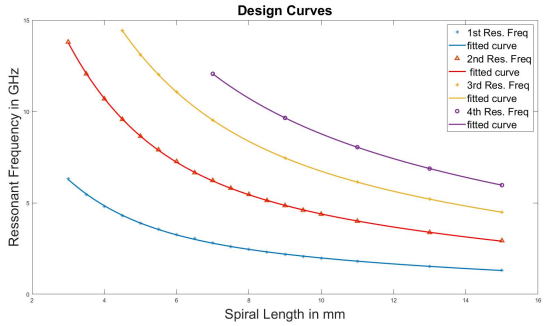

Fig. 13. Design curves obtained from the fitting of the obtained data points with exponential curves.

As we can see, these curves fit the data points appropriately which means that one can infer the circuit resonant frequency from the spiral length with a high degree of confidence. Bear in mind that these equations are valid only for the set of design parameters establish in Table I although the procedure is easily extended to all variations of those parameters.

The authors also computed the variation of the $\|S12\|$ parameter in function of the resonant frequency. Such relationship is presented in Figure 14. From this graph, one can conclude that by increasing the value of the length of the spiral, its multiple resonant frequencies decrease in value as well as in attenuation. This provides precious insight to better and easily design multi-resonant circuits.

VI. CONCLUSIONS

This paper presents the main problem with designing multi-resonant circuits: the lack of models. To the authors knowledge, few work as been done in this regard and so, the pinpointing of this problem in this paper aims to stimulate its resolution by the scientific community. This paper also exploits the adequateness of three simulators while exploring the behaviour of the multi-resonant circuit by performing a wide range of simulations. The existence of multiple resonant

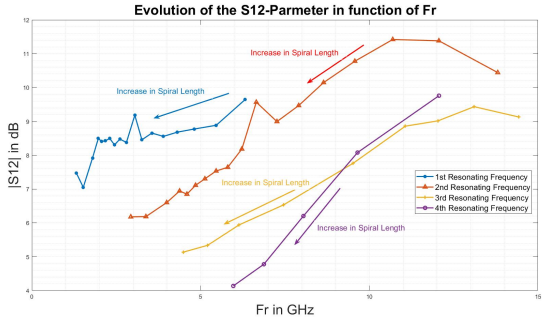

Fig. 14. Relationship between the $\|S12\|$ parameter and the resonant frequency as the spiral length increases.

frequencies per spiral resonator is highlighted as it is very important factor in the design of the circuit and it's not asserted by the literature. Finally, the authors propose a methodology to compute a set of equations that can easily relate the length of the spiral with the circuit's multiple resonant frequency. This greatly aids the design of the circuit as the designers can effortlessly compute the length of the spiral to resonate at a certain frequency and vice-versa.

The work done is an important first step to better define the multi-resonant circuit frequency behaviour. It would be of great interest to explore and define the influence of adjacent spiral resonators.

ACKNOWLEDGEMENT

This work is funded by FCT/MEC through national funds and when applicable co-funded by FEDER – PT2020 partnership agreement under the project UID/EEA/50008/2019

REFERENCES

[1] S. Preradovic and N. C. Karmakar, "Chipless RFID: Bar Code of the Future," in IEEE Microwave Magazine, vol. 11, no. 7, pp. 87-97, Dec. 2010. doi: 10.1109/MMM.2010.938571,URL:http://ieeexplore.ieee.org/stamp/stamp.jsp?tp=&arnumber=5590347&isnumber=5590337

[2] Elprocus, "RFID - a basic introduction & simple application." https://www.elprocus.com/rfid-basic-introduction-simple-application/#comments, 2015. [Online; accessed 03-July-2018].

[3] Finkenzeller, Klaus. (2005). RFID Handbook: Fundamentals and Applications In Contactless Smart Cards and Identification. 10.1002/0470868023.ch1.

[4] Karmakar, N. C., Kalansuriya, P., Azim, R. E., & Koswatta, R. (2016). Chipless radio frequency identification reader signal processing. (1 ed.) (Wiley Series in Microwave and Optical Engineering). Hoboken NJ USA: John Wiley & Sons.https://doi.org/10.1002/9781119215783

[5] Preradovic, S., Karmakar, N.C., & Balbin, I. (2008). RFID Transponders. IEEE Microwave Magazine, 9.

[6] Ni, Yi-Zhan & Huang, Xiao-dong & Cheng, Chong-Hu. (2017). Improved chipless tag based on multifilters. Microwave and Optical Technology Letters. 59. 1890-1896. 10.1002/mop.30647.

[7] S. Preradovic, I. Balbin, N. C. Karmakar and G. F. Swiegers, "Multiresonator-Based Chipless RFID System for Low-Cost Item Tracking," in IEEE Transactions on Microwave Theory and Techniques, vol. 57, no. 5, pp. 1411-1419, May 2009. doi: 10.1109/TMTT.2009.2017323 URL: http://ieeexplore.ieee.org/stamp/stamp.jsp?tp=&arnumber=4814553&isnumber=4909499

[8] J. Joubert, "Spiral microstrip resonators for narrow-stopband filters," in IEE Proceedings - Microwaves, Antennas and Propagation, vol. 150, no. 6, pp. 493-496, 8 Dec. 2003.

[9] Bahl, I. J. (2003). Lumped elements for RF and microwave circuits. Boston: Artech House.

[10] Zunfu Jiang, P. S. Excell and Z. M. Hejazi, "Calculation of distributed capacitances of spiral resonators," in IEEE Transactions on Microwave Theory and Techniques, vol. 45, no. 1, pp. 139-142, Jan. 1997. doi: 10.1109/22.552045, URL:http://ieeexplore.ieee.org/stamp/stamp.jsp?tp=&arnumber=552045&isnumber=11976

[11] Z. M. Hejazi, P. S. Excell and Z. Jiang, "Accurate distributed inductance of spiral resonators," in IEEE Microwave and Guided Wave Letters, vol. 8, no. 4, pp. 164-166, April 1998. doi: 10.1109/75.663521, URL: http://ieeexplore.ieee.org/stamp/stamp.jsp?tp=&arnumber=663521&isnumber=14529

[12] Young-Taek Lee, Jong-Sik Lim, Chul-Soo Kim, Dal Ahn, & Sangwook Nam. (2002). A compact-size microstrip spiral resonator and its application to microwave oscillator. IEEE Microwave and Wireless Components Letters, 12(10), 375–377. doi:10.1109/lmwc.2002.804556

[13] Elelimy, A. M., Ahmed, H. N., & El-Tager, A. M. (2010). A low phase noise microwave oscillator based on a planar microstrip spiral resonator. IEEE Middle East Conference on Antennas and Propagation (MECAP 2010). doi:10.1109/mecap.2010.5724202

[14] S. S. Mohan, M. del Mar Hershenson, S. P. Boyd and T. H. Lee, "Simple accurate expressions for planar spiral inductances," in IEEE Journal of Solid-State Circuits, vol. 34, no. 10, pp. 1419-1424, Oct. 1999. doi: 10.1109/4.792620, URL: http://ieeexplore.ieee.org/stamp/stamp.jsp?tp=&arnumber=792620&isnumber=17209

[15] Preradovic, Stevan & Karmakar, Nemai. (2014). Multiresonator-Based Chipless RFID - Barcode of the Future. 10.1007/978-1-4614-2095-8.

C Appendix C

IMOC 2019 - SBMO/IEEE MTT-S International Microwave and Optoelectronics Conference

Simulation of a Chipless RFID System using discreet FrFT to recover individual tags IDs

Bernardo Lopes
Universidade de Aveiro
Instituto de Telecomunicações
Aveiro, Portugal
bernardobentolopes@ua.pt

João N. Matos
Universidade de Aveiro
Instituto de Telecomunicações
Aveiro, Portugal
matos@ua.pt

***Abstract*—This paper presents a model of a real environment case of a Chipless RFID System using discreet FrFT algorithm to retrieve the ID of tags that share the same interrogation zone. The simulation is implemented in *MATLAB R20018b* and is based of physical measurements of the frequency behaviour of printed Multi-Resonant Circuits in order to achieve a better understanding of the challenges faced when designing said systems.The results show that the Multi-Resonant Circuit Frequency behaviour can be approximated by a band-stop FIR filter and that the tags IDs can be exceptionally well decoded by performing windowing in a fractional domain. The results show that the Multi-Resonant Circuit Frequency behaviour can be approximated by a band-stop FIR filter and that the tags IDs can be exceptionally well decoded by performing windowing in a fractional domain.**

***Index Terms*—Chipless RFID, RFID System, Multi-Resonant Circuit, Fractional Fourier Transform**

I. Introduction

Radio-Frequency Identification (RFID) is an emerging technology that allows data capturing based on the propagation of radio frequency (RF) electromagnetic waves through open space. The goal is to use RFID to substitute the use of optical reading printed barcode labels enabeling an non-automated trackin [1]. However, the penetration of the RFID technology in this market is hindered due to the high price of the tag, which is located on the object to be identified, when compared to the simple printed barcode [2].

The chipless RFID technology , appears from an effort to design low-cost RFID tags without the use of traditional silicone Application Specific Integrated Circuits (ASICs) that are the price bottleneck of the tags. In this way, tags become fully passive and without any active processing unit, thus the Chipless RFID system have more similarities with the Radio Detection And Ranging (RADAR) systems than with the typical RFID systems. The main challenge with these systems is to successfully recover ID's from superimposed backscatter signals.

This paper provides an example of an implementation of a Chipless RFID System using a discreet FrFT algorithm to retrieve the ID of tags that share the same interrogation zone. The simulation is implemented in *MATLAB R20018b* and is based of physical measurements of the frequency behaviour of printed Multi-Resonant Circuits.

II. Working Principle

Data can be encoded in many ways in chipless RFID tags. So far, tags that encode their data as a spectral signature are known to be more efficient in terms of coding capacity and, thus, are more studied by the scientific community [3]. One embodiment of the spectral signature coding technique are the Multi-Resonant-Based Chipless RFID Tags.

In these tags, the information is coded by the presence/absence of information in pre-determined frequency by either a logical '1' or '0'. This effect is achieved by deviating the signal flowing from the RX antenna through the transmission line to the TX antenna, to the ground through the coupled resonators at specific frequencies. The codding is performed by the Multi-Resonating circuit depicted in Figure 1.

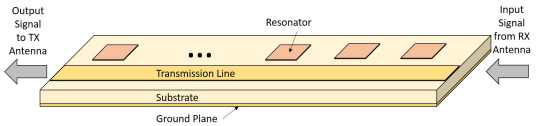

Fig. 1. Block diagram of the multi-resonantor circuit from a perspective view.

The resonant structures have a huge impact on the quality of the tag and therefore, the choice of the resonator must be done thoughtfully. In his work [4], Joubert sorted out that the spiral resonators are indicated to act as a band-stop filter. For this reason, the authors also used spiral resonators.

Because the tag functions by backscattering the received signal with it's unique ID encoded in it's spectrum, when multiple tags share the same interrogation zone, the signal received by the reader may be a overlap of several responses that encode different information in the same interrogation signal, as seen in Figure 2. This results in an information overlap in both time and frequency domain and thus, conventional techniques can't be applied in order to retrieve and distinguish the ID of the tags.

III. Fractional Fourier Transform (FrFT)

The fractional Fourier Transform can be explores as a technique to separate Linear Frequency Modulated (LFM) signals (such as the interrogation signal), providing means to manipulate signals in both time and frequency, allowing

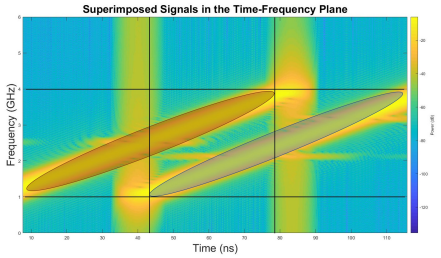

Fig. 2. Signal composed of two superimposed LFM signals that interfere both the time and frequency domain.

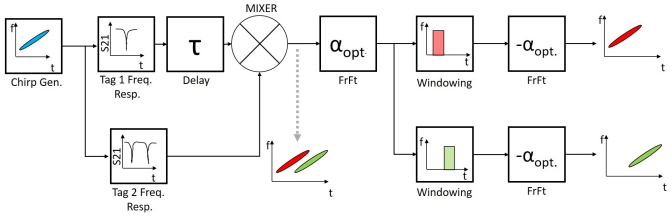

Fig. 3. Block diagram of the simulated Chipless RFID System.

separation of signals overlapping simultaneously in both domains. The FrFT is nothing more than a generalization of the Fourier transform, whereas the conventional Fourier transform allows signal in the time domain to be transformed to the frequency domain and vice versa, the FrFT allows signals to be transformed to a fractional domain that is neither time nor frequency but an intermediate domain in between. The discreet FrFT rotates the time-frequency plane around the intersection of the zero-frequency axis with half the total duration of the time domain signal [5]. The rotating angle is directly proportional the order of the transform α.

The separation of overlapping LFM signals can be achieved by performing an FrFT of order $\alpha_{optimum}$ transforming the overlapping signals into separable pulses in the fractional domain. The individual pulses can in this way be windowed creating sub-versions of overlapping signal containing only one pulse each. The signal can be recovered by performing an FrFT of inverse order - $-\alpha_{optimum}$.

IV. Chipless RFID System Simulation

In order to test the viability of using a discreet FrFT algorithm to recover the ID information tags sharing the same interrogation zone, the authors simulated in Matlab a Chipless RFID System. The system simulates the transition of a chip signal (a LFM signal) from the reader to two tags with different distances from the reader, the encoding of their ID in the signal, the corresponding backscattered signal of each tag, the received signal composed of the overlap of the two backscatter signals and the extraction of the both tag's ID from that signal. The equivalent implemented system is displayed in Figure 3. It does not account for any lost of power of the propagating signals, the existence of noise and assumes that the receiving and transmitting antenna are orthogonal thus not existing collision between the transmitted and received signal in the tag.

First, a chirp signal is generated, emulating the interrogation signal created from a reader. This signal is then capture by both tags that encode their unique ID by removing certain frequencies. The signal from one of the tags is then delayed simulating a scenario where here tags aren't at the same distance from the reader and thus, one of the backscatters signals will arrive later. The signals are then mixed together simulating the interference that may occur when the tags share the same interrogation zone. This signal is the one received by the reader that will start an algorithm to extract both tags unique ID. This is achieved by performing the discreet FrFT algorithm with an α_{opt} and then isolating each signal rectangular windows. The opposite process is the made in order to fully recover the original signals. The system was fully simulated in *MATLAB R20018b*.

In order to closer approximate the results from the simulated system to the ones expected in a real environment, the authors printed two Multi-Resonant Circuits on a Rogers RO4725JXR substrate with $hight = 0.78mm$ and $\epsilon_r = 2.55$. The conductor used was copper with $tickness = 0.017mm$. The multi-resonant circuit has a lot of variable that influence its frequency response. Every spiral resonator has five different physical parameters that directly influence its resonant frequency. Additionally, the transmission line also has two physical parameters that influence the frequency response of the circuit. Such parameters are depicted in Figure 4. Additionally, the number of turns n is also used and it accounts for the number of turns of a spiral resonator.

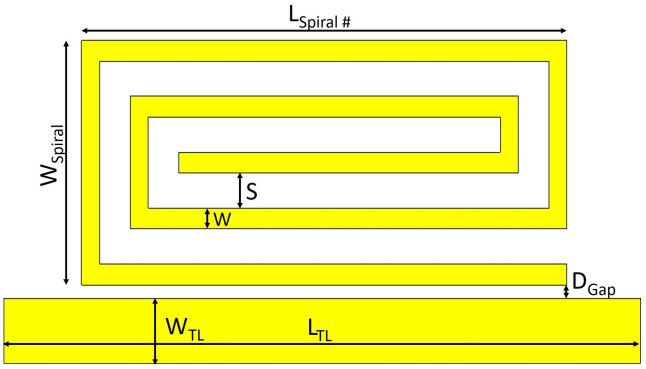

Fig. 4. Spiral Resonator coupled to a transmission line highlighting the physical parameters of the structure: $L_{spiral\#}$ is the length of the spiral numbered by #; W_{spiral} is the width of the spiral; S is the spacing between turns; W is the width of the spiral arm; D_{Gap} is the distance between the spiral resonator and the transmission line; W_{TL} is the width of the transmission line and the L_{TL} is the length of the transmission line.

The authors defined the frequency range of interest from 2 to 3 GHz and the coding frequencies of 2, 2.5 and 3 GHz. It was constructed a multi-resonant circuit that resonated at 2.5 GHz and one that resonated both at 2 and 3 GHz. Said circuits are depicted in Figure 5.

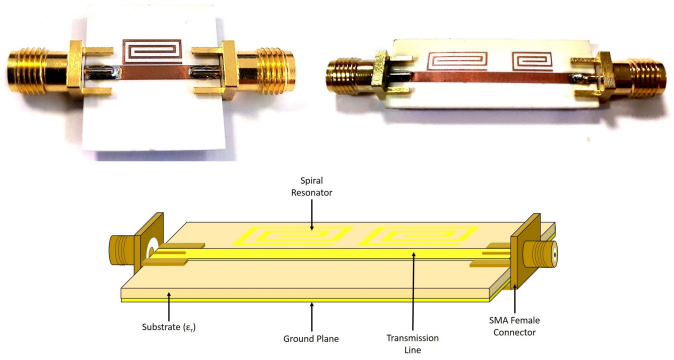

Fig. 5. Multi-Resonant Circuits printed and tested. At the left, on top, is a Multi-Resonant Circuit with a single spiral resonator that is projected to resonate at 2.5 GHz. At the right, on top, is a Multi-Resonant Circuit with two spiral resonators that are projected to resonate at 2 and 3 GHz.

The length of each spiral resonator were computed by performing a comparative study between three different models created using two different simulators and computing a set of equations capable of describing the behaviour of the circuit's resonance frequency in function of the spiral resonator's length. Due to the page limit of this paper, such method could not be described. The remaining parameters used in the circuit design are presented in Table I.

TABLE I
DESIGN PARAMETERS

Circuit Parameter	**Value [mm]**	**Circuit Parameter**	**Value [mm]**
S	0.5	D_{Gap}	0.2
W	0.3	W_{TL}	1.912
W_{Spiral}	3.5	L_{TL}	$L_{Spiral\#} + 10$

The S-Parameters of the circuits were extracted using a Agilent Technologies's PNA-X Network Analyser. In order to simplify the simulation, the authors re-created the circuits frequency response using narrow-bandstop equivalent FIR filters. The comparison between the measured signals and the ones from the equivalent filters is shown in Figure 6.

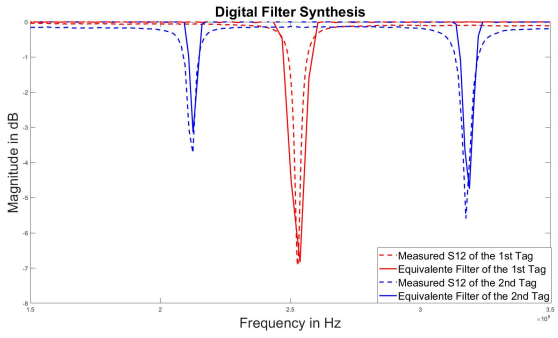

Fig. 6. Multi-resonant circuit S12 parameter versus the synthesised FIR filters frequency response.

From the results displayed we can see a good agreement between the simulated and measured frequency response of the Multi-resonant Circuit.

Due to the page limit, the authors cannot fully explain the details of the implementation of the system in the *MATLAB R20018b*. The results obtained from the implemented system are depicted in Figure 7.

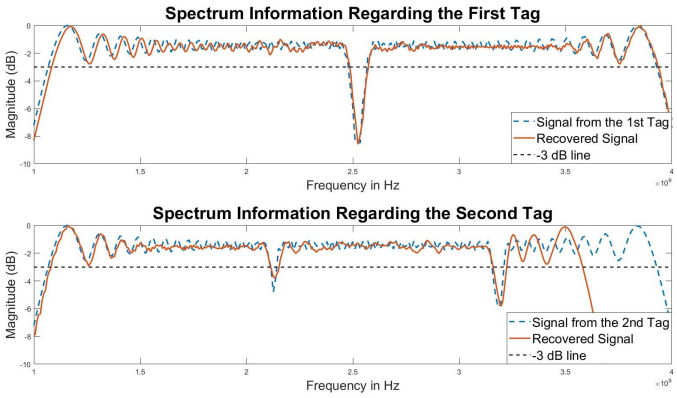

Fig. 7. Comparation between the original and recovered spectral information of both tag 1 and 2.

The results show that the signal can be almost perfectly recovered within the frequency band of interest, thus decoding successfully the information of each tag.

V. CONCLUSIONS

This paper highlights the potential of the use of the discreet FrFT algorithm to retrieve the information of the individual tag's ID. The implemented system was created to be a close approximation of a Chipless RFID System operating in a real environment. The results show that the Multi-Resonant Circuit Frequency behaviour can be approximated by a band-stop FIR filter and that the tags IDs can be exceptionally well decoded by performing windowing in a fractional domain.

ACKNOWLEDGEMENT

This work is funded by FCT/MEC through national funds and when applicable co-funded by FEDER – PT2020 partnership agreement under the project UID/EEA/50008/2019

REFERENCES

[1] S. Preradovic and N. C. Karmakar, "Chipless RFID: Bar Code of the Future," in IEEE Microwave Magazine, vol. 11, no. 7, pp. 87-97, Dec. 2010.

[2] Karmakar, N. C., Kalansuriya, P., Azim, R. E., & Koswatta, R. (2016). Chipless radio frequency identification reader signal processing. (1 ed.) (Wiley Series in Microwave and Optical Engineering). Hoboken NJ USA: John Wiley & Sons.

[3] Ni, Yi-Zhan & Huang, Xiao-dong & Cheng, Chong-Hu. (2017). Improved chipless tag based on multifilters. Microwave and Optical Technology Letters.

[4] J. Joubert, "Spiral microstrip resonators for narrow-stopband filters," in IEE Proceedings - Microwaves, Antennas and Propagation, vol. 150, no. 6, pp. 493-496, 8 Dec. 2003.

[5] D. M. J. Cowell and S. Freear, "Separation of overlapping linear frequency modulated (LFM) signals using the fractional fourier transform," in IEEE Transactions on Ultrasonics, Ferroelectrics, and Frequency Control, vol. 57, no. 10, pp. 2324-2333, October 2010.